THE EFFECT OF SOIL IMPROVEMENT UNDER EARTHQUAKE LOADING CONDITIONS

by

Kenan Yıldırım

B.S., Civil Engineering, Boğaziçi University, 2014

Submitted to the Institute for Graduate Studies in

Science and Engineering in partial fulfillment of

the requirements for the degree of

Master of Science

Graduate Program in Civil Engineering

Boğaziçi University

2019

To my family,

ACKNOWLEDGEMENTS

While preparing this thesis, I had very precious helps from very important individuals. At first, I would like to thank Professor Erol Güler for his valuable sharing and contributions throughout my master which expansed my vison and knowledge. I would also thank to my jury members Associate Professor İsmail Hakkı Aksoy and Associate Professor Özer Çinicioğlu.

I would express my gratitude to all Destech family for their encouragement and sharing their knowledge and experience in any case.

I profoundly want to thank my father, my mother, my wife, my sisters and my children who did not spare any support during that difficult period, make feel their love all the time and stand behind me in my all decisions.

ABSTRACT

THE EFFECT OF SOIL IMPROVEMENT UNDER EARTHQUAKE LOADING CONDITIONS

Earthquake is the rapid and sudden release of a huge energy resulting from the rupture of earth crust which cause the creation of seismic waves. The effect of earthquakes on soil conditions has been investigating for a long time by earthquake engineers.

The common practice in the past was mainly pseudo-static analysis and experiences. In the last ten years due to development of finite element programs to overcome many complex problems, researchers started to use computer programs to simulate and analyze earthquake conditions.

In that study, effect of soil improvement on site response during earthquake loading conditions is studied through response spectrum, PGA values measured from different points and amplification factors. For that purpose, three models are created with same dimensions and material properties, which represents the initial condition, raft foundation condition and deep foundation condition. Seven-time history records are selected and scaled with appropriate selection, scaling and filtering criteria.

Results show that, the soil improvement through pile construction does not create any shifts in the response spectrum, thus it does not change the soil class in most of the cases for the given loading and soil conditions, but for some records, the spectrum may change depending on the loading. Beside we checked the PGA values at different points. It is seen that there is amplification as the wave travels within soil in most cases. And based on amplification factors, it is stated that amplification factors of deep foundation are lower than initial condition. Thus, the soil improvement through the construction of piles deamplifies the earthquake loading much better than natural condition.

ÖZET

ZEMİN İYİLEŞTİRMESİNİN DEPREM DURUMUNDA ETKİSİ

Deprem yer kabuğunun kırılması sonucu ortaya çıkan ve sismik dalgaların oluşmasına sebep olan ani ve hızlı enerji salınımıdır. Depremlerin lokal zemin koşulları üzerine etkisi deprem mühendisleri tarafından uzun bir süredir araştırılmaktadır.

Geçmiş dönemlerdeki genel uygulama pseudo-statik yaklaşımlar ve deneyimlerdi. Fakat son on yılda, sonlu elemanlar programlarının birçok karmaşık problemin üstesinden gelmesiyle birlikte, araştırmacılar deprem analizlerini ve simülasyonlarını yapmak için bilgisayar programlarını kullanmaya başladılar.

Bu çalışmada, tepki spektrumu, farklı noktalardan ölçülen PGA değerleri ve büyütme katsayıları üzerinden zemin iyileştirmesinin deprem durumundaki etkisi araştırılmıştır. Bu amaçla, aynı ölçüler ve parametrelere sahip ve Doğal durumu, yüzeysel temel durumunu ve kazıklı temel durumunu göstermek üzere üç model oluşturulmuştur. Belirli kriterler çerçevesinde yedi deprem kaydı seçilmiş ve filtre ve ölçeklendirilmiştir.

Sonuçlara göre kazık ile yapılan zemin iyileştirmesinde birçok durumda tepki spektrumunun değişmediği görülmüştür. Bu durumda belirtilen yükleme ve zemin koşullarında zemin sınıfını da değiştirmemiştir. Fakat yükleme durumuna bağlı olarak bazı durumlarda spektrumda değişiklikler olmuştur. Bununla beraber farklı noktalarda PGA değerleri ölçüldü. Ve görüldü ki, dalgalar zeminde ilerlerken çoğu durumda büyütmeye uğradılar. Ve büyütme faktörlerine göre, derin temel durumunda büyütme faktörlerinin doğal duruma göre daha düşük olduğu belirlendi. Buna göre, kazık imalatı ile yapılan zemin iyileştirmesi deprem durumunda doğal duruma göre büyütmeyi daha çok engelledi.

TABLE OF CONTENTS

LIST OF FIGURES

LIST OF TABLES

LIST OF SYMBOLS

$a(t)$	Initial (unscaled) earthquake time history
A	Incident wave amplitude
A_o	Amplitude of harmonic loading on a SDOF system
A_{loop}	Area of hysteretic loop
b	Amplitude coefficients related with f(t)
B	Reflected wave amplitude
c_{ik}	Spectral response at ti resulting from the application of fk(t)
F_{ij}	Transfer function relating disp. amplitudes of ith and jth strata
F_s	Spectral acceleration coefficient for short periods
F_1	Spectral acceleration coefficient for 1-second periods
$\|F_n(w)\|$	Amplification function relating case n
G	Shear modulus
$Gmax$	Maximum shear modulus
$Gsec$	Secant shear modulus
$Gtan$	Tangent shear modulus
G_N	Shear modulus at cycle N
k	Wave number
M_w	Moment magnitude
PI	Plasticity Index
R_{jb}	Joyner-Boore distance
S_s	Spectral acceleration for short periods
S_1	Spectral acceleration for a 1-second period
t	Time
T	Period of vibration
u	Ground displacement along the direction of wave stresses
$\ddot{u}$	Ground acceleration along the direction of wave stresses
Vs	Shear-wave velocity
V_{s30}	Mean shear-wave velocity down to 30m from ground surface
z	Location of the point at which stresses\strains are calculated

W_D	Dissipated energy
W_S	Maximum strain energy
ϕ	Friction angle
γ	Shear strain
γ_c	Cyclic shear strain
τ	Shear stress
τ_c	Cyclic shear stress
ρ	Material density
τ (z,t)	Shear stress at depth z and time t
ξ	Damping ratio
υ	Poisson ratio
ω	Circular frequency
ω_n	Natural circular frequency

LIST OF SYMBOLS

AASHTO	American Association of State Highway and Transportation Officials
FHWA	Federal Highway Administration
NEHRP	National Earthquake Hazards Reduction Program
OCR	Overconsolidation Ratio
PEER	Pacific Earthquake Engineering Research Center
PGA	Peak Ground Acceleration
PGV	Peak ground velocity
PSHA	Probabilistic Seismic Hazard Analysis
SA	Spectral Acceleration
TBDY	Turkish Earthquake Code for Buildings
UHS	Uniform Hazard Spectra

1. INTRODUCTION

Earthquake is the rapid and sudden release of a huge energy resulting from the rupture of earth crust which cause the creation of seismic waves. The effect of earthquakes on soil conditions has been investigating for a long time by earthquake engineers. Papers and researches existing from early 1800s indicates the effect of ground motions on local soil conditions. Many different soil types are investigated to understand the seismic response of soils to earthquake waves.

The common practice in the past was mainly pseudo-static analysis and experiences. In the last ten years due to development of finite element programs to overcome many complex problems, researchers started to use computer programs to simulate and analyze earthquake conditions. The effect of a variety of soil improvement techniques is studied by means of software with real or synthetic earthquake records. M. Naghizadehrokni has studied the effect of soil improvement via piled abutments based on the numerical analysis of natural ground in Babol city (5). Siegel et al. searched the seismic response of site improved with stone column in the eastern United States. (6) R.J. Armstrong and R.W. Boulanger had studied the liquefaction effect of piled abutments by comparing the results of centrifuge tests and numerical analysis. (7) Bouckovalas had studied the seismic response of ground improved with rigid inclusions. (8) Vucetic et al. had obtained the effect of soil improvement with column piles on seismic soil response. (9) Ge and Liu had investigated the effect of foundation stabilization on seismic site response, etc. (10)

In that study, the aim is to understand the effect of soil improvement on site response. Earthquake loading conditions. In that sense, three models are created with same dimensions and material properties, which represents the initial condition, raft foundation condition and deep foundation condition. Seven-time history records are selected and scaled with appropriate selection, scaling and filtering criteria. The aim is to understand of seismic response of ground for strong ground motions in terms of PGA values and response spectrums.

2. CYCLIC SOIL PARAMETERS AND SITE CHARACTERIZATION

The soil behavior can be very complex under cyclic conditions. In such a condition, characterization of the parameters of soil as accurate as possible is the main concern for the geotechnical engineers.

The widely used models are mainly, equivalent linear models, cyclic nonlinear models and advanced constitutive models. The complexity and hardship of each type increases respectively. Equivalent linear models are the easiest and most common models; however, they have limited capacity of representing the soil behavior during cyclic or earthquake loading. But advanced models reflect many details of cyclic behavior of soils, but they are very complex and difficult, therefore impractical in many problems relating with seismic design. (1)

2.1. Equivalent Linear Model

The soil having a great depth and far away from the structures may show hysteretic behavior under earthquake loading, which is shown in the Figure 2.1. The curve of that figure can be described via the path of the curve or variables identifying the general shape. Two main characteristics describing the shape are the inclination (slope) and breath of the cycle (loop). (3) The slope of that cycle (loop) depends on the soil stiffness that can be identified during loading process at any point by G_{tan}, tangent shear modulus. Since the tangent modulus changes throughout the cyclic loading, it can be approximated over entire loop by secant shear modulus, which describes general inclination of hysteresis loop.

$$G_{sec} = \frac{\tau_c}{\gamma_c}$$

The breath of cycle (loop) is interrelating with energy dissipation mechanism including friction, heat generation and plastic yielding which can be determined by damping ratio.

$$\xi = \frac{W_D}{4 * \pi * W_s} = \frac{1}{2\pi} * \frac{A_{loop}}{G_{sec} * \gamma_c^2}$$

G_{sec} and $\boldsymbol{\xi}$ are equivalent linear material parameters.

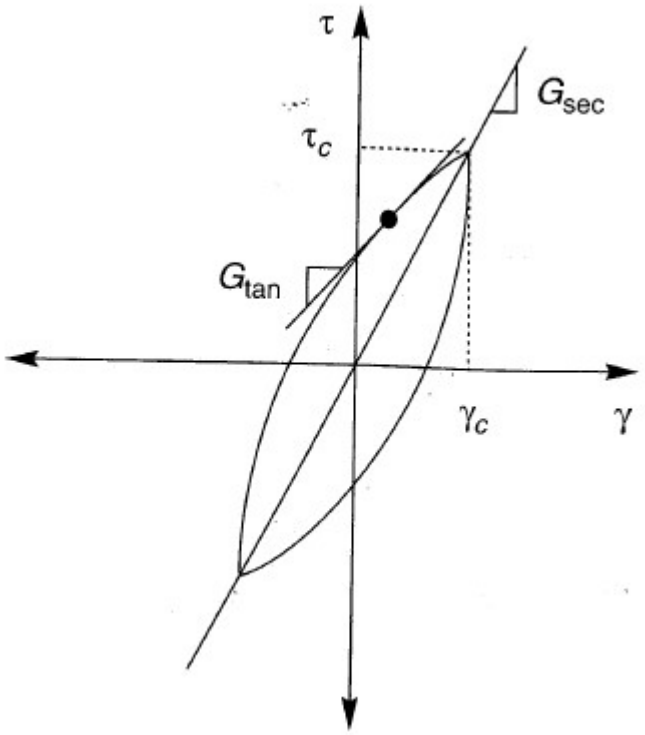

Figure 2.1. Secant shear modulus G_{sec} and tangent shear modulus G_{tan}. (3)

2.1.1. Shear Modulus

According to the laboratory tests, the parameters that affect the soil strength are effective stresses, atterberg limits, principal effective stresses, pre-overburden pressure condition and dynamic strain amplitude. (1) The change in the shear modulus of a soil element depends on dynamic strain amplitude. The path that describes the nonlinear behavior of soil by stress-strain curve is called *backbone curve*. (Figure 2.2.) At zero cyclic(dynamic)

strain amplitude (origin) the slope of the curve shows the maximum value of the shear modulus, (G_{max}). The, G_{sec}/G_{max}, (modulus ratio) decreases to the values lower than 1 as the cyclic shear strain amplitudes get greater values. (G and G_{sec} represents the same meaning.) Therefore, soil stiffness characterization requires both G_{max} and G/G_{max} (modulus ratio). The change in G/G_{max} is depicted by the curve named as modulus reduction curve which gives the similar information with backbone curve. (Figure 2.2.) (3)

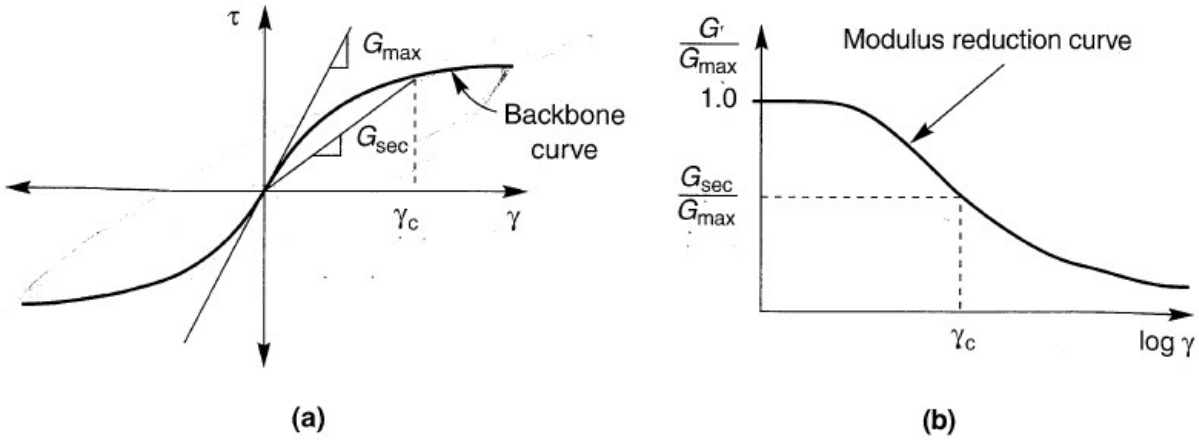

Figure 2.2. Backbone curve showing change in G_{sec} with shear strain. (3)

Maximum Shear Modulus, G_{max}: G_{max} value can be determined both from laboratory tests and in-situ tests. Since most of the geophysical tests use low strain values, G_{max} value can be determined from measured shear wave velocity as

$$G_{max} = \rho * v_s^2$$

Shear wave velocity is most reliable method to evaluate G_{max} and many geophysical tests are used for that purpose like seismic refraction or reflection tests, suspension-logging test, Rayleigh wave test, seismic cross hole and down-hole test, seismic cone test etc. In-situ tests should be carefully conducted due to anisotropy of the soil which may cause wrong interpretation of the shear wave velocity.

G_{max} value can be found from laboratory tests too, in case of lack of Vs (shear wave velocity). However, in-situ tests are more reliable than laboratory tests due to disturbance effect, stress prehistory etc.

Table 2.1. Empirical relationships between G_{max} and in-situ test parameters (3)

In Situ Test	Relationship	Soil Type	References	Comments
SPT	$G_{max} = 20{,}000(N_1)_{60}^{0.333}(\sigma'_m)^{0.5}$	Sand	Ohta and Goto (1976), Seed et al. (1986)	G_{max} and σ'_m in lb/ft²
	$G_{max} = 325N_{60}^{0.68}$	Sand	Imai and Tonouchi (1982)	G_{max} in kips/ft²
CPT	$G_{max} = 1634(q_c)^{0.250}(\sigma'_v)^{0.375}$	Quartz sand	Rix and Stokoe (1991)	G_{max}, q_c and σ'_v in kPa; Based on field tests in Italy and on calibration chamber tests
	(Figure 6.41)	Silica sand	Baldi et al. (1986)	G_{max}, q_c and σ'_v in kPa; Based on field tests in Italy
	$G_{max} = 406(q_c)^{0.695}e^{-1.130}$	Clay	Mayne and Rix (1993)	G_{max}, q_c and σ'_v in kPa; Based on field tests at worldwide sites
DMT	$G_{max}/E_d = 2.72 \pm 0.59$	Sand	Baldi et al. (1986)	Based on calibration chamber tests
	$G_{max} = 2.2 \pm 0.7$	Sand	Bellotti et al. (1986)	Based on field test
	$G_{max} = \frac{530}{(\sigma''_v/p_a)^{0.25}} \frac{\frac{\gamma_D}{\gamma_W} - 1}{2.7 - \frac{\gamma_D}{\gamma_W}} K_o^{0.25}(p_a\sigma'_v)^{0.5}$	Sand, silt, clay	Hryciw (1990)	G_{max}, pq_c, σ'_v in same units; γ_D is dilatometer-based unit weight of soil; based on field tests
PMT	$3.6 \le \frac{G_{max}}{G_{ur,c}} \le 4.8$	Sand	Bellotti et al. (1986)	G_{urc} is corrected unloading-reloading modulus from cyclic PMT
	$G_{max} = \frac{1.68}{\alpha_p} G_{ur}$	Sand	Byrne et al. (1991)	G_{ur} is secant modulus unloading-reloading portion of PMG; α_p is factor that depends on unloading-reloading stress conditions; based on theory and field test data

Modulus Reduction, G/G_{max}: According to the recent searches, unlike the past idea that the G/G_{max} behavior of fine and coarse grained is evaluated separately, recent researches and studies, however, shows that there is an incremental changeover among that behavior of plastic fine soil and non-plastic coarse soil. (3)

Kokushu (1982) and Zen (1978) have revealed the effect of soil plastification based on the curve shown in Figure 2.2. that the increase of plasticity cause decrease of shear modulus with shear strain. (3) After wide studies and searches, Vucetic (1987) and Dobry and Sun (1988) agree in the idea that the effect of plasticity on that curve is much greater than void ratio and had presented it with graph shown in the Figure 2.3. It can be understood from graph that linear cyclic(dynamic) threshold, γ_{tl}, is higher for soils of high plasticity than low plastic soils. (3) That characteristic affects the soil whether it amplifies or attenuates the earthquake motions. The curve shown in Figure 2.3. were generally used for sands when PI=0 by Sedd and Idriss. (1970). That means the Figure 2.3. may be used for both fine soils and granular soils. (that can be confirmed for the granular soil which shows aging and cementation effect.

The behavior of curve shown in Figure 2.2. is affected by effective peripheral (confining) pressure, especially for soils that show low plastic characteristics. (Iwasaki; Kokoshu,1980) The effective confining pressure increases the linear cyclic(dynamic) threshold shear strain, γ_{tl}. (Figure 2.4.) (3)

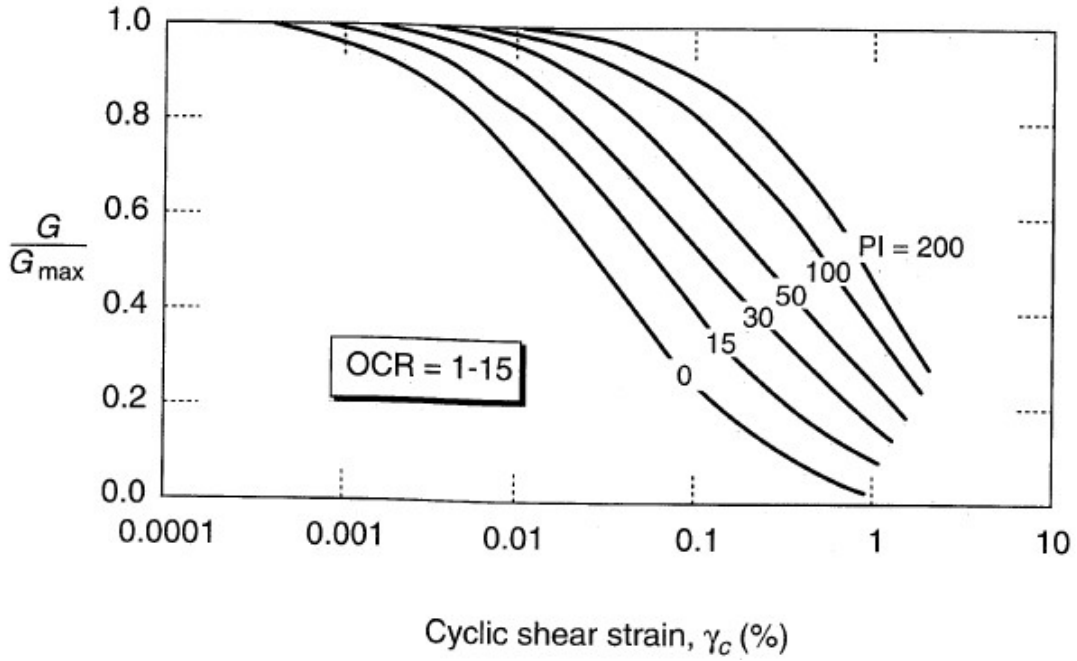

Figure 2.3. Modulus reduction curve for fine-grained soils of different plasticity (3)

Table 2.2. Effect of environmental and loading conditions on maximum shear modulus of normally consolidated and moderately overconsolidated soils (3)

Increasing Factor	G_{max}
Effective confining pressure, σ'_m	Increases with σ'_m
Void ratio, e	Decreases with e
Geological age, t_g	Increases with t_g
Cementation, c	Increases with c
Overconsolidation ratio, OCR	Increases with OCR
Plasticity index, PI	Increases with PI if OCR>1; stays about constant if OCR=1
Strain rate, $\dot{\gamma}$	No effect for non-plastic soils; increases with $\dot{\gamma}$, for plastic soils (up to~10% increase per log cycle increase in $\dot{\gamma}$)
Number of loading cycles, N	Decreases after N cycles of large γ_c, but recovers later with time in clays; increases with N for sand

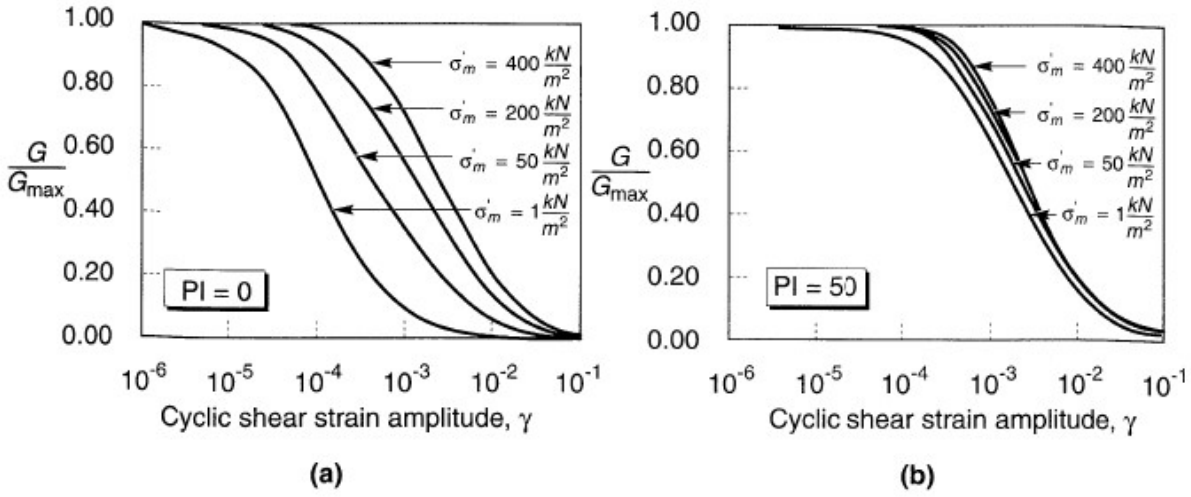

Figure 2.4. Effect of mean effective confining pressure on modulus reduction curves for (a) non-plastic (pi=0) and (b) plastic (pi=50) soil. (after Ishibashi 1992). (3)

The generation of pore pressure or structural changes can change the shear strain of soils in cyclic loading situations if the stress is controlled and the number of cycles change. The shear stress would increase as the cycles of loading decreases clay or saturate sand of undrained condition and if stain is controlled. (1) Stiffness of specimen decreases under both conditions. For clayey or silty soils, the relation between the shear modulus at the beginning (G1) and after N cycles (G_N) can be shown as below by degradation index, δ, and degradation parameter, t. (Idriss et.al. 1978).

$$G_N = \delta * G_1$$

$$\delta = N^{-t}$$

The degradation parameter increases with decrease of PI and pre-overburden pressure and decreases with decrease of cyclic strain amplitude. The effect of stiffness change is shown in the Figure 2.5. The effects the modulus ratio of clays is described in Table 2.3. (3)

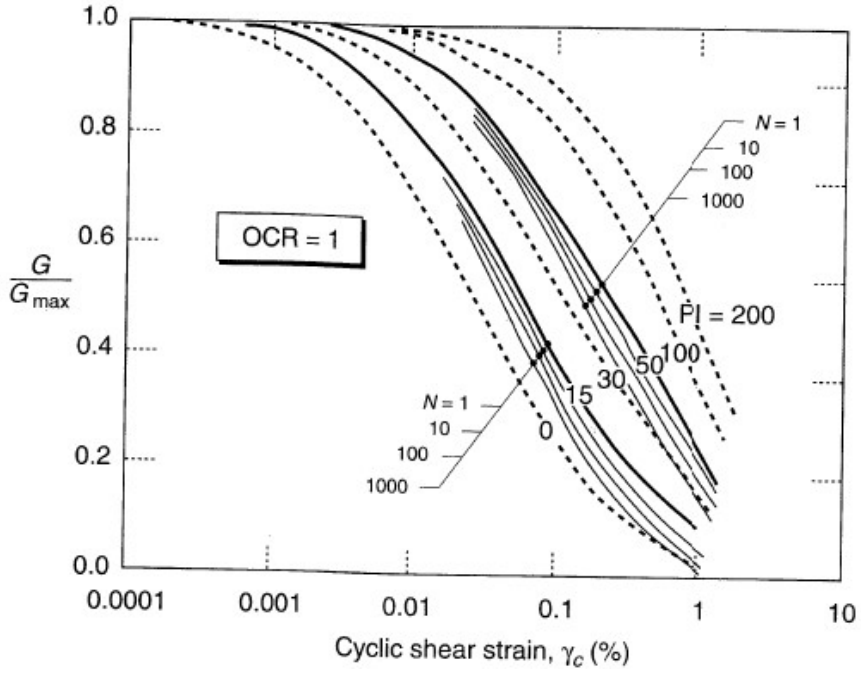

Figure 2.5. Effect of plasticity and cyclic degradation on shear modulus (after Vucetic and Dobry, 1991). (3)

Table 2.3. Effects on modulus ratio of clays (3)

Increasing Factor	G/G_{max}
Confining pressure, σ'_m	Increases with σ'_m; effect decreases with increasing PI
Void ratio, e	Increases with e
Geological age, t_g	May increase with t_g
Cementation, c	May increase with c
Overconsolidation ratio, OCR	Not affected
Plasticity index, PI	Increase with PI
Cyclic strain, γ_c	Decreases with γ_c
Strain rate, $\dot{\gamma}$	G increases with $\dot{\gamma}$, but G/G_{max} probably not affected ig G and G_{max} are measured at same $\dot{\gamma}$
Number of loading cycles, N	Decreases after N cycles of large γ_c (G_{max} measured before N cycles) for clays; for sands, can increase (under drained conditions) or decrease (under undrained conditions)
Source: Modified from Dobry and Vucetic (1987).	

2.1.2. Damping Ratio

Experiments have indicated that there is energy dissipation even at levels below cyclic limit strain, which means damping never gets value of zero. Above threshold strain damping ratio decreases with decreasing shear strain. Damping characteristic is affected by plasticity properties of soil like modulus reduction behavior. (3) According to Figure 2.6. damping ratio of soils with low plasticity is lower than the soils with high plasticity at the same cyclic strain level. The curves in Figure 2.6. are applicable to both cohesive and cohesionless soils. The gravel shows the same characteristic with sand in term of damping. (Seed 1984). (3)

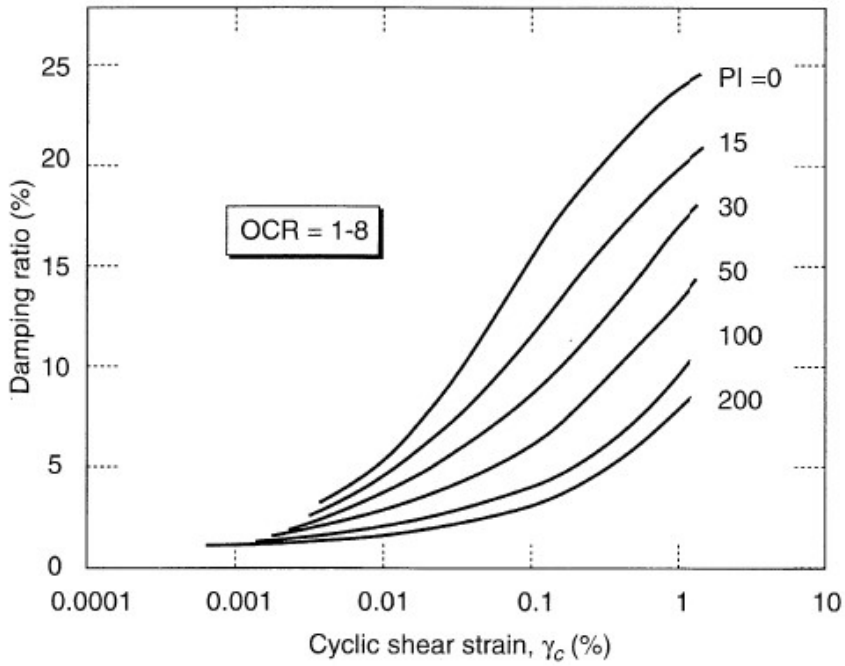

Figure 2.6. Variation of damping ratio of fine-grained soil with cyclic shear strain amplitude and plasticity index. (after Vucetic and Dobry 1991) effect of soil plasticity on cyclic response (3)

Table 2.4. Effects on damping ratio of clays

Increasing Factor	Damping ratio, ξ
Confining pressure, σ'_m	Decreases with σ'_m; effect decreases with increasing PI
Void ratio, e	Decreases with e
Geological age, t_g	Decreases with t_g
Cementation, c	May increase with c
Overconsolidation ratio, OCR	Not affected
Plasticity index, PI	Decreases with PI
Cyclic strain, γ_c	Increases with γ_c
Strain rate, $\dot{\gamma}$	Stays constant or may increase with $\dot{\gamma}$,
Number of loading cycles, N	Not significant for moderate γ_c and N
Source: Modified from Dobry and Vucetic (1987).	

2.2. Cyclic Nonlinear Models

These models characterize the nonlinear soil behavior more accurately because they pursue the real stress circle(path) in a cyclic(dynamic) loading condition. The main characterization parameters of these models are backbone curve and the rules that is valid for unloading-reloading behavior of soils and stiffness degradation and other effects. (3) Many complex models can be formed by incorporating many rules to represent the soil properties better, however, such models are mainly restricted with many initial conditions and stress paths.

The shear strength and initial stiffness are the main parameters for construction of backbone curve. For a simple example, backbone shape can be illustrated by a hyperbolic formula as below, and the curve can be shown as in the Figure 2.7.
The quantities G_{max} and τ_{max} can be measured directly or calculated by empirical correlations.

$$F_{bb}(\gamma) = \frac{G_{max} * \gamma}{1 + \left({}^{G_{max}}/_{\tau_{max}}\right) * \gamma}$$

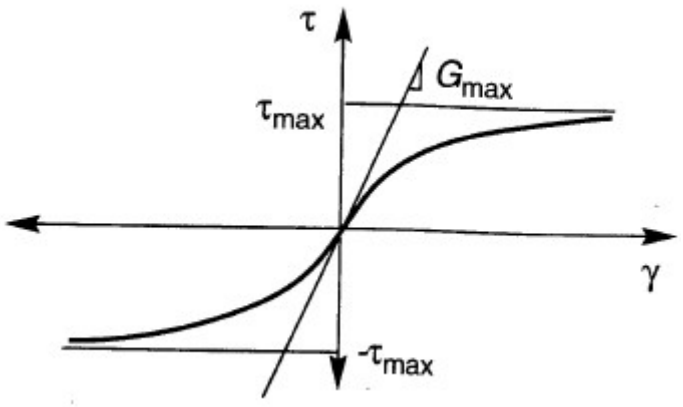

Figure 2.7. Hyperbolic backbone curve asymptotic to $\tau=G_{max}*\gamma$ and $\tau=\tau_{max}$ ($\tau=-\tau_{max}$)

The rules that are to characterize the seismic response for the example model are; (3)

- Stress path follows the backbone curve for the initial loading.
- The other loading and reloading graph(curve) have the same shape with backbone curve but enlarged with two. These two-rules are called Masing behavior
- The unloading and reloading curve pursues the backbone curve for the next time that the stress reverse back if it passes over the maximum strain in the past and has the intersection with the backbone curve.
- The stress strain curve traces the previous one If an unloading-reloading curve intersects an unloading-reloading curve from the previous cycle.

If these rules govern any such model, that model is named as extended Massing model and the curve in the Figure 2.8. can be shown as an example.

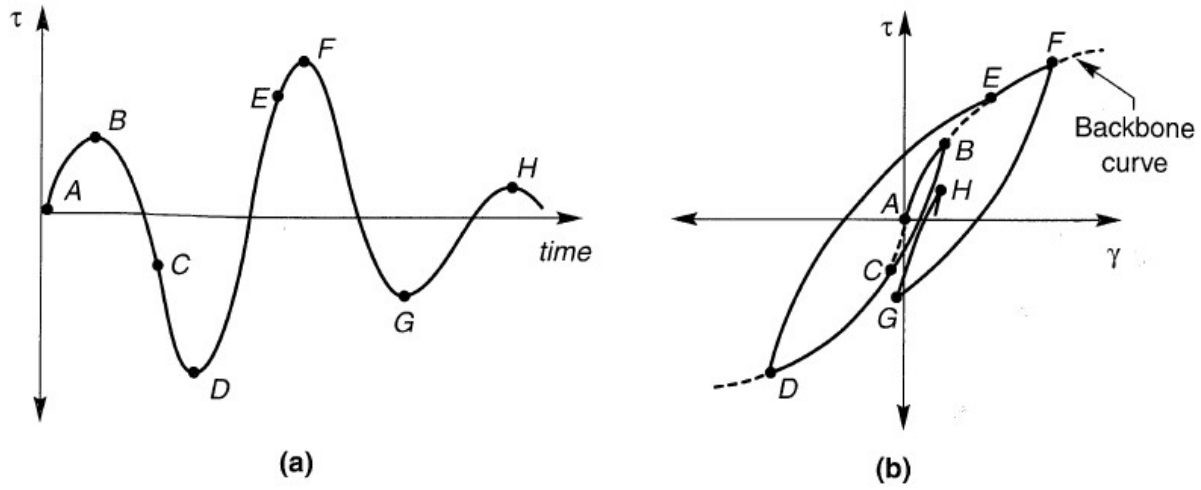

Figure 2.8. Extended Masing rules: (a) variation of shear stress with time; (b) resulting stress-strain behavior (3)

Shear strain is not necessarily zero for cyclic nonlinear models when shear stress is null. The capability of those models to reflect the development of permanent strain is one of the most essential property when compared to equivalent linear models. Another important characteristic of these models is the ability of computation of pore pressures, hence effective pressure. (3)

2.3. Advanced Constitutive Models

Advanced models represent soil behavior most accurately. Basic rules of mechanic are used for describing soil behavior for stress paths, stress conditions, principal stresses, cyclic loading and drained or undrained conditions.

Advanced constitutive models require a yield surface, where yield surface is the limit of elasticity under stress combinations, a hardening law, where hardening law defines the shape of yield surface when plastic deformation occurs and a flow rule, where flow rule provides the relation between the plastic strain and stress. (3)

Although these models provide considerable flexibility in characterizing soil behavior, their formation and description require many more parameters than other models. Since determination of those parameters is very complex and difficult, and it requires many in-situ or laboratory test, it makes the models impractical.

3. SEISMIC SITE RESPONSE ANALYSIS

The researchers have been studying the effect of local soil conditions during earthquake loading for many years. The local soil condition may change the duration, intensity and frequency of shaking. Amplification of order three or more of peak acceleration of bedrock at small values (0.05g to 0.10g) has been measured. In fact, the only effect of soil conditions is not amplification, it may also change the frequency content of bedrock ground motions. In proximity of fundamental site period, To, an amplification of order of ten is documented.

Traditionally, seismic hazard analyses give the ground motions for rock having Vs30, as 760 m/sec for top 30m, which represents Site Class B according to Turkish Earthquake Code, TBDY, or AASHTO. The effect of ground motion for the sites different than Site Class B can be taken into consideration in a variety of ways. One is to modify the PGA, by an empirical amplification value. Another option is to modify the PGA and spectral acceleration values by site specific factors, FPGA, Fa and Fv. Then new spectral acceleration graph can be drawn. (The construction of acceleration graph (response spectrum) is explained in the next chapter). As a third alternative, a site-specific analysis can be conducted by different attenuation relationships, which definitively count for site conditions.

General acceptance of engineers is that one of these methods is enough for evaluation of seismic properties of sites. However, if the aim is to observe the soil conditions within details, or the use of empirical amplification factors is not suitable, a formal site-specific soil response analysis must be performed. Moreover, The Class F according to TBDY requires site-specific seismic analysis. Sites having very different properties in top 60m also requires. Sites that has soil part 150m or more at top require site-specific seismic response analysis too. (2)

3.1. Site-Specific Seismic Response Analysis

The most widespread type is one dimensional analysis. The main assumption of that type is a vertically propagating shear wave within uniform infinite horizontal layers. In fact, that assumption is valid in engineering-wise. Since the Vs increases with depth, the wave refracts and propagates near vertical as it gets closer to ground surface as shown in the Figure 3.1. In conventional one-dimensional analysis, the effect of vertical motions waves, compressional waves and lateral non-uniform soil conditions. In such a case, where these properties must be taken into consideration, two-dimensional site response analysis must be performed.

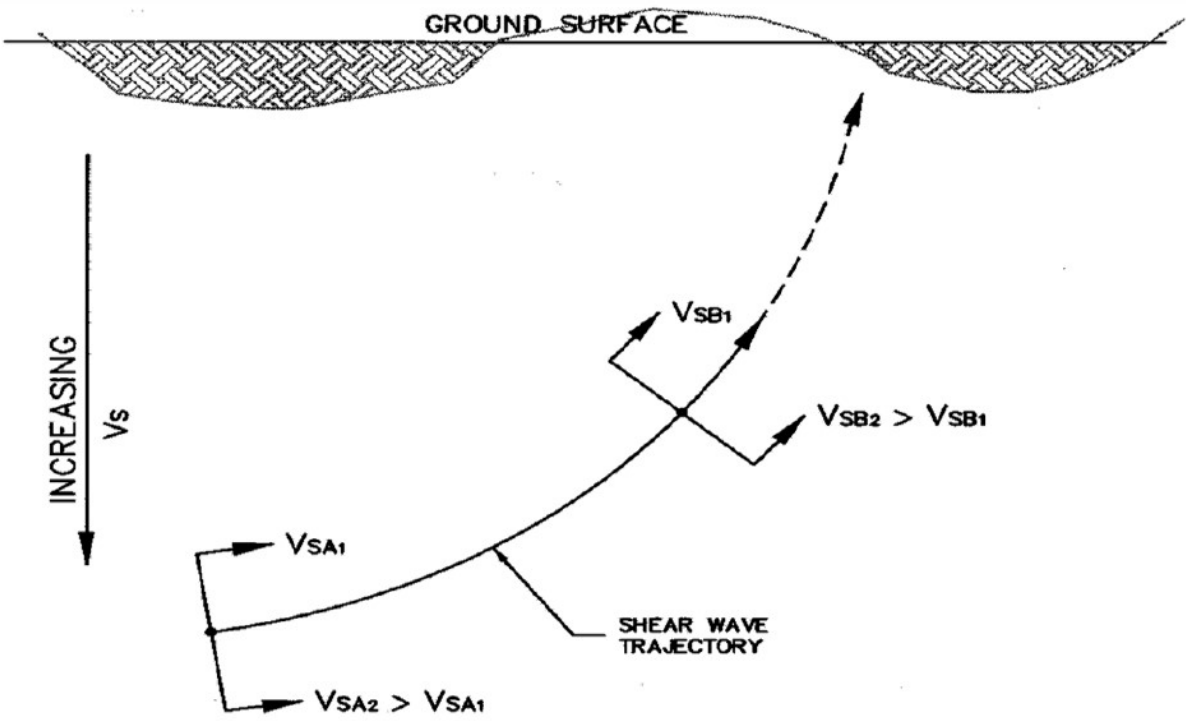

Figure 3.1. Refraction of shear waves approaching the ground surface (3)

The assumption of vertically propagating waves is consistent with design and code practices. It is also suitable for seismic lope stability and liquefaction potential analysis which take the horizontal component of ground motion into consideration.

There are three approaches for such one-dimensional analysis; (1)

- Simplified analysis
- Linear one-dimensional site response analysis
- Advanced (non-linear) one dimensional site response analysis

3.2. Simple Empirical Relationships

The effect of local soil behavior on seismic response is approximated by using empirical relations which relates the bedrock motion to site motion. (1) The correlations are determined by observational data from ground motions during earthquake or linear one-dimensional site response analysis. These correlations give the site response factors to be used in the specified site.

One of the most prevalent types is given in the TBDY, which modifies the acceleration response spectra by site response factors based on V_{S30}. The procedure for modifying PGA, S_s and S_1 values with site factors F_{PGA}, F_{Ss} and F_{S1} is presented below. (2)

Step 1: The first step is to determine PGA, Ss and S1 values from national hazard map through the coordinates, in Turkey it is found from AFAD website. (AFAD, 2019)

Step 2: As second step, design spectral acceleration factors, S_{DS}, S_{D1} are calculated using site factors, which are given below.

$$S_{DS} = S_S * F_S \quad (3.1.1)$$

$$S_{D1=}S_1 * F_1 \quad (3.1.2)$$

Table 3.1. TBDY Site Classification System

Site Class	Soil Profile	Average Properties in top 30 m		
		Soil Shear Wave Velocity, Vs30 (m/sec)	Standart Penetration Resistance, N_{60}	Soil Undrained Sshear Strength , c_u (kPa)
ZA	Hard Rock	>1500	-	-
ZB	Slightly Weathered Rock	760 - 1500	-	-
ZC	Very Dense Sand, Gravel and Hard Clay or highly Weathered Rock	360 - 760	>50	>250
ZD	Medium Dense to Dense Sand, Gravel and Very Stiff Clay	180 - 360	15 - 50	70 - 250
ZE	Loose Sand, Gravel and Soft to Stiff Clay Any Profile with more than three D3m of soil having following characteristics 1.PI>20 2.w>40% 3. c_u<25	>180	<15	<70
ZF	Any Profile having one or more of the following characteristics 1.Soils vulnerable to potential failure or collapse under seismic loading such as liquefable soils, quick and highly sensitive clays, collapsible weakly cemented soils 2.Peats and/or highly organic clays (H>3m) 3.Very high plasticity clays (H>8m and PI>50) 4. Very thick soft/medium stiff clays (H>35m)			

Table 3.2. Spectral Acceleration Factor at Short Period, Fs

Site Class	Spectral Response Acceleration Factor at Short Period					
	$S_s \leq 0.25$	$S_s = 0.50$	$S_s = 0.75$	$S_s = 1.00$	$S_s = 1.25$	$S_s \geq 1.50$
ZA	0.8	0.8	0.8	0.8	0.8	0.8
ZB	0.9	0.9	0.9	0.9	0.9	0.9
ZC	1.3	1.3	1.2	1.2	1.2	1.2
ZD	1.6	1.4	1.2	1.1	1.0	1.0
ZE	2.4	1.7	1.3	1.1	0.9	0.8
ZF	Site specific Analysis required					

Table 3.3. Spectral Acceleration Factor at Short Period, Fs

Site Class	Spectral Response Acceleration Factor at 1.0 second Period					
	$S_1 \leq 0.25$	$S_1 = 0.50$	$S_1 = 0.75$	$S_1 = 1.00$	$S_1 = 1.25$	$S_1 \geq 1.50$
ZA	0.8	0.8	0.8	0.8	0.8	0.8
ZB	0.8	0.8	0.8	0.8	0.8	0.8
ZC	1.5	1.5	1.5	1.5	1.5	1.4
ZD	2.4	2.2	2	1.9	1.8	1.7
ZE	4.2	3.3	2.8	2.4	2.2	2.0
ZF	Site specific Analysis required					

Step 3-1: Constructing horizontal acceleration response spectra by computing horizontal elastic design acceleration, $S_{ae}(T)$.

$$S_{ae}(T) = \left(0.4 + 0.6 * \frac{T}{T_A}\right) * S_{DS} \qquad (0 \leq T \leq T_A) \qquad (3.1.3)$$

$$S_{ae}(T) = S_{DS} \qquad (T_A \leq T \leq T_B) \qquad (3.1.4)$$

$$S_{ae}(T) = \frac{S_{D1}}{T} \qquad (T_B \leq T \leq T_L) \qquad (3.1.5)$$

$$S_{ae}(T) = \frac{S_{D1} * T_L}{T^2} \qquad (T_L \leq T) \qquad (3.1.6)$$

$$T_A = 0.2 * {}^{S_{D1}}/_{S_{DS}} \;\; ; \;\; T_B = {}^{S_{DS}}/_{S_{DS}} \qquad (3.1.7)$$

T_L is assumed as 6 sec according to TBDY.

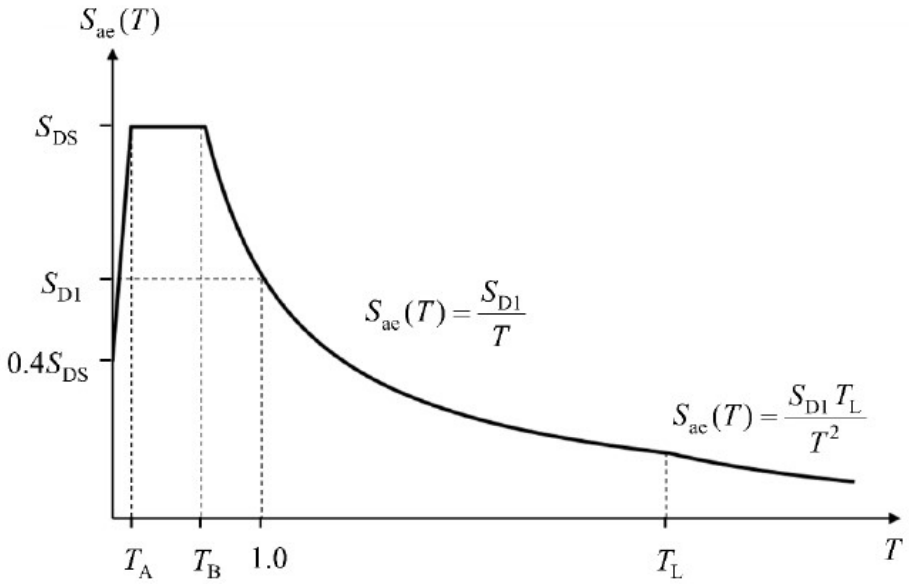

Figure 3.2. Horizontal Design Acceleration Spectrum

Step 3-1: Constructing vertical acceleration response spectra by computing vertical elastic design acceleration, $S_{aeD}(T)$.

$$S_{aeD}(T) = \left(0.32 + 0.48 * \frac{T}{T_{Ad}}\right) * S_{DS} \qquad (0 \le T \le T_{AD}) \qquad (3.1.8)$$

$$S_{aeD}(T) = 0.8 * S_{DS} \qquad (T_{AD} \le T \le T_{BD}) \qquad (3.1.9)$$

$$S_{aeD}(T) = 0.8 * S_{DS} * {}^{T_{BD}}/_{T} \qquad (T_{BD} \le T \le T_{LD}) \qquad (3.1.10)$$

$$T_{AD} = {}^{T_A}/_{3} \;\; ; \quad T_{BD} = {}^{T_B}/_{3} \;\; ; \quad T_{LD} = {}^{T_L}/_{2} \qquad (3.1.11)$$

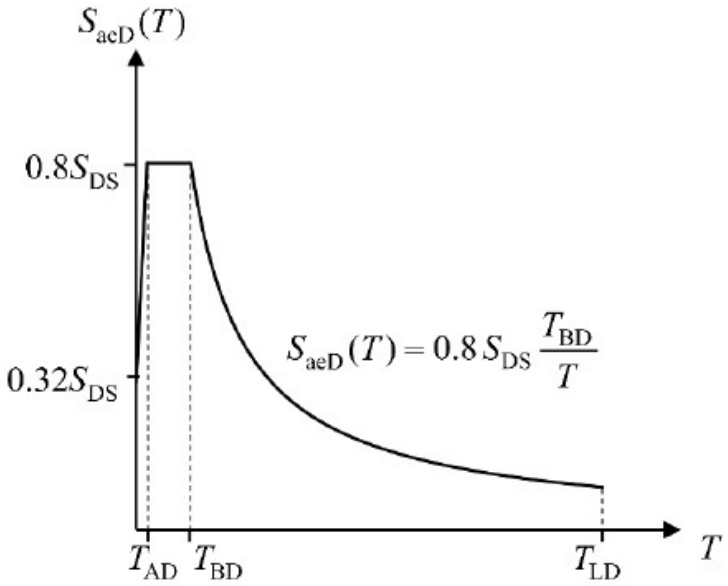

Figure 3.3. Vertical Design Acceleration Spectrum

This method is not appropriate for Site Class F. Moreover, that procedure cannot be applied to sites which have strong impedance at top 60m. (Impedance is the product of mass density and shear wave velocity). And the site factors should be used cautiously for the sites having more than 150m thick soil.

Many researchers propounded different empirical relationships between PGA values at hypothetical bedrock outcrop and project site. One of these relationships developed by Seed and Idriss(1982), which gives relation between PGA at bedrock and different soil profiles. Whereas, there is no detailed definition for these soil profiles. The graph belonging to that relation is given in Figure 3.4. However, that relation is out-of-date. It is not used, and it should not be used in site response analysis. Indeed, if the values are not considered, the general shape of curve remains unchanged. The ground motion amplifies at low PGA values and it attenuates at high PGA values. (1) The attenuation is due to inadequate shear strength of soil. As far as motions having great PGA steps up to the ground surface, the soil yields and the waves cannot transmit, which results in decrease of PGA values.

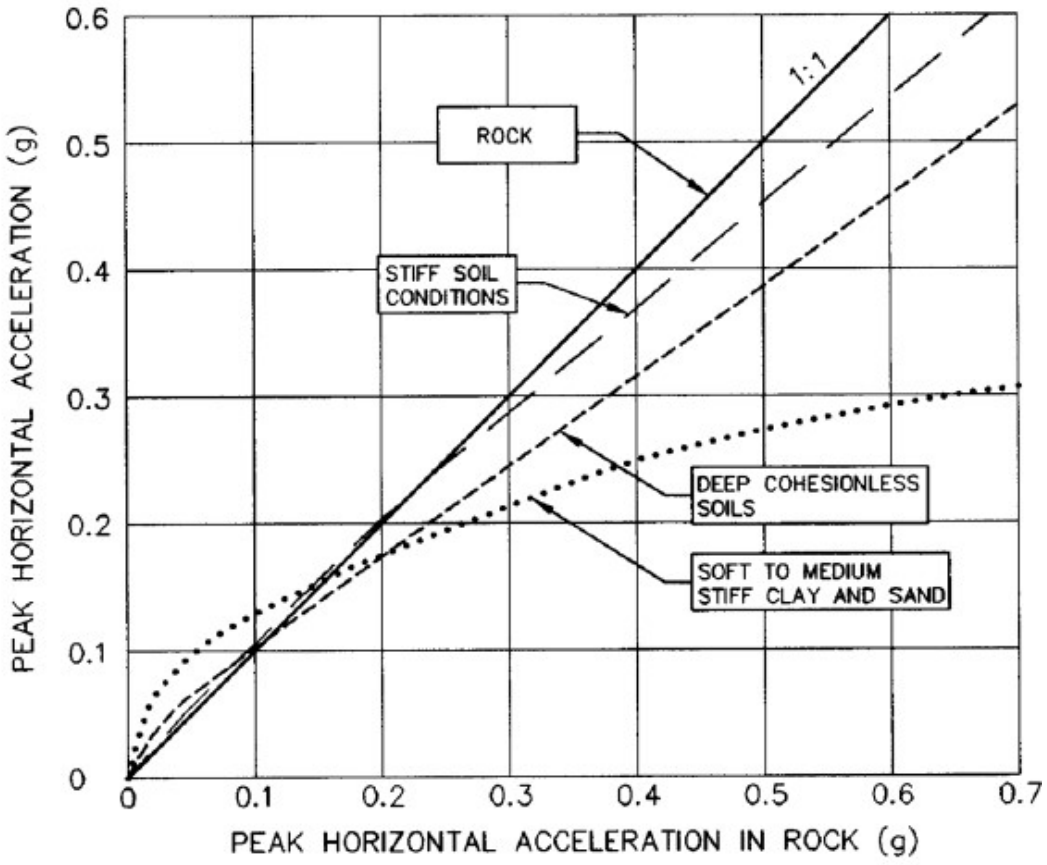

Figure 3.4. Relationship between PGA on rock and on other local soil conditions (After Seed and Idriss, 1982) (1)

Another empirical relation is developed by Idriss (1990) for soft soils. The graph is shown in Figure 3.5. The development of that curve relies on both field observations and results of equivalent linear one-dimensional analysis. The graph represents the PGA amplification for soft soils including Site Class F.

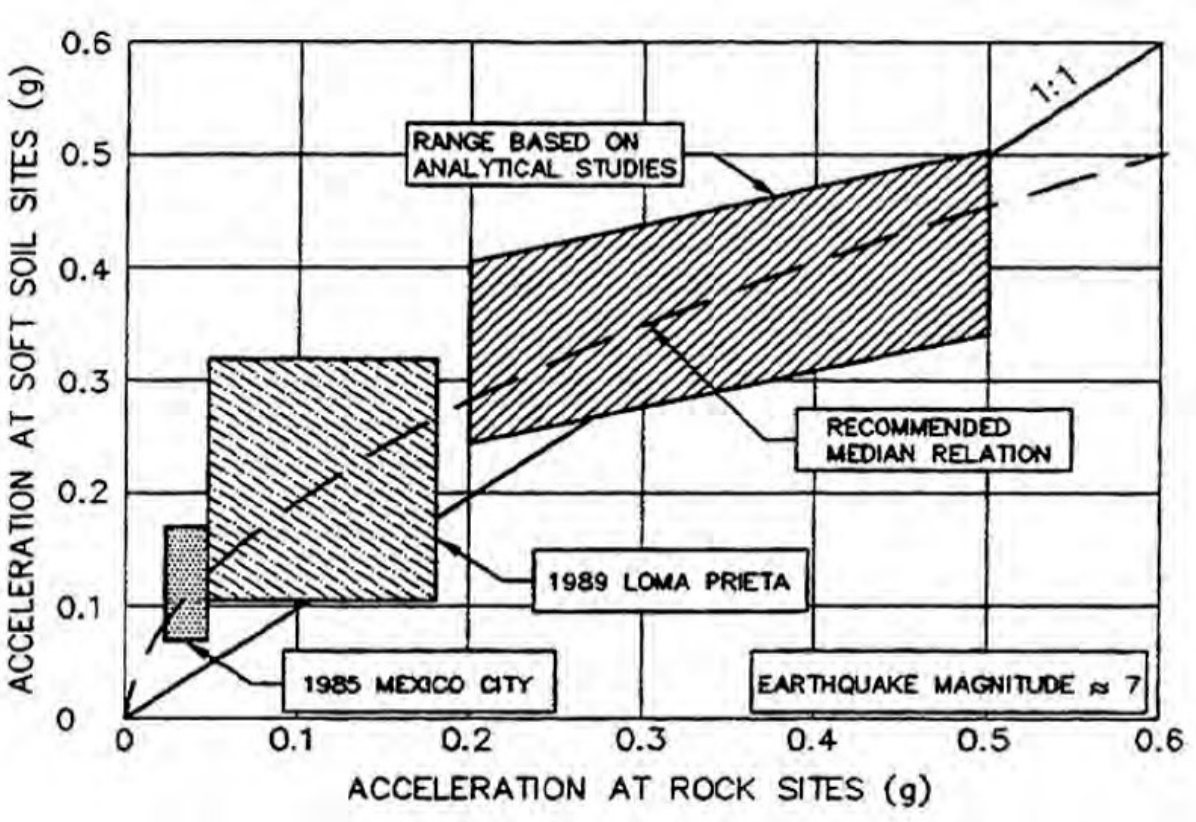

Figure 3.5. Relationship between PHGA on rock and on soft soil sites (Idriss, 1990) (1)

Figure 3.6. is constructed based on observations and recordings at the base and crest of several earthen dams (Harder, 1991). It is understood from the figure that the smaller amplification is expected in the free field surface than in the earthen structures. However, that curve limits the amplification with a boundary curve and the curve is used for transverse acceleration of embankment. That means it is not valid for longitudinal acceleration and for cut slopes. Because it is expected much little amplification than the transverse acceleration.

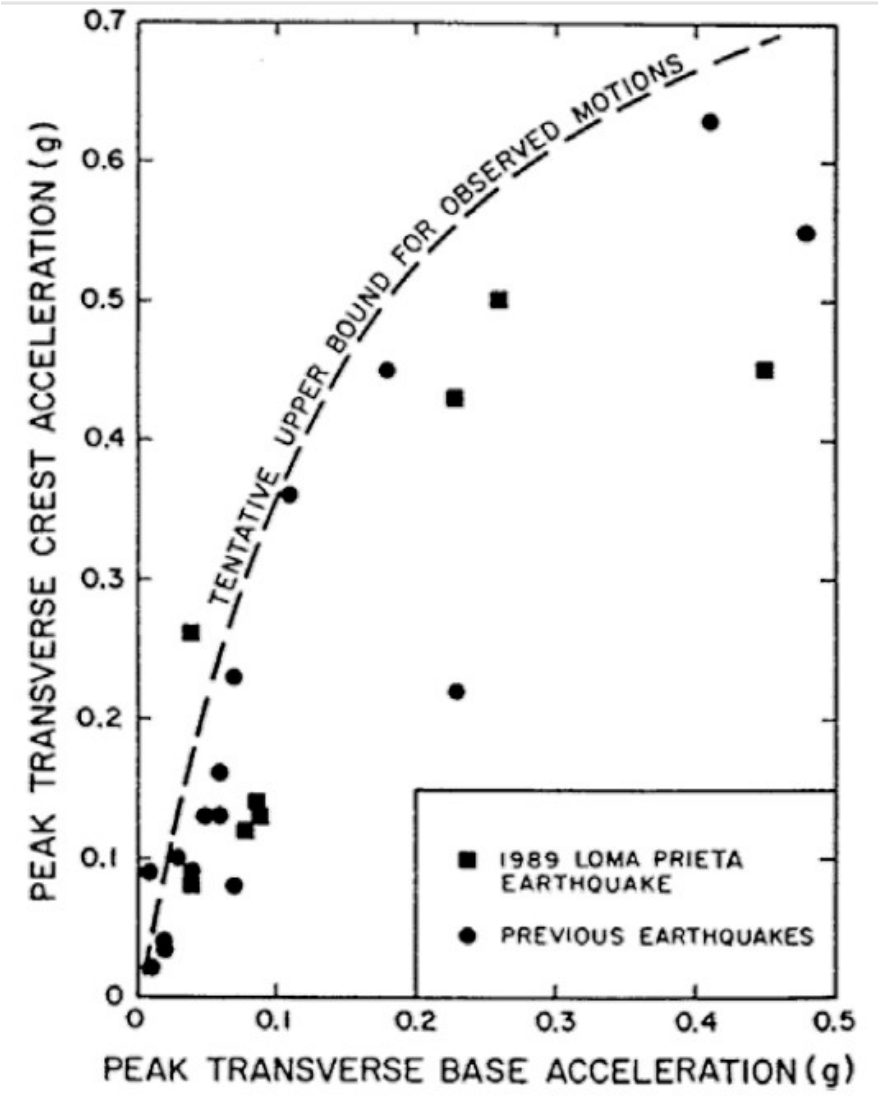

Figure 3.6. Base and crest peak accelerations recorded at the earth dams (1)

3.3. One-Dimensional Site Response Analysis

When earthquake occurs result from rupture of earth crest, waves propagate. The reflect and refract as passing through different geological formations. As they come closer to ground surface, the waves get vertical. Because the shear wave velocity of bottom parts is usually greater than upper sides. The main assumption for one-dimensional analysis, as explained in the previous part, is infinite horizontal uniform layers, which means the soil properties does not change inherently.

Some important definitions are explained to describe ground motions before expressing ground response models. The reference for the terms is the figure below, Figure 3.7. The term *free surface motion* is the motion at the top of the soil, Figure 3.7-a. *Bedrock motion* is called for the one at the bottom of the soil layer or at the top of the rock. A *rock outcropping motion* is the one at which the bedrock exists at surface. (1) Bedrock outcropping motion is the one at the top of the bedrock where there is no soil deposit.

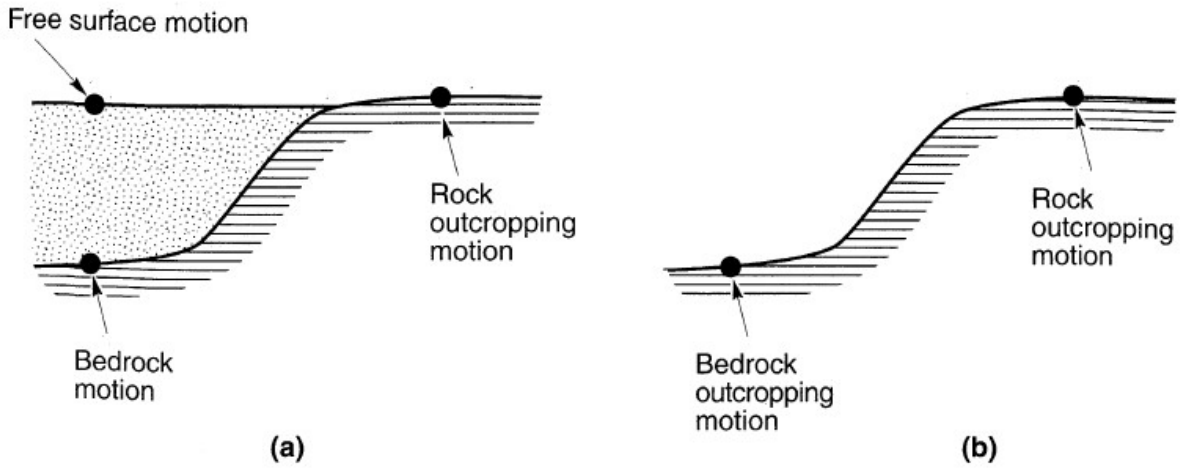

Figure 3.7. Ground response nomenclature: a) soil overlying bedrock, b) no soil overlying bedrock

3.3.1. Linear One-Dimensional Site Response Analysis

In liner approach, transfer functions are used to explain different ground response parameters such as displacement, velocity acceleration, shear stress and shear strain. That method is limited to linear system analysis because it is based on superposition principle. Nonlinear systems are solved by the approximation to linear approach by an iterative procedure.

The representation of earthquake motion of bedrock and ground surface is derived through Fourier Series, which are called Transfer Functions. Thus, the amplification or deamplification of ground motion is represented by transfer functions.

In the following sections, derivation of the transform functions is going to be explained with the simplest to the most complicated functions. The derivation of these functions depends upon the geotechnical boundary conditions. Indeed, the simple transfer functions are not widespread due to lack of capability of illustration of all geotechnical aspects. Complex functions are commonly used for describing of ground response more accurately. Transfer functions are explained for different geotechnical conditions. (3)

3.3.1.1. Uniform Undamped Soil on Rigid Rock. The definition of that function assumes of a rigid bedrock underlying a uniform, isotropic, linear elastic sol layer. The bedrock ground motion generates shear waves that propagates vertically. Then the displacement (horizontal) is described as;

$$u(z,t) = A * e^{i*(\omega t+kz)} + B * e^{i*(\omega t-kz)} \tag{3.3.1}$$

According to the boundary conditions at free surfaces, shear stress and shear strain have to be zero. That means;

$$\tau(0,t) = G * \gamma(0,t) = G * \frac{\partial u(0,t)}{\partial z} = 0 \tag{3.3.2}$$

After substitution of displacement equation and differentiation of that equation, it yields;

$$G * i * k\left(A * e^{ik(0)} - B * e^{-ik(0)}\right) * e^{i\omega t} = G * i * k(A-B) * e^{i\omega t} = 0 \tag{3.3.3}$$

That equation satisfies if A=B. Then displacement equation becomes;

$$u(z,t) = 2 * A * \frac{e^{ikz}+e^{-ikz}}{2} * e^{i\omega t} = 2 * A * coskze^{i\omega t} \tag{3.3.4}$$

That function describes a fixed shape waves with respect to depth, which is called standing wave. That is produced by upward and downward travelling waves. After describing those equations, transfer function is constructed through that displacement function. By choosing max and min value of z, the subbase 1 represents the assumption 1;

$$F_1(\omega) = \frac{u_{max}(0,t)}{u_{max}(H,t)} = \frac{2*A*e^{i\omega t}}{2*A*\cos kHe^{i\omega t}} = \frac{1}{\cos kH} = \frac{1}{\cos(\omega H/v_s)} \quad (3.3.5)$$

The modulus of that transfer function is amplification function which is formulated below:

$$|F_1(\omega)| = \sqrt{Re(F_1(\omega))^2 + Im(F_1(\omega))^2} = \frac{1}{|\cos(\omega H/v_s)|} \quad (3.3.6)$$

According to amplification function, the displacement of the soil is always equal or greater than the displacement of bedrock. Because the denominator is cosine function which is always equal or lower than 1. The graph of amplification function is shown below.

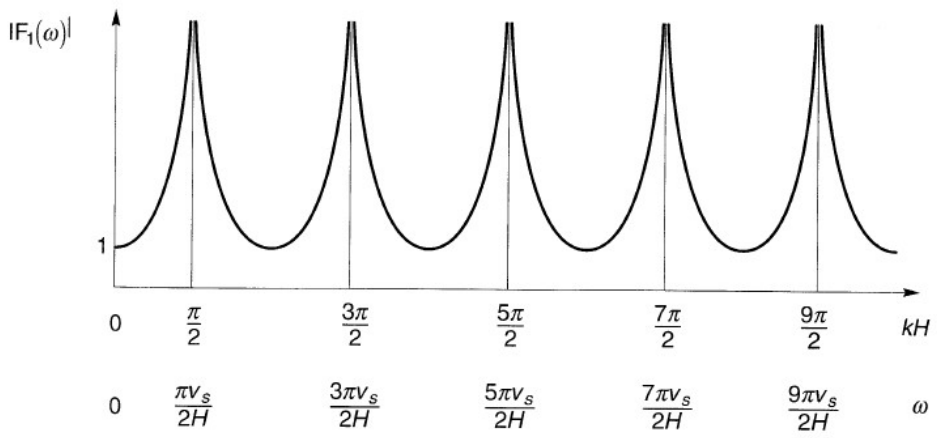

Figure 3.8. Influence of frequency on steady state response of undamped linear elastic layer

3.3.1.2. Uniform Damped Soil on Rigid Rock. Actually, the assumption explained above is physically not possible. Because the that assumption requires no energy loss and no damping. However, there is damping almost in all soils (or rock). Thus, to get more healthy results, the assumption is repeated with damping condition. In that part, the details of all equations are not included, instead the transfer functions, the amplification functions and the graph of amplification function are stated below. The details of the functions can be found from "Geotechnical Earthquake Engineering, Kramer, S.L.". The transfer and amplification functions are shown below, respectively.

$$F_2(\omega) = \frac{1}{\cos k(1-i\xi)H} = \frac{1}{\cos(\omega H/\ _{s}*(1+i\xi))} \tag{3.3.7}$$

$$|F_2(\omega)| = \frac{1}{\sqrt{cos^2(kH)+si\ \ ^2(\xi kH)}} \tag{3.3.8}$$

Since $\sinh^2 y \approx y^2$ for small y;

$$|F_2(\omega)| = \frac{1}{\sqrt{cos^2(kH)+(\xi kH)^2}} = \frac{1}{\sqrt{cos^2(\omega H/v_S)+(\xi(\omega H/v_S)^2}} \tag{3.3.9}$$

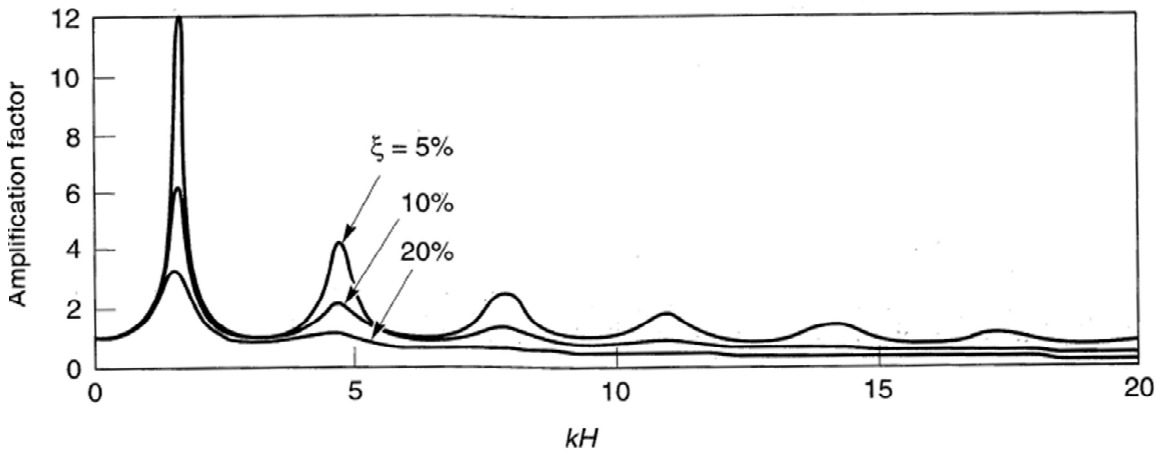

Figure 3.9. Influence of frequency on steady-state response of damped, linear elastic layer

The amplification factor represents the ratio of amplitude of free surface motion to amplitude of bedrock motion. Moreover, the local maximum points are the natural frequency of soil. The first peak point represents the *fundamental frequency* and the period corresponds to that frequency is named as *characteristic site period*. (3)

3.3.1.3. Uniform Damped Soil on Elastic Rock. By this point, the expressions explained are based on the idea of soil overlying rigid bedrock. A rigid base or rigid rock means a fixed boundary for the travelling waves. That means the energy is captured in soil. However, if rock is elastic, not all the waves reflect. Some travels downward in the rock, which means part of energy in the soil dissipates. In that case, the amplitude of the free surface is smaller than the rigid base conditions.

In that part the derivation of transfer and amplification function is skipped too. Like the other conditions, these functions stem from the displacement function of waves and geotechnical boundary conditions. The transfer function, amplification function and the amplification factor graph are put below.

$$F_3(\omega) = \frac{2}{(1+a_z^*)e^{ik_S^*H}+(1-a_z^*)e^{-ik_S^*H}} \tag{3.3.10}$$

By using Euler's law, it can be rewritten as;

$$F_3(\omega) = \frac{1}{\cos k_S^**H+i*a_z^**sink_S^**H} = \frac{1}{\cos(\omega H/v_{SS}^*)+i*a_z^**\sin(\omega H/v_{SS}^*)} \tag{3.3.11}$$

As it can be understood from the expression, very compact form of F3(ω) is not possible. Then the amplification factor is expressed by assuming the damping as zero.

$$|F_3(\omega, \xi = 0)| = \frac{1}{\sqrt{cos^2(k_SH)+a_z^2sin^2(k_SH)}} \tag{3.3.12}$$

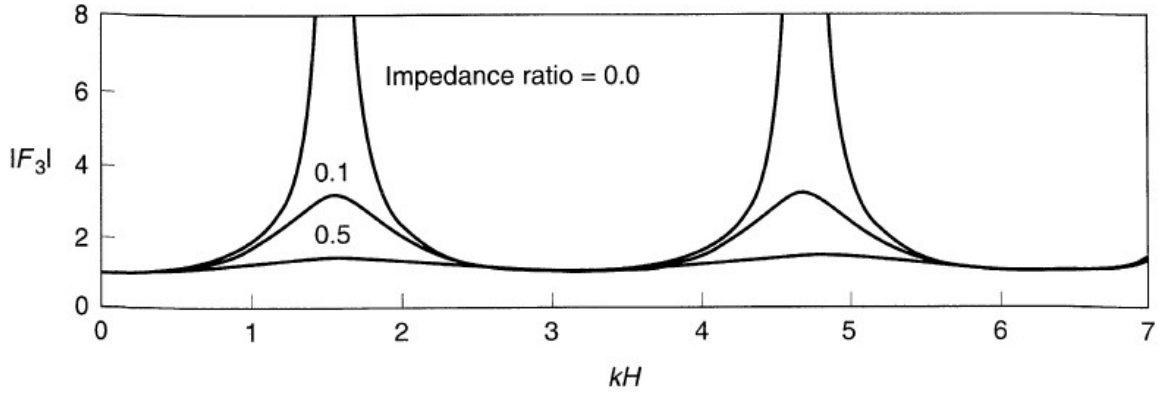

Figure 3.10. Effect of impedance ratio on amplification factor for case of undamped soil

3.3.1.4. Layered Damped Soil on Elastic Rock. The case above is very useful to understand the behavior of soil and rock. However, it is not suitable for many cases. Because the soil is not uniform most of the times, instead it is layered with different properties of materials. In such a case, a layered damped soil condition must be taken into consideration.

In layered soil conditions the displacement at two points must be equal which are the bottom of overlying soil and top of underlying soil. Then if the displacement equation is written according to the Figure 3.11, it yields

$$u_m(Z_m = 0, t) = (A_m + B_m) * e^{i\omega t} \tag{3.3.13}$$

$$u_m(Z_m = h_m, t) = \left(A_m * e^{ik_m^* h_m} + B_m * e^{-ik_m^* h_m}\right) * e^{i\omega t} \tag{3.3.14}$$

After appliying the boundary conditions of layer m and layer m+1, the equations becomes

$$u_m(Z_m = h_m, t) = u_{m+1}(Z_{m+1} = 0, t) \tag{3.3.15}$$

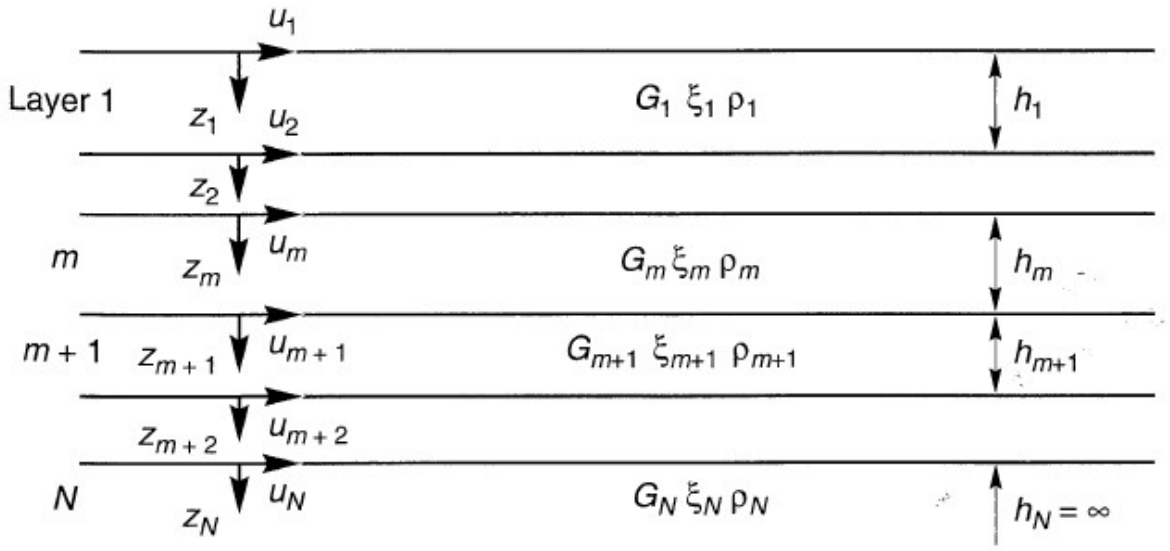

Figure 3.11. Case showing for layered soil deposit

Transfer function is derived by considering the shear stress compatibility conditions with shear strain, which means, like displacement, shear stress at those two points must be equal too. After skipping the details of derivation, transfer function relating the motion of I layer to the j layer is given as;

$$F_{ij}(\omega) = \frac{|u_i|}{|u_j|} = \frac{a_i(\omega)+b_i(\omega)}{a_j(\omega)+b_j(\omega)} \quad (3.3.16)$$

According to the equation, if any motion in any layer is konown then the function for other layer can be found.

3.3.2. Equivalent Linear Approximation of Nonlinear Response

It is obvious that the soil behavior is not linear all the time. Thus, some approximation must be performed to estimate the soil problems in an easy and practical way. The equivalent linear properties assist to approximate the real nonlinear behavior of soil. The equivalent linear soil properties are equivalent linear shear modulus, G, which is usually assumed as secant modulus, and equivalent linear damping ratio, $\boldsymbol{\xi}$.

As the heading implies, the method itself is linear. Therefore, it requires constant parameters of damping and shear modulus. The aim is to liken the time history record to a laboratory-produced motion with same peak values as in the Figure 3.12. The cyclic effect of two waves are not same in terms of shear stress and shear strain, the laboratory-induced motion would create disastrous results due to many numbers of peaks. Then it is a need to describe a strain level for earthquake motion in terms of effective shear strain, which generally remains between 50-70% of peak strain. Moreover, it is generally assumed as 65%. (3)

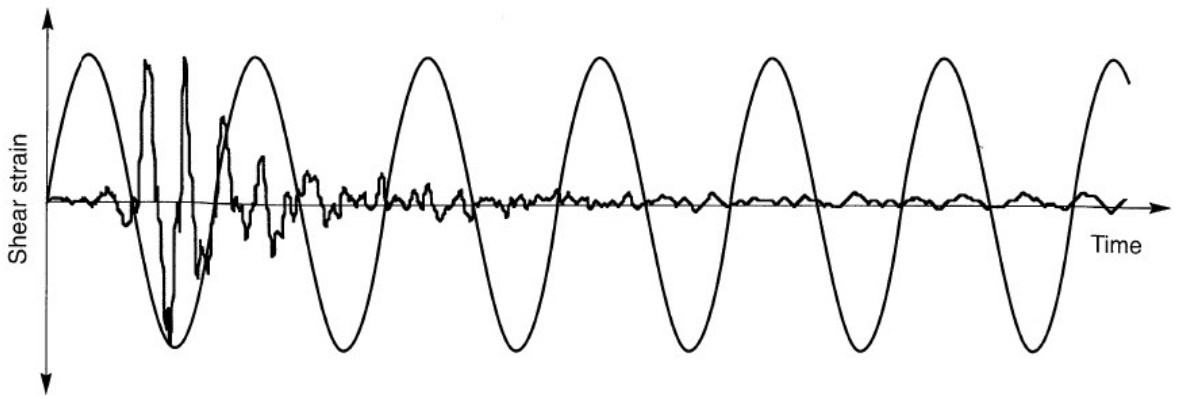

Figure 3.12. Harmonic (laboratory) motion and earthquake motion

As it is stated previously that method requires equivalent linear parameters. Therefore, an iterative procedure is required to understand the compatibility of these linear properties and computed strain level. (3) The procedure, which is depicted on Figure 3.13, is as following;

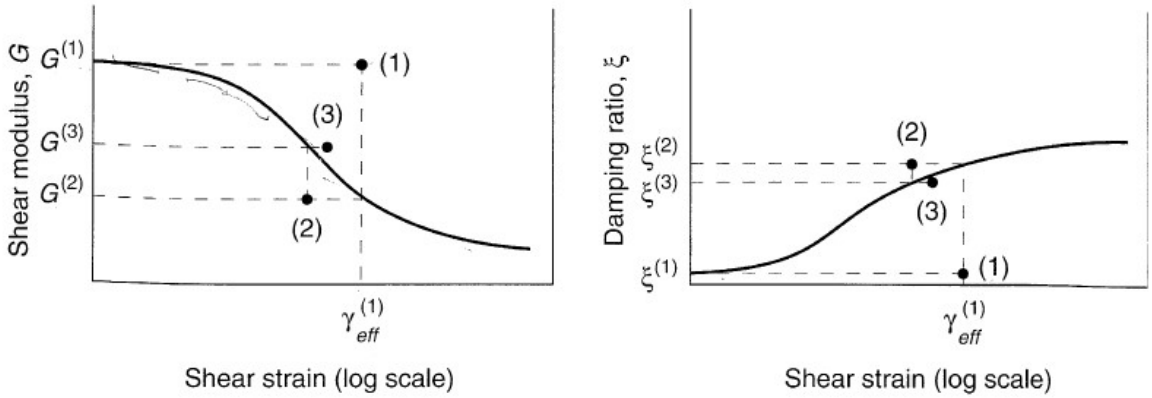

Figure 3.13. Iteration of shear modulus and damping ratio in equivalent linear approximation method

a) Estimate G and $\boldsymbol{\xi}$ for each layer
b) Compute ground response for each layer including time histories of shear strain
c) As mentioned before, the effective shear stain is related to maximum shear strain.

The relation can be formulized as below:

$$\gamma_{eff\,j}^{(i)} = R_\gamma * \gamma_{\max j}^{(i)} \tag{3.3.17}$$

Where j represents the layer name, i is the iteration number and R_x is the ratio of effective shear strain to max shear strain. That ratio is dependent to earthquake magnitude (Idriss and Sun, 1992).

$$R_\gamma = \frac{M-1}{10} \tag{3.3.18}$$

d) New damping ($\xi^{(i+1)}$) and shear modulus values ($G^{(i+1)}$) are determined for next iteration through effective shear strain.
e) Step b to d is repeated until the differences between computed parameters for successive two iterations fall below approximately 5% to 10%.

Although that method provides to understand nonlinear behavior of soil, it is still a linear method. The parameters are assumed constant during the earthquake. That results in incapability of describing soil properties during earthquake.

3.4. Advanced (Non-Linear) One-Dimensional Site Response Analysis

Another method is advanced (nonlinear) one-dimensional analysis. That method is based on direct integration in time domain. Any models can be used through integration of the motion equation in very small increments. Since that integration by hand is very complex, computer programs are used with different stress-strain models such as, Martin-Davidenkov model, Iwan-type model, hyperbolic model etc. In the table below, there are some basic programs and models that are used in non-linear one-dimensional analysis. There are a variety of techniques for direct integration, however finite difference is the easiest to be explained.

Table 3.4. Computer programs and soil models for nonlinear one-dimensional analysis (1)

Program	**Soil Model**	**Reference**
CHARSOIL	Ramberg-Osgood	Streeter et al. (1973)
DESRA-2	Hyperbolic	Lee and Finn (1978)
DYNAID	Nested yield surface	Prevost (1989)
MASH	Martin-Davidenkov	Martin and Seed (1978)
NONLI3	Iwan-type	Joyner (1977)
TESSI	HDCP	Pyke (1985)

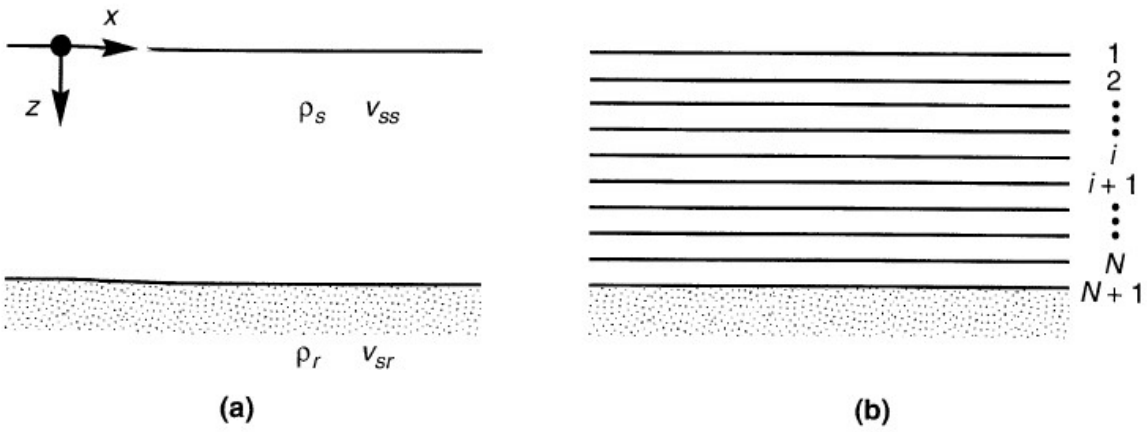

Figure 3.14. a) infinite lateral soil deposit overlying bedrock, b) discretization of soil into sublayers (3)

Referring to the Figure 3.14, the soil response to a bedrock motion can be expressed as;

$$\frac{\partial \tau}{\partial z} = \rho * \frac{\partial^2 u}{\partial t^2} \tag{3.4.1}$$

The idea of finite-difference method is based on the Figure 3.15. To understand the method, that f(x) function must be considered first. The first derivative of f(x) at x=$\tilde{x}$ is given below;

$$\frac{df(\tilde{x})}{dx} = \lim_{\Delta x \to 0} \frac{f(\tilde{x}+\Delta x) - f(\tilde{x})}{\Delta x} \tag{3.4.2}$$

Then since the soil is discretized into sublayers of thickness Δz, the derivative in time domain of very small increments of length Δt for shear stress and velocity of wave is given by

$$\frac{\partial \tau}{\partial z} \approx \frac{\tau_{i+1,t} - \tau_{i,t}}{\Delta z} \tag{3.4.3}$$

$$\frac{\partial \dot{u}}{\partial t} \approx \frac{\dot{u}_{i+1,t} - \dot{u}_{i,t}}{\Delta t} \tag{3.4.4}$$

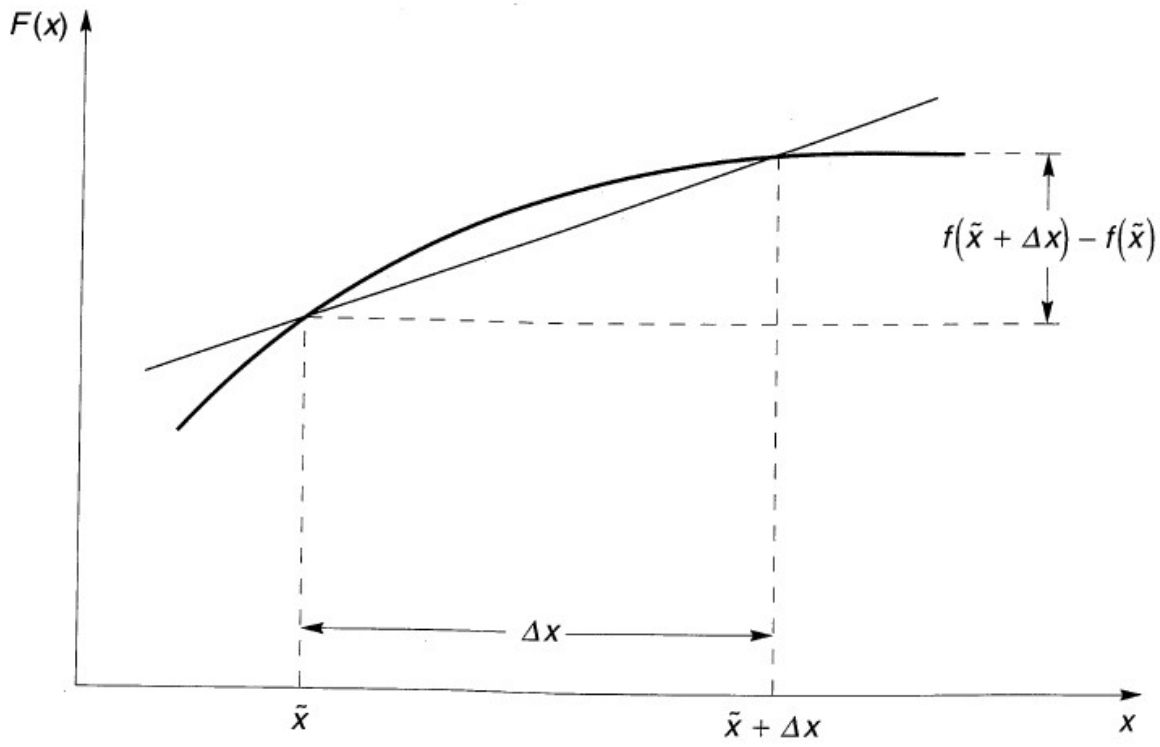

Figure 3.15. Forward difference approximation of f(x) (3)

The detail of equations is not present here. After proceeding the equations from bottom to the top the incremental displacement in each time step and shear strain in each layer is given by the formulas below:

$$\Delta u_{i,t} = \dot{u}_{i,t} * \Delta t \tag{3.4.5}$$

$$\gamma_{i,t} = \frac{\partial u_{i,t}}{\partial z} \approx \frac{u_{i+1,t} - u_{i,t}}{\Delta z} \tag{3.4.6}$$

The current shear strain resulting from shear stress is used if the soil is linear elastic. However, if its nonlinear shear stress is determined from stress path. Then the integration process is as following; (3)

a) The total displacement and velocity for each layer are known at the beginning of each time step.
b) The shear stain in each layer is determine though the displacement profile.

c) Shear stress is determined by stress path.
d) The motion at each time increment is determined by input motion.
e) Then the motion for next time increment is calculated from bottom to the top. Then these 4 steps are repeated for all time increments.

All in all, by that point one dimensional site response analysis techniques are explained. However, the main idea is to understand the assumptions underlying these techniques, main operation system and understanding their limitation of use. Because as it is expressed previously the calculation methods and assumptions are different. Therefore, the techniques give different results. The point is to choose the correct one. In that way, the designer/engineer must take the points below into consideration.

Equivalent linear analyses may result in artificial resonances due to inherent linearity. However, the shear strength of an actual nonlinear soil may change, throughout the earthquake, which prevents the high amplification to occur. Moreover, equivalent analysis is getting more practical as the characterization of motion gets more accurate. However nonlinear analysis may allow more detailed properties than equivalent linear analysis. Nonlinear analyses give more detailed results by more detailed parameters, but that may require a substantial laboratory or field testing. Degree of nonlinearity is the biggest factor that creates difference between equivalent linear and nonlinear site response analysis. İf the strain level is low, then both methods may give similar results, but if the strain level is high, then nonlinear analyses probably give more reasonable results.

3.5. Two- and Three-Dimensional Site Response Analysis

One-dimensional analyses are widespread among geotechnical earthquake engineering. However, there may be some conditions where two- or three-dimensional analyses are required. These conditions may be irregular geometry of the stratigraphy or irregular geometry of the project. In time, by the development of commercial finite element programs, two-dimensional analyses get wider too, but three-dimensional analyses are still rarely used.

The quasi-two-dimensional analyses are the most accustomed sort of two-dimensional analyses. Indeed, the main procedure behind that idea is one-dimensional analysis. Because it is modeled by using one dimensional analysis, especially with an equivalent linear model. Generally, one-dimensional analysis results within 5 to 10% accuracy with the two-dimensional analysis, which is enough for most of the engineering facilities. However, for a more detailed analysis finite element software may be used to search for soil-structure interaction.

Just as one-dimensional analysis, there are different type of solutions for two-dimensional analysis too. Some of which are Dynamic Finite Element Analysis, Equivalent Linear Approach and Nonlinear Approach. The use of these methods depends on the underlying assumptions and calculation methods.

4. ANALYSIS AND RESULTS

In that study, it is aimed to determine the effect of piled soil improvement to understand whether soil improvement change the natural soil class. In that purpose, seven-time history records were selected and scaled by Seismosignal software (30) and dynamic analyses were performed via Plaxis software (31). The project description, selection and scaling procedure, material properties that are used in Plaxis and the finite element model itself are explained within details in the following headings.

Indeed, the soil-pile-structure interaction analysis under earthquake loading is a very difficult process for design engineers due to the complexity of the interaction within soil. In this study, as specified in the Turkish Earthquake Code (2), seven records are selected, and analyses are performed. For each record, three models are created namely initial(natural) condition, raft foundation condition and piled foundation condition. In the results, peak spectral accelerations of each model and amplification factors are compared to check whether there is any shift in the periods and to see the PGA variation while the wave propagates through soil.

4.1. Project Description

Three models are created as shown in the Figure 4.1, Figure 4.2, Figure 4.3. In the Figure 4.1, initial(natural) condition is modelled at which there is no structure. In the second model, which is shown in Figure 4.2, the raft foundation is created at which a 50 cm-depth foundation and to represent a 7-story building, 100 kPa of surcharge over foundation are assumed. For the third model, shown in Figure 4.3 and which is the most important part of the study, a pile foundation is modelled. Like the raft foundation model, a 50 cm-depth foundation and 100 kPa of surcharge over foundation are assumed. For each model last phase is performed as dynamic analysis. For each model, six points are selected for comparison of results which are depicted in Figure 4.4. The coordinates of each point are given in the parentheses. The details of each model and the materials used in models are explained in next heading.

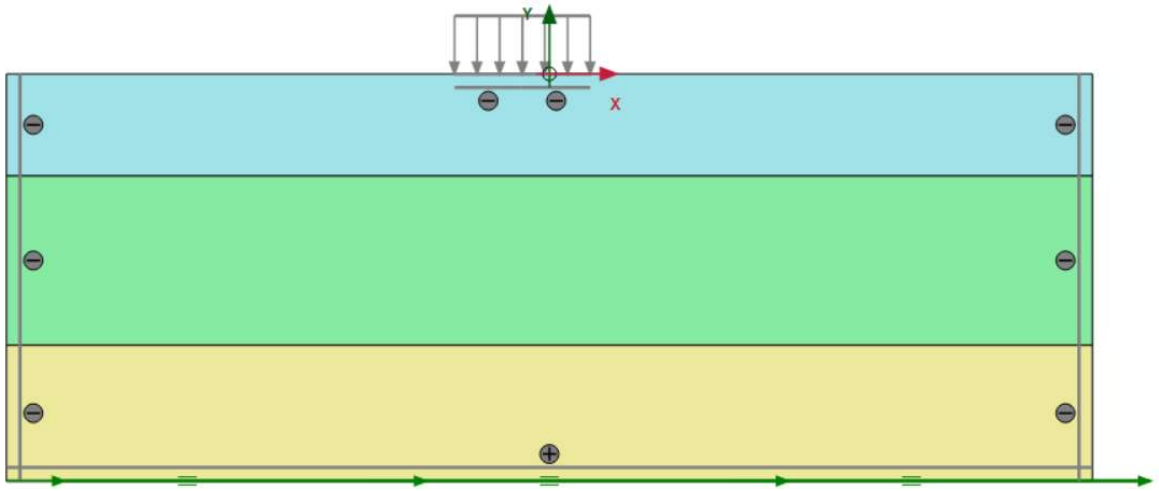

Figure 4.1. Model representing initial condition

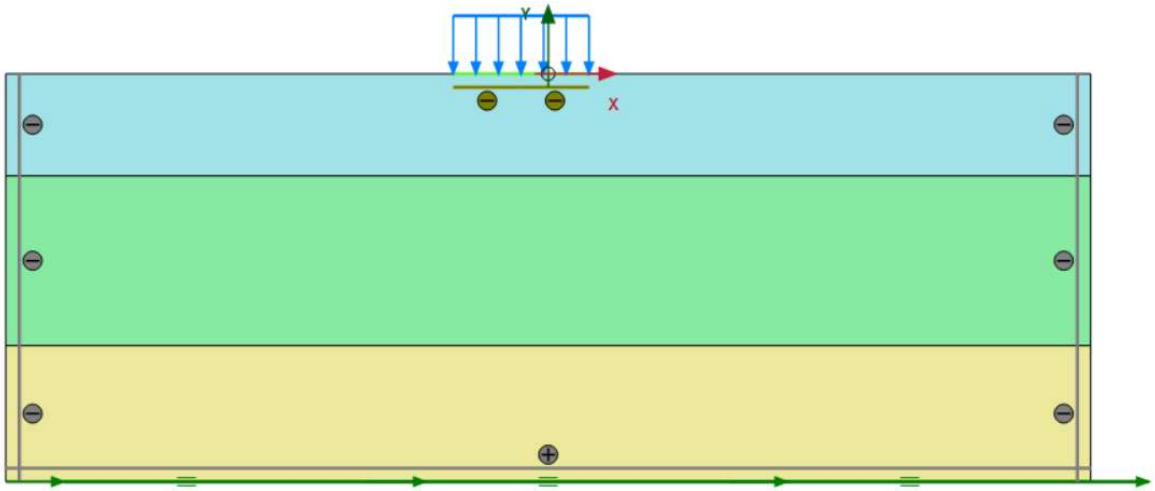

Figure 4.2. Model representing raft foundation condition

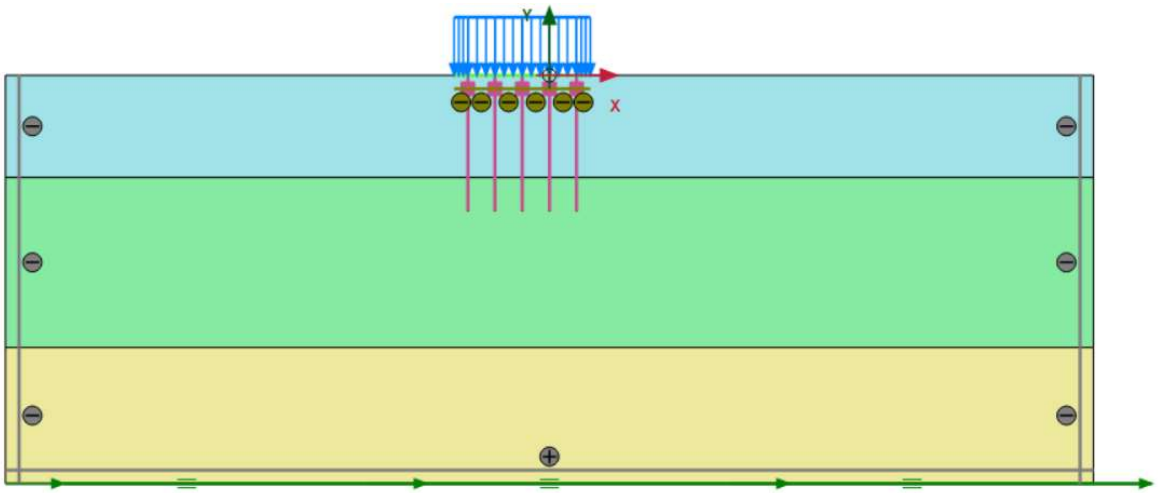

Figure 4.3. Model representing deep foundation condition

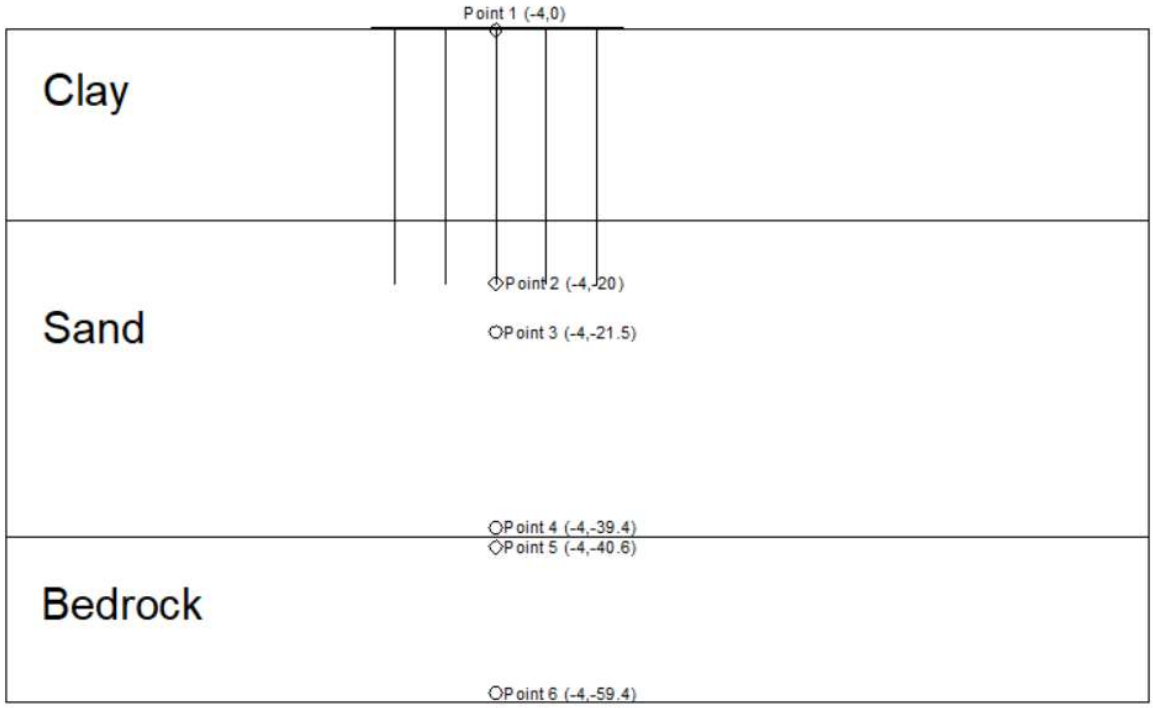

Figure 4.4. Comparison points

4.2. Project Model

The soil-pile-structure interaction is investigated by plane-strain finite element model of Plaxis 2D 2019 Dynamic module. Plaxis is a finite element software which can take the different aspects into consideration in geotechnical earthquake engineering such as elastic and elasto-plastic soil behavior, dynamic loading and earthquake loading conditions, anisotropic soil behaviors, drainage conditions, time-dependent behavior of soils etc. It has a user-friendly interface. Stress-strain of soils can be investigated through quadratic 6-node and 4^{th} order 15-node triangular elements.

For representing the effect of wave propagation, dynamic boundary conditions are used in software. For the bottom side, *Compliant base boundary condition* is applied which consist of prescribed displacement and viscous boundary. The prescribed displacement is transferred into load history. The combination of viscous boundary and load history allows for input of earthquake motion while still absorbing energy. For lateral boundaries, *free-field boundary condition* is used. That condition simulates the wave propagation in the far field with minimum reflection.

The mechanical behavior of soil is characterized by HS Small model. The piles are modelled as embedded beam row. The properties of soil model, plate element and embedded beam row element is described in part 4.2.1, part 4.2.2 and part 4.2.3. The generated meshes of each model are shown in the figures below. The parameters are presented in Table 4.1, Table 4.2 and Table 4.3.

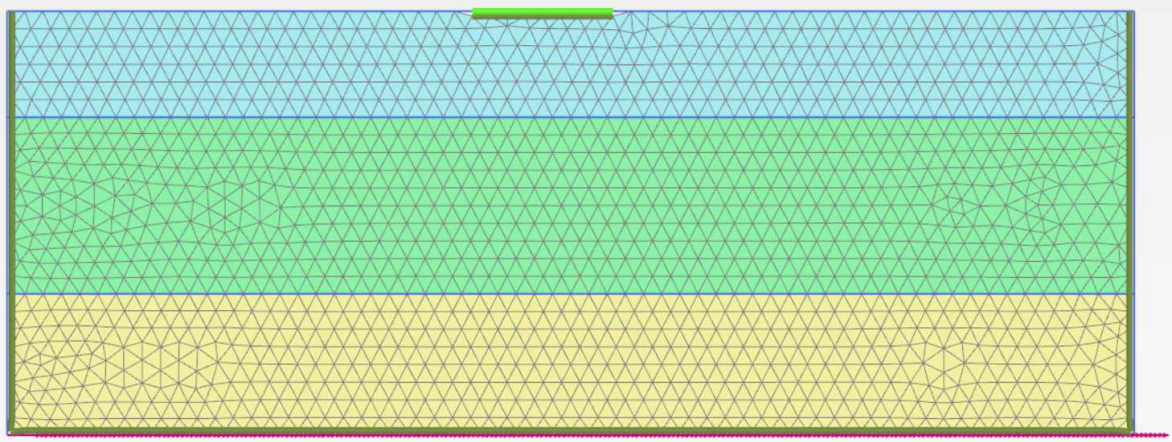

Figure 4.5. Mesh of initial condition

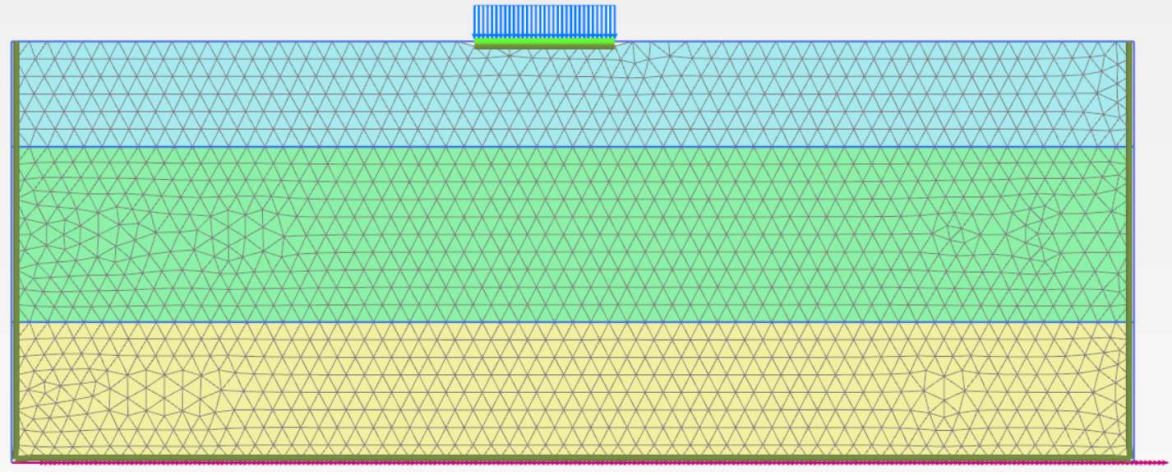

Figure 4.6. Mesh of raft foundation condition

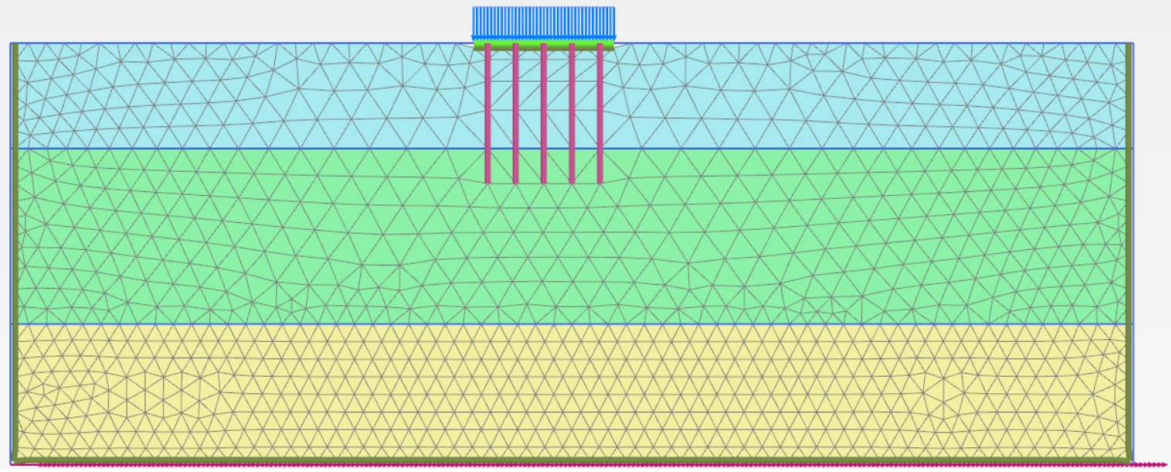

Figure 4.7. Mesh of deep foundation condition

Table 4.1. Soil properties

0-15m	**15-40m**	**40-60m**
Clay	**Sand**	**Bedrock**
HS Small	**HS Small**	**Linear Elastic**
Drained	Drained	Drained
γ_{unsat} (kN/m^3)	**γ_{unsat} (kN/m^3)**	**γ_{unsat} (kN/m^3)**
17	19	24
γ_{sat} (kN/m^3)	**γ_{sat} (kN/m^3)**	**γ_{sat} (kN/m^3)**
18	20	25
E_{50}^{ref} (kN/m^2)	**E_{50}^{ref} (kN/m^2)**	**E (kN/m^2)**
20000	50000	3400000
E_{oed}^{ref} (kN/m^2)	**E_{oed}^{ref} (kN/m^2)**	**E_{oed}^{ref} (kN/m^2)**
20000	50000	3800000
E_{ur}^{ref} (kN/m^2)	**E_{ur}^{ref} (kN/m^2)**	**E_{ur}^{ref} (kN/m^2)**
60000	150000	-
c' (kN/m^2)	**c' (kN/m^2)**	**V_s(m/s)**
10	5	760
Ø' (phi)^o	**Ø' (phi)^o**	**V_p(m/s)**
26	28	1241
Ψ (psi)^o	**Ψ (psi)^o**	**Ψ (psi)^o**
0	0	-
G_0^{ref}(kN/m^2)	**G_0^{ref}(kN/m^2)**	**G (kN/m^2)**
270000	100000	1400000
$\gamma_{0.7}$	**$\gamma_{0.7}$**	**$\gamma_{0.7}$**
0.00012	0.00015	-

Table 4.2. Plate element properties

Parameter	Name	Foundation	Unit
Material Type	Type	Elastic;Isotropic	-
Normal Stiffness	EA	1.20E+07	kN/m
Flexural Rigidity	EI	1.60E+05	$kN.m^2/m$
Weight	w	20	kN/m/m
Poisson's Ratio	ν	0.15	-

Table 4.3. Embedded beam row element parameters

Parameter	Name	Ø120 Pile	Unit
Material Type	Type	Elastic	-
Stiffness	E	1.13E+07	$kN.m^2$
Unit Weight	γ	25	kN/m^3
Beam Type	Type	Predefined	-
Predefined Beam Type	Type	Massive Circular Beam	-
Diameter	D	1.2	m
Pile Spacing	$L_{spacing}$	3	m
Skin Resistance	T_{skin}	300	kN/m
Base Resistance	F_{max}	350	kN/m
Interface Stiffness Factor	-	Default Values	-

4.2.1. HS Small Model (Hardening Soil Model with Small-Strain Stiffness)

Hardening Soil with Small Strain Model is defined to deal with the high stiffness problem of soils while there is very small strain level in the material. The original Hardening Soil Model overpassed the very small strain in the reloading-unloading procedure. For both models, all parameters are same, however two more parameters are needed for HS Small model, namely shear modulus at very small strains, G_0^{ref} and threshold shear strain, $\gamma_{0.7}$. The number 0.7 represents the shear strain level where, G_s, secant shear modulus decreases about 70% of G_o. The strain level that can be measured near the geotechnical structures or can be applied for laboratory test is given in the Figure 4.8. with characteristic stiffness reduction curve.

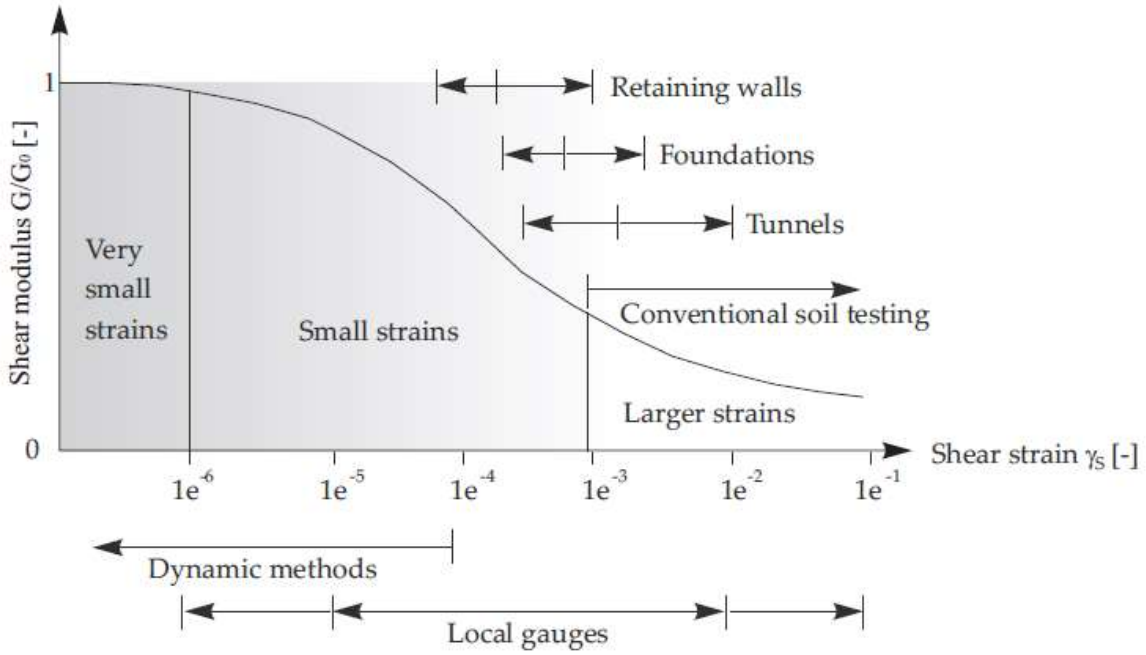

Figure 4.8. Characteristic stiffness-strain behavior of soil with typical strain ranges for laboratory tests and structures (after Atkinson & Sallfors (1991)) (31)

Since poisson's ratio, μ_{ur} is assumed as constant, the reference shear modulus is calculated as below:

$$G_0^{ref} = \frac{E_0^{ref}}{2 * (1 + \mu_{ur})}$$

The $\gamma_{0.7}$ value is the shear strain where secant shear modulus decreased to $0.722G_0^{ref}$. That parameter is used for virgin (initial) loading. The model stiffness parameters are shown in Figure 4.9. in a drained triaxial test and they are shown in Figure 4.10. in a cyclic shear test.

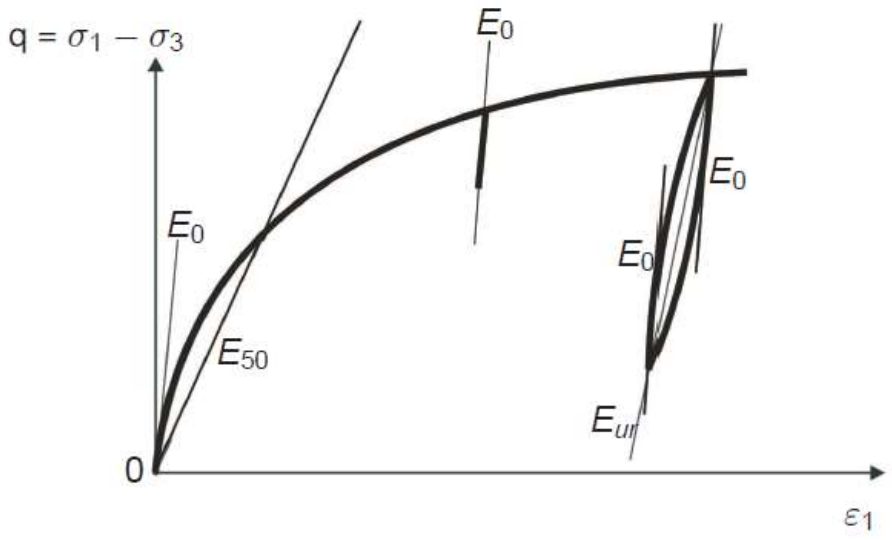

Figure 4.9. HS Small model stiffness parameters in a triaxial test

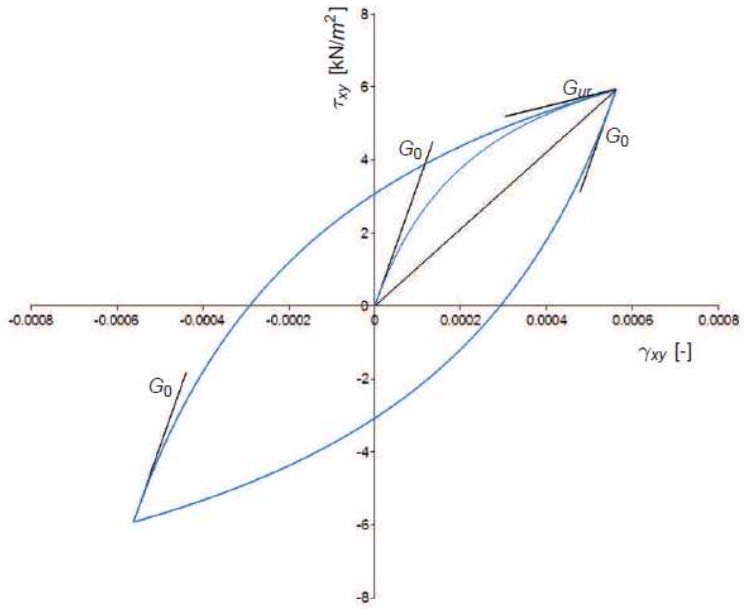

Figure 4.10. HS Small model stiffness parameters in a cyclic shear test

4.2.2. Plate

Plate elements are 3-node or 5-node elements with flexural rigidity and normal stiffness. These elements have three degrees of freedom per node, namely two translational and one rotational. The coordinate system of plate elements is;

One axial displacement (u_x*)

One transverse displacement (u_y*)

One rotation (ϕ_z)

The plate element is integrated over its length by 2-point Gaussian (also known as Euler-Poisson integration) for 3-node elements and 4-point Gaussian integral for 5-node elements. And it is integrated over its height by 2-point Gaussian integration method.

4.2.3. Embedded Beam Row

Embedded beam row element, which is created for embedded piles based on embedded beam approach in Plaxis, consists of beam elements for pile itself and interface element at the surface and tip to for representing the interaction between soil and pile. The beam element allows for deflections resulting from shear or bending. Moreover, the embedded beam row elements cope with out-of-plane direction in contrast to plate elements, which means the mesh is not just 2D, it is also 3D mesh. That property of element is succeeded by a special out-of-plane mesh system. The strength of that interface should be determined by considering load transfer between soil and pile.

4.3. Selection and Scaling of Time-History Records

The selection and scaling are processed according to Turkish Earthquake Code 2019. By this process, at first design acceleration spectrum is constructed for D soil class. The details of procedure of constructing design spectrum are explained in chapter 3. The spectrum is constructed through the https://tdth.afad.gov.tr/ (accessed in April 2019) website shown in Figure 4.11. (29) The site is chosen so that it is an earthquake-vulnerable place on North Anatolian Fault. The properties and location of place are presented in the figure and table below.

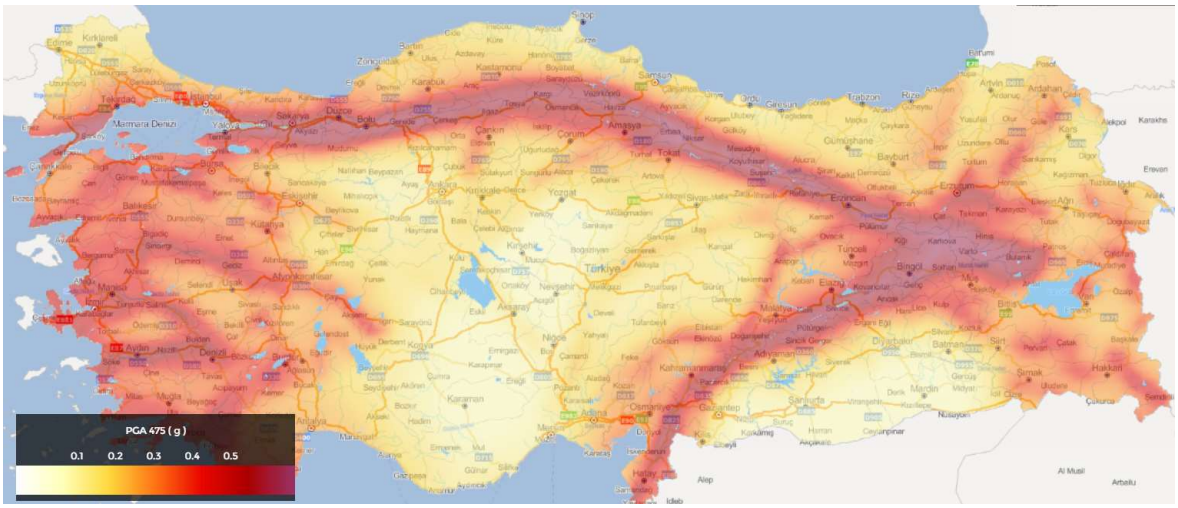

Figure 4.11. Turkish Seismic Hazard Map

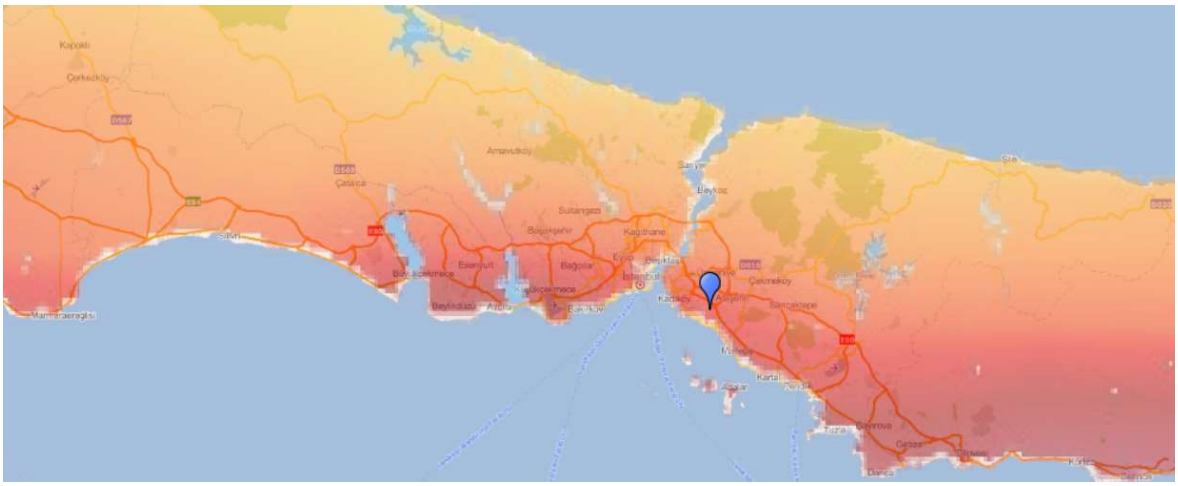

Figure 4.12. Location of studied place

Table 4.4. Properties of studied place

PGA	0.457
S_s	1.19
S_1	0.58
Earthquake Design Class	DD-2
S_{DS}	1.219
S_{D1}	0.998

After construction of design acceleration spectrum, by using "*https://ngawest2.berkeley.edu/"* website (28), related time-history records are found. The

peer search interface is shown in the Figure 4.13. below. The search parameters are chosen so that they represent the earthquakes occurred on North Anatolian Fault. Thus, the fault type is chosen as strike slip. Since epicentral distance of most of the earthquakes in Turkey are not deep, so the R_{jb} value is put as 0,10 meaning the depth of earthquake is between 0 to 10 km. Moreover, the records on outcrop is chosen, so shear wave velocity is selected as 700 m/s to 2000 m/s. And the earthquakes having great magnitudes (between 6 to 10) are chosen. The periods are selected to be within $0.2T_n$ and $1.5T_n$ where T_n is the natural period of the soil. T_n is determined based on one-dimensional analysis of specified area. The analysis is performed by Deepsoil v7.1 Software which is provided by Illinois University. The result is shown in Figure 4.14. After determining natural period, the design spectrum is constructed which is given in Figure 4.15. The summary of earthquake records found based on design spectrum is given in Table 4.5. The detailed properties of each record are presented in chapter 4.4.

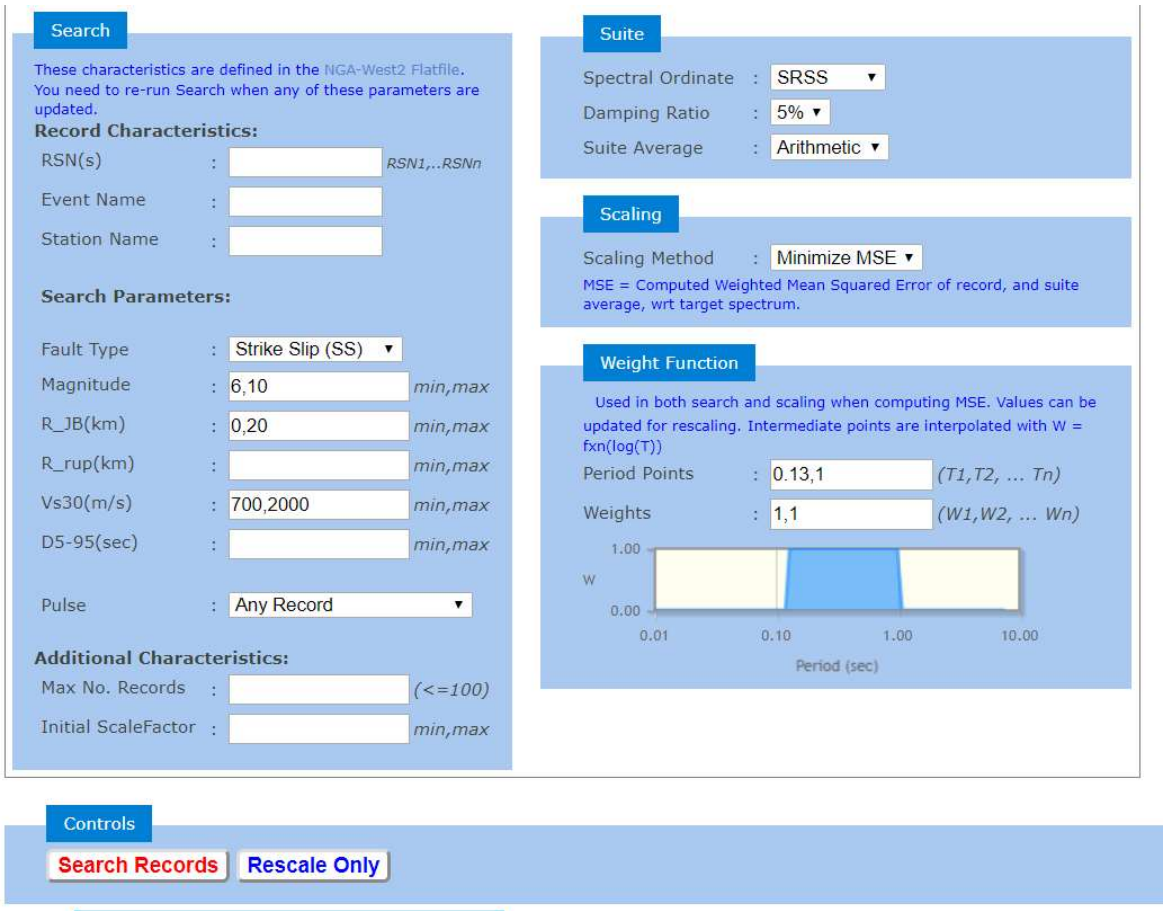

Figure 4.13. Peer Search Interface

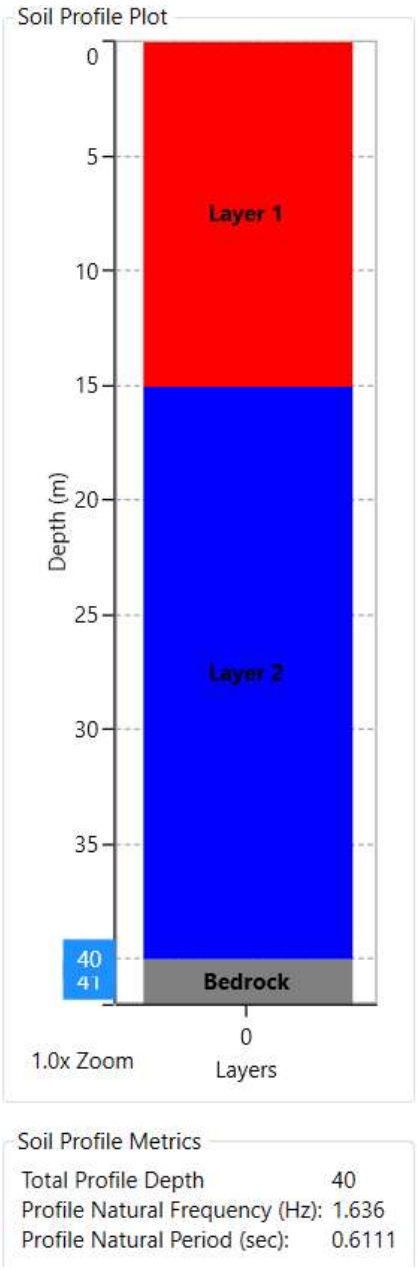

Figure 4.14. Deepsoil analysis result

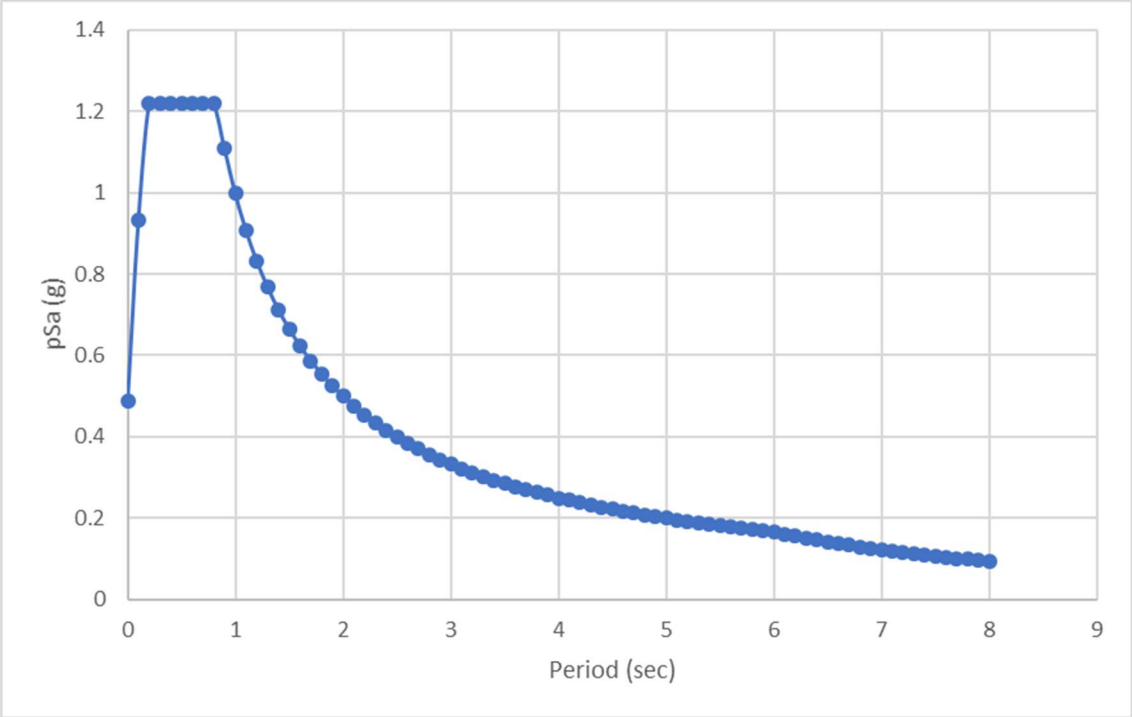

Figure 4.15. Design Spectrum

Table 4.5. Summary of earthquake records

Result ID	Mean Squared Error	Scale Factor	Earthquake Name	Year	Station Name	Magnitude	Mechanism	Rjb (km)	Rrup (km)	Vs30 (m/sec)
1	0.2021	1.0318	"Landers"	1992	"Lucerne"	7.28	strike slip	2.19	2.19	1369
2	0.0351	1.4157	"Kobe_ Japan"	1995	"Kobe University"	6.9	strike slip	0.9	0.92	1043
3	0.0595	2.1176	"Kocaeli_ Turkey"	1999	"Gebze"	7.51	strike slip	7.57	10.92	792
4	0.1103	1.834	"Kocaeli_ Turkey"	1999	"Izmit"	7.51	strike slip	3.62	7.21	811
5	0.0992	1.3454	"Hector Mine"	1999	"Hector"	7.13	strike slip	10.35	11.66	726
6	0.4642	2.162	"Tottori_ Japan"	2000	"SMNH10"	6.61	strike slip	15.58	15.59	967.27
7	0.8753	0.7087	"Duzce_ Turkey"	1999	"IRIGM 496"	7.14	strike slip	4.21	4.21	760

After selection of earthquakes scaling of earthquakes is a very important phenomenon too. One of the substantial things in dynamic analysis is the appropriateness of the records to the design spectrum. For that purpose, the records are spectrally matched, at which spectrum is assimilated to the design spectrum by scaling both in time domain and frequency domain, or scaled, at which the amplitude of all record is scaled to make similar spectrum. In this study second method is used, scaling. The scale values are determined according to peer search interface. The values are given in Table 4.5. Each acceleration value is scaled by that specified scale factor. The graph of both scaled and unscaled values of each time-history record is given in the chapter 4.4. The scaling, baseline correction and filtering of records

are carried out by Seismosignal software. Baseline correction is applied for avoiding linear errors. It is necessary to meet the spectrum fit requirements. Filtering is applied to exclude undesirable noise effect from acceleration record. Both low pass and high pass filtering are applied.

4.4. Properties of Selected Earthquake Records

The records are selected from Landers, Kobe, Kocaeli (Gebze and Izmit stations), Hector Mine, Tottori and Duzce earthquakes as given in Table 4.5. The detailed properties of each record are given in Table 4.6.

Table 4.6. Earthquake records' properties

ID	Earthquake Name	Station Name	PGA-Unscaled (g)	PGA-Scaled-Uncorrected (g)	PGA-Scaled-Corrected (g)	Time of Maximum Accelaration-Corrected (sec)	Total Earhqauke Duration (sec)	Selected Time Interval (sec)
1	"Landers"	"Lucerne"	0.79	0.81	0.80	8.875	48.12	6-23
2	"Kobe_ Japan"	"Kobe University"	0.31	0.44	0.44	4.960	32.00	2-11
3	"Kocaeli_ Turkey"	"Gebze"	0.26	0.55	0.47	2.945	28.00	4-13
4	"Kocaeli_ Turkey"	"Izmit"	0.23	0.42	0.41	6.550	30.00	1-18
5	"Hector Mine"	"Hector"	0.33	0.44	0.48	5.440	45.30	3-17
6	"Tottori_ Japan"	"SMNH10"	0.23	0.50	0.53	3.825	99.97	20-27
7	"Duzce_ Turkey"	"IRIGM 496"	1.03	0.73	0.76	12.456	30.00	7-27

The scaled time-history records and acceleration and velocity graphs of each record are presented below. In the analyses, the critical horizontal component of record is selected. For prevent time consuming, not all recorded time duration is used in the analysis. Instead related time intervals are used which is specified in the Table 4.6. The red line in the spectrum graphs represents the target spectrum.

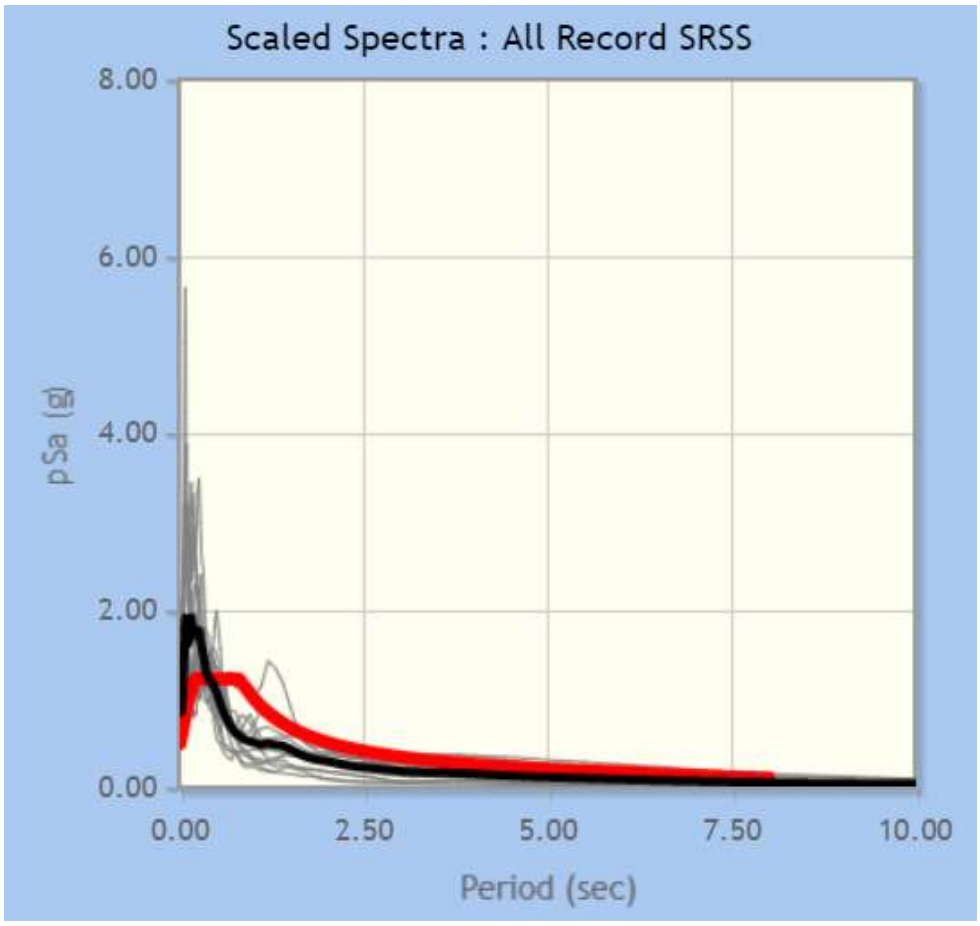

Figure 4.16. Design spectrum and scaled earthquake records

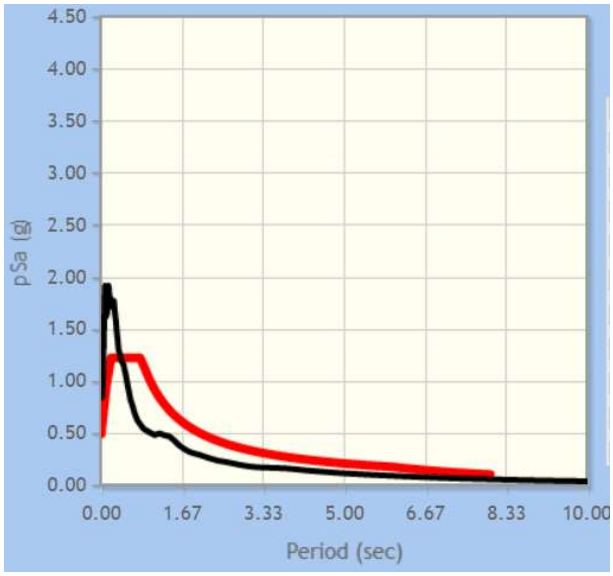

Figure 4.17. Landers scaled record and design spectrum comparison

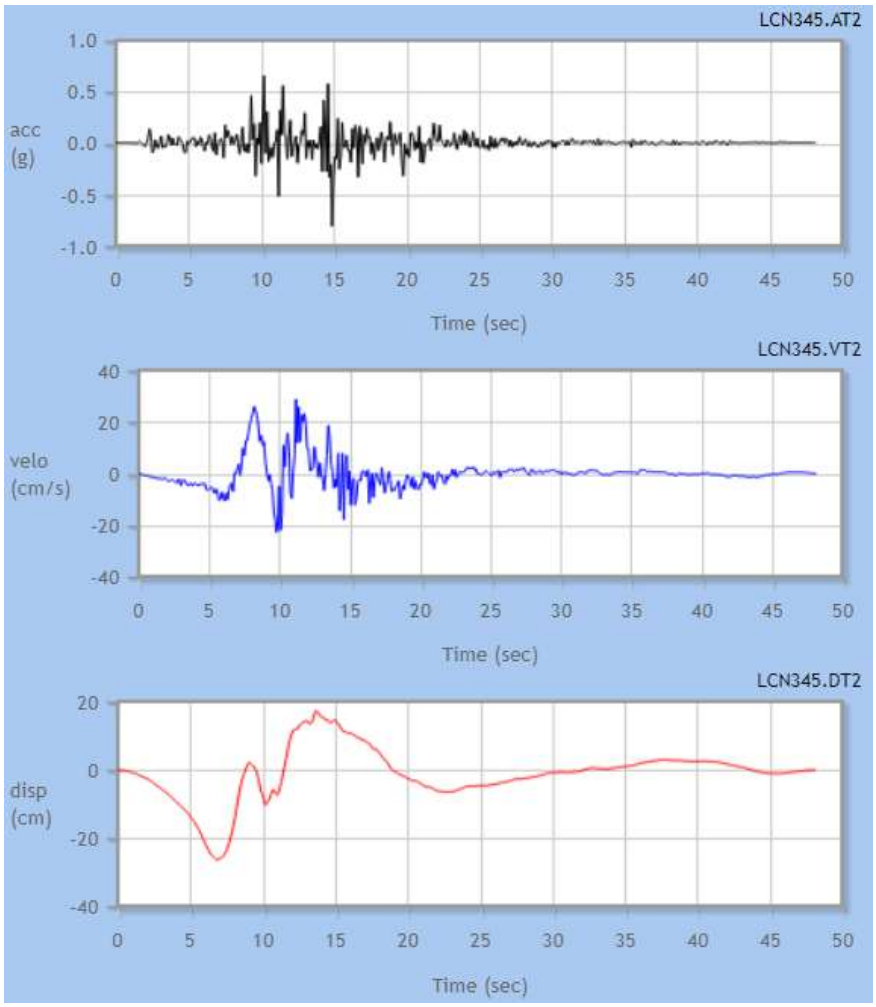

Figure 4.18. Landers Earthquake Acceleration-Time, Velocity-Time and Displacement-Time Record (Scaled)

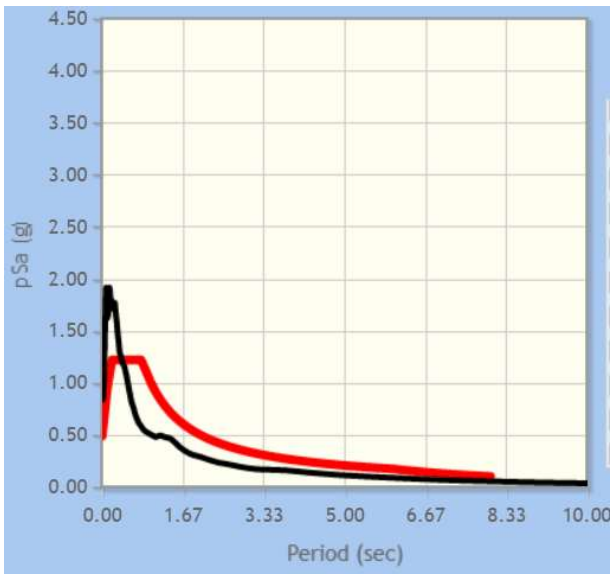

Figure 4.19. Kobe earthquake scaled record and design spectrum comparison

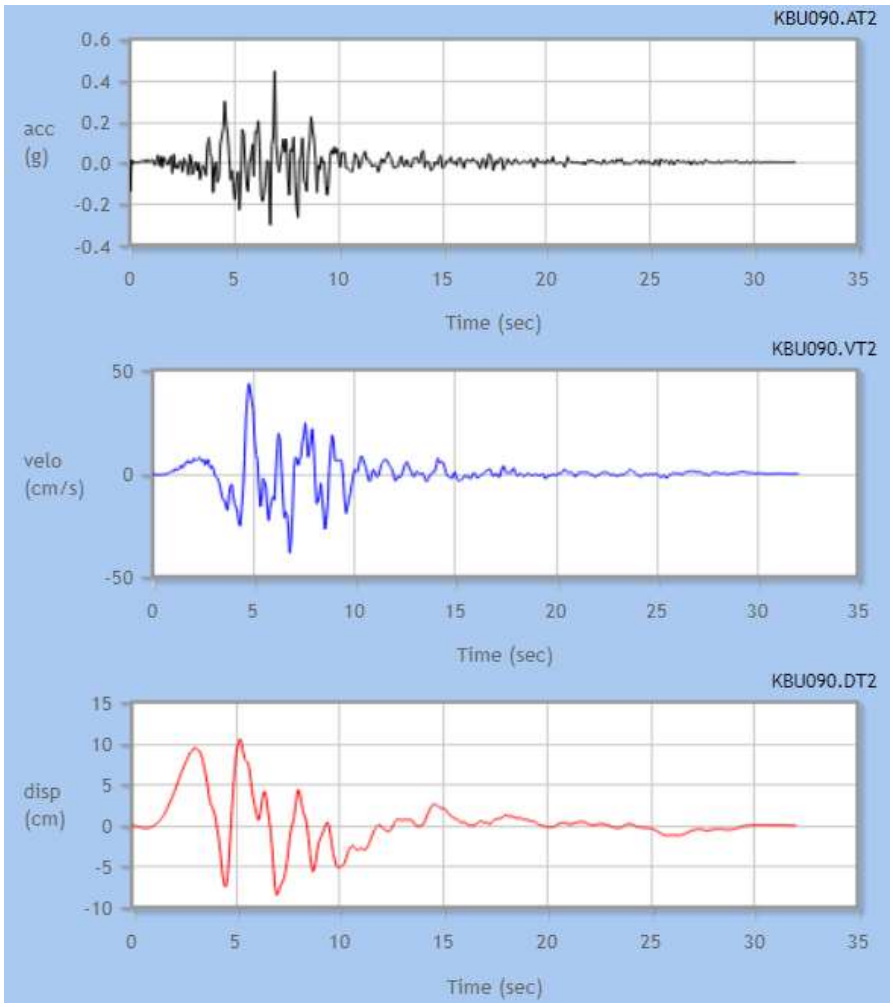

Figure 4.20. Kobe earthquake acceleration-time, velocity-time and displacement-time record (scaled)

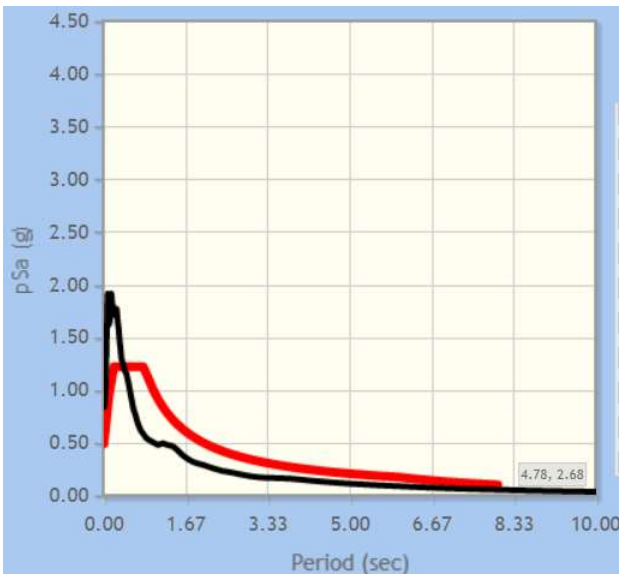

Figure 4.21. Kocaeli-Gebze earthquake scaled record and design spectrum comparison

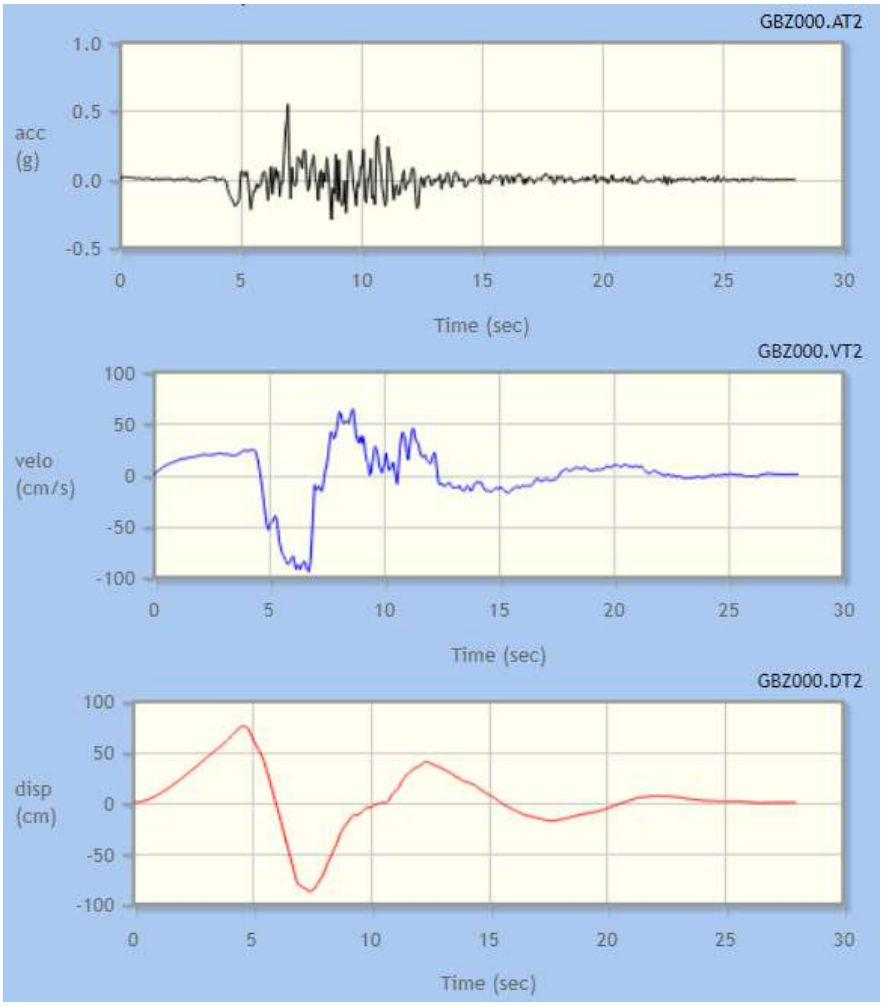

Figure 4.22. Kocaeli-Gebze earthquake acceleration-time, velocity-time and displacement-time record (scaled)

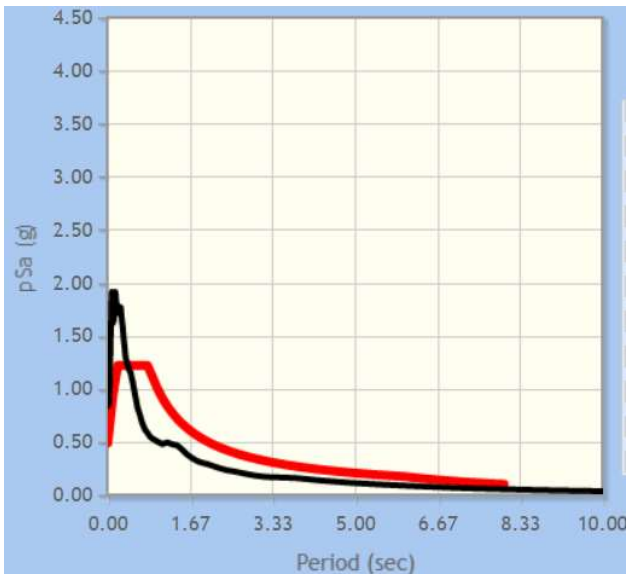

Figure 4.23. Kocaeli-Izmit earthquake scaled record and design spectrum comparison

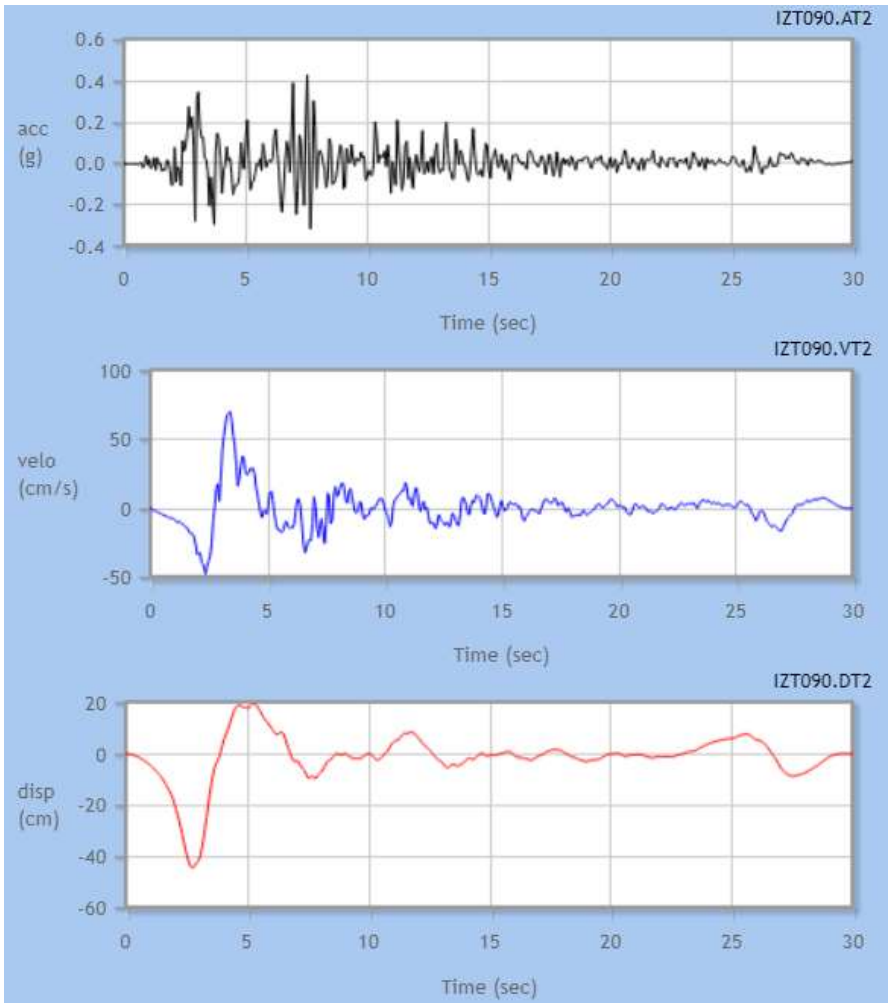

Figure 4.24. Kocaeli- Izmit earthquake acceleration-time, velocity-time and displacement-time record (scaled)

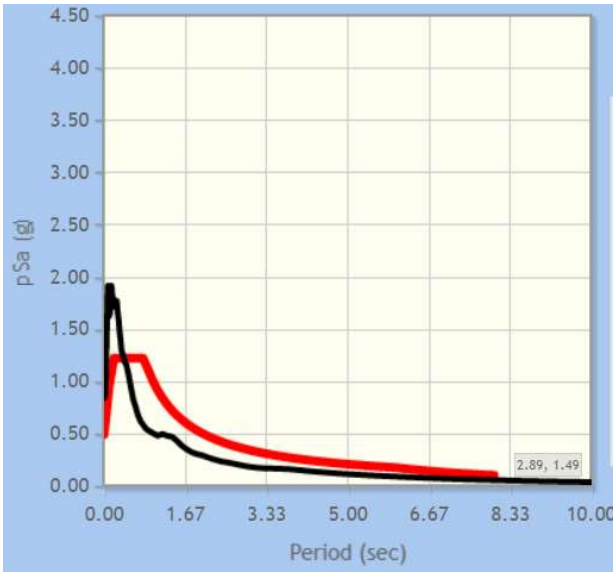

Figure 4.25. Hector Mine earthquake scaled record and design spectrum comparison

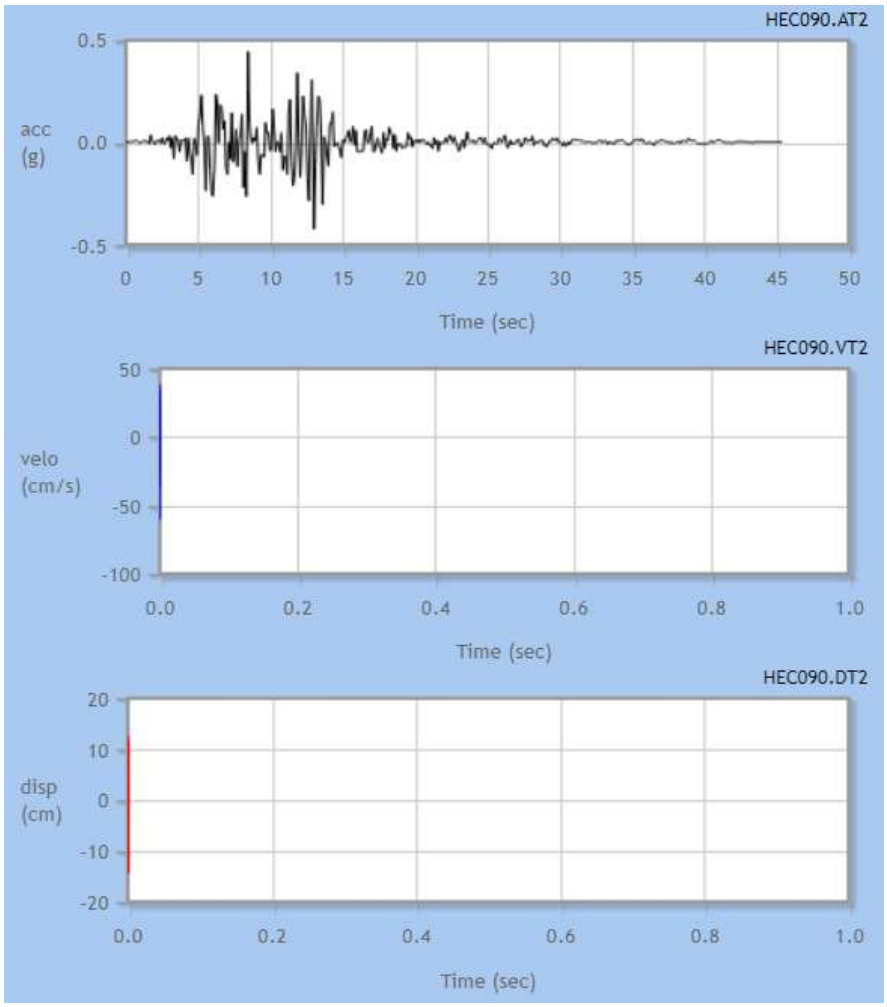

Figure 4.26. Hector Mine earthquake acceleration-time, velocity-time and displacement-time record (scaled)

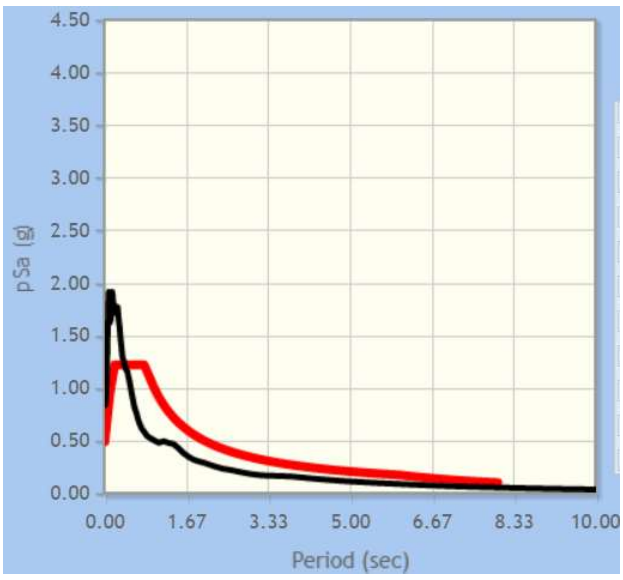

Figure 4.27. Tottori earthquake scaled record and design spectrum comparison

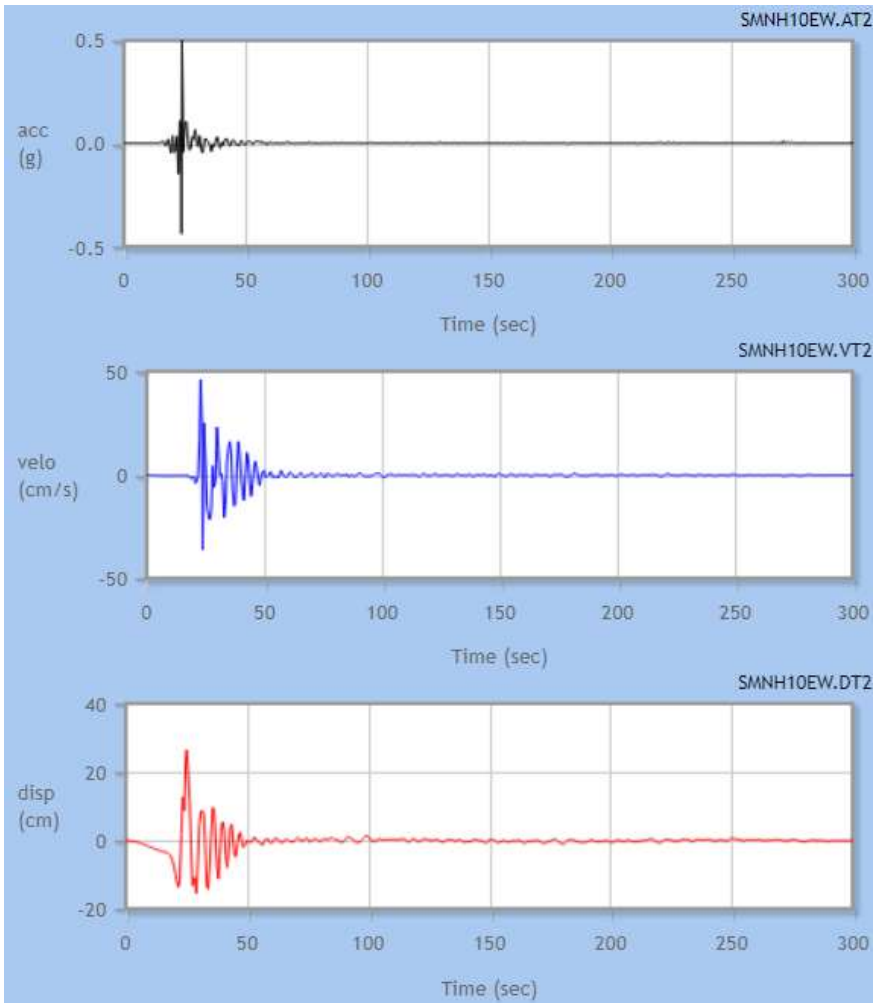

Figure 4.28. Tottori earthquake acceleration-time, velocity-time and displacement-time record (scaled)

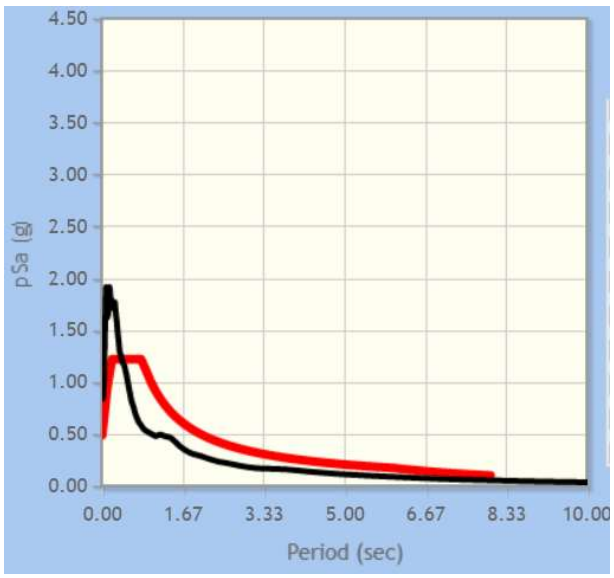

Figure 4.29. Duzce earthquake scaled record and design spectrum comparison

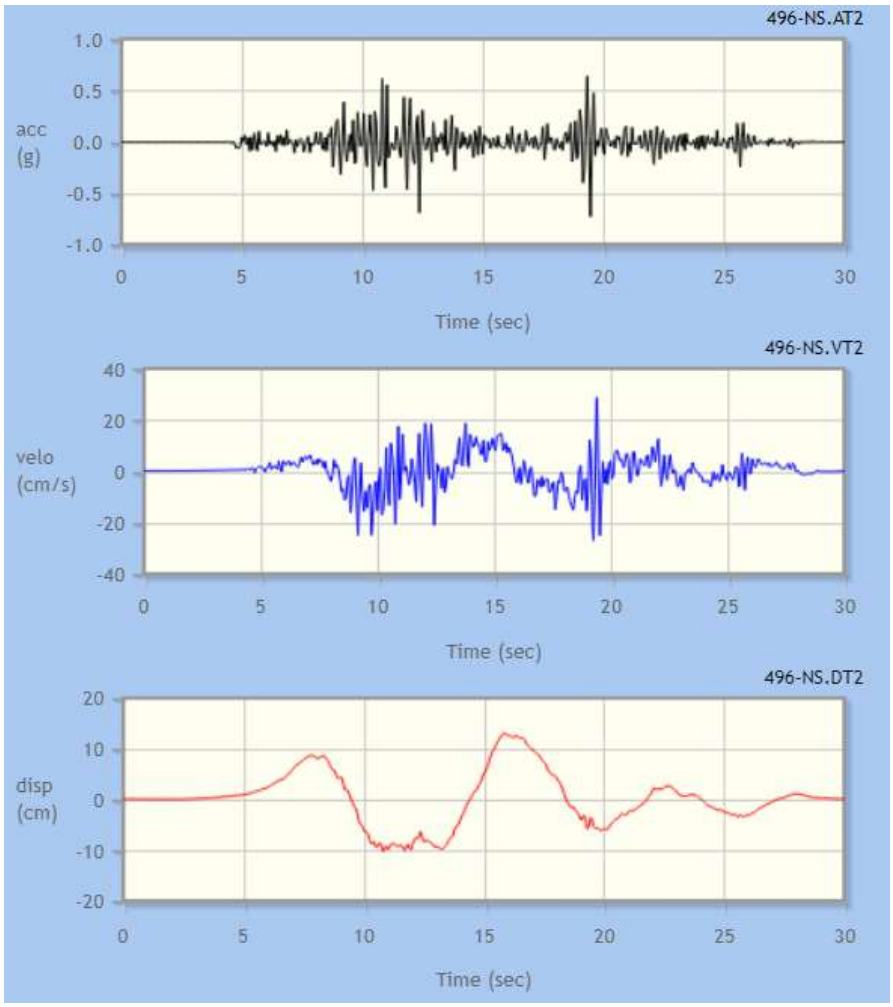

Figure 4.30. Duzce earthquake acceleration-time, velocity-time and displacement-time record (scaled)

4.5. Results

In this section, the results of analyses are presented and discussed. In the study, as stated previously, it is mainly focused on the change in natural frequency of soil after improvement. It is done by drawing acceleration response spectrum of each case. Besides, the effect of PGA amplification is discussed too. For comparison purposes, 6 points are selected at mesh stage. The points are shown in Figure 4.4. For each point, both spectral accelerations and acceleration-time graphs are drawn. In fact, at locations under improvement, numerated as Point 4, Point 5 and Point 6, no change is expected. Because the improved soil is much over that level. However, they are checked whether there is any effect

of improvement at underlying layers. Moreover, since all PGA values are chosen as high, it can be sum as that the effect of severe earthquakes are investigated in this study.

4.5.1. Landers

According to results, there is not a significant change in response spectrum. In Figure 4.32 and in Figure 4.33, which shows the end of piles and just beneath the end of piles , the peak values decreased, but at surface, which is given in Figure 4.31, the peak values increased after piling. Moreover, after a depth under the piles, such as just over and under the clay layer and at the base of rock layer, which are numerated as point 4,5 and 6, there is a clear match among each curve. As result, it can be concluded that at the locations of pile constructed, due the effect of improvement the peaks in response spectra have decreased. Besides, since the shape of curves for the locations of pile constructed do not shape, it can be concluded that the improvement does not change soil class in that area for given conditions. The reason of increase at the surface may be explained by response of increase in rigidity of free surface. Besides, at the locations under the end of piles, there is no change as expected, because the improvement does not affect the underlying layers. Thus, the effect of dynamic loading is the same for all three locations (point 4,5 and 6).

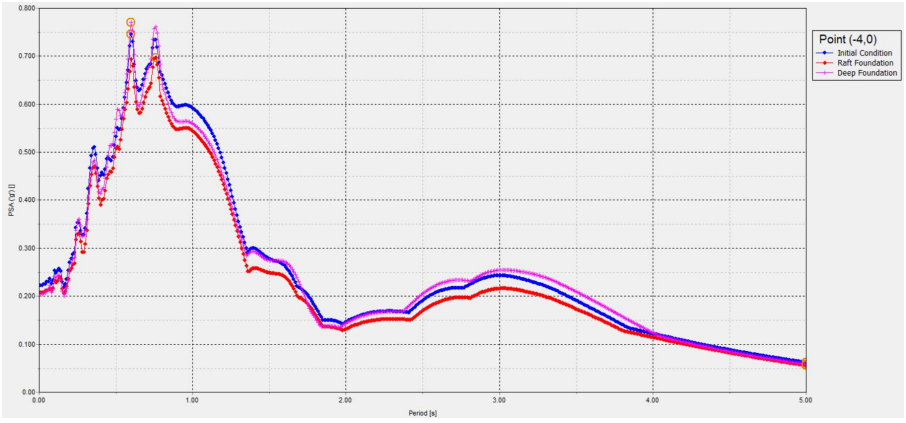

Figure 4.31. Acceleration response spectrum for point 1

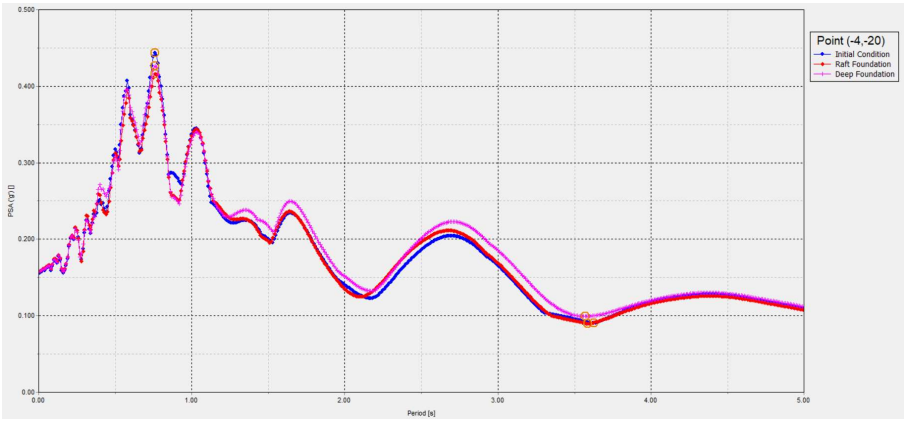

Figure 4.32. Acceleration response spectrum for point 2

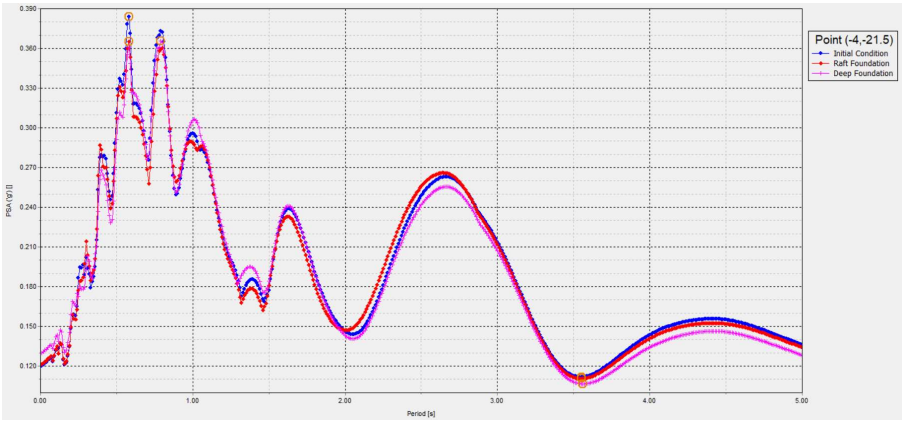

Figure 4.33. Acceleration response spectrum for point 3

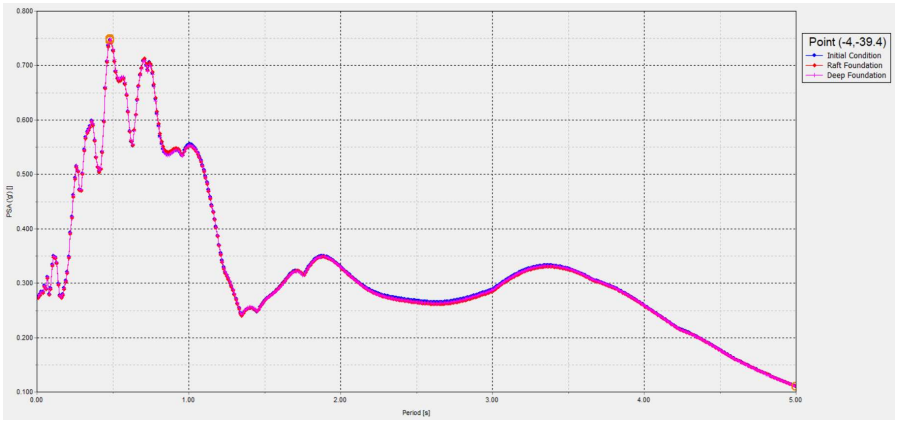

Figure 4.34. Acceleration response spectrum for point 4

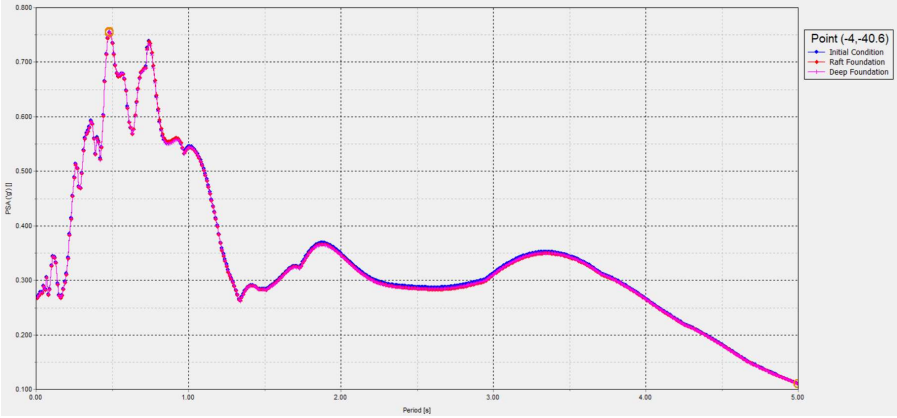

Figure 4.35. Acceleration response spectrum for point 5

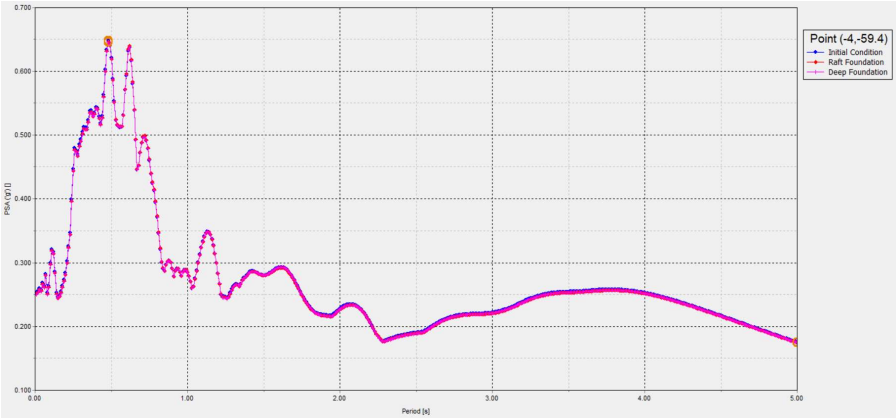

Figure 4.36. Acceleration response spectrum for point 6

Based on acceleration vs dynamic time graphs, as previously stated, since there would not be the effect of improvement in underlying layers, the response spectrum and acceleration would not have shifted in these points. Indeed, there is not a very clear shift at upper levels too. But there is decreases of peak accelerations at the end of piles and just beneath the piles. In contrast there is increase at surface which may be due to the increase in rigidity in free surface.

We look to the he amplification behavior by taking the ratio of accelerations at various points and dividing it to the acceleration at the base (point 6). According to values given in Table 4.7 and Table 4.8, there is an amplification as the wave travels within the sand. But as the wave reaches the surface the degree of amplification decreases. Based on Table 4.8, it can be stated that the amplification factors for deep foundation are lower than initial

condition. Thus, the construction of pile deamplify the dynamic loading better than natural condition under those specified conditions.

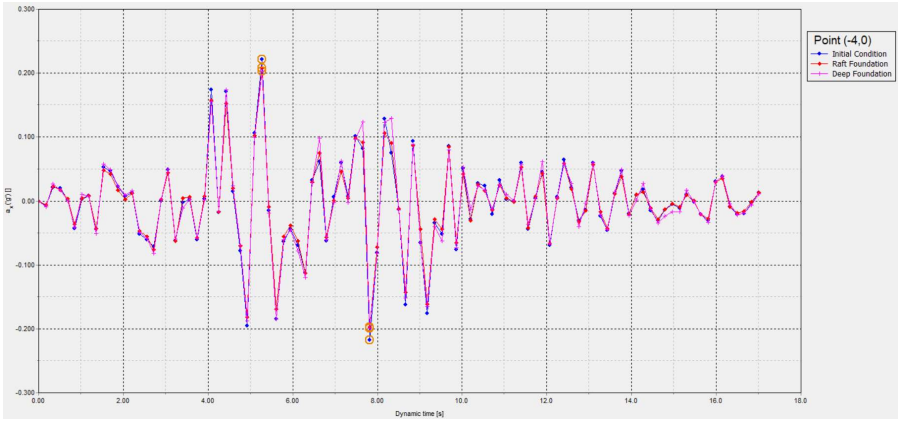

Figure 4.37. Acceleration vs Dynamic Time for Point 1

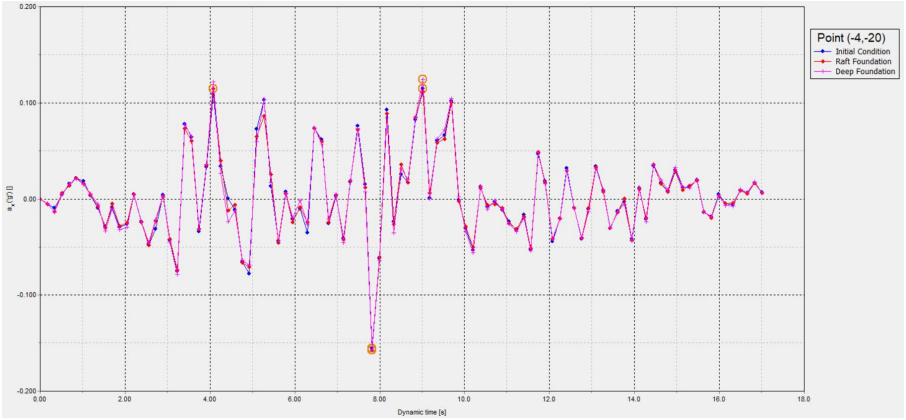

Figure 4.38. Acceleration vs Dynamic Time for Point 2

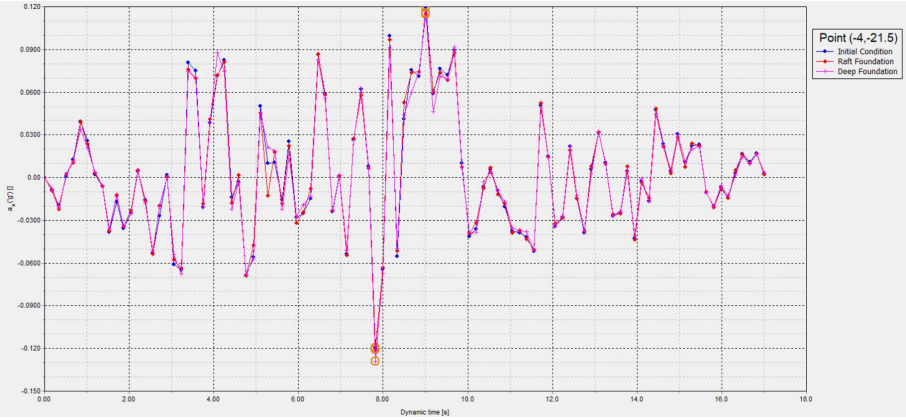

Figure 4.39. Acceleration vs Dynamic Time for Point 3

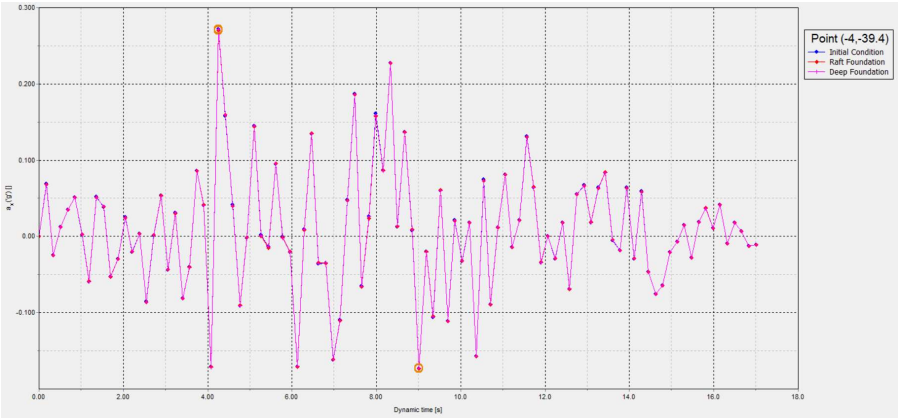

Figure 4.40. Acceleration vs Dynamic Time for Point 4

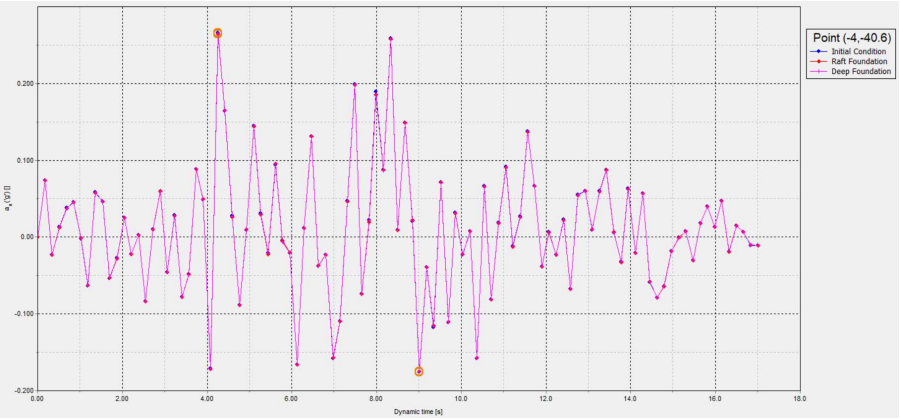

Figure 4.41. Acceleration vs Dynamic Time for Point 5

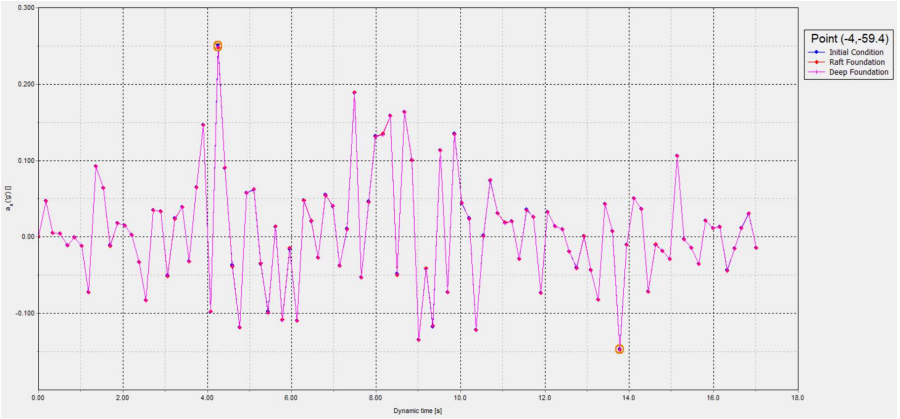

Figure 4.42. Acceleration vs Dynamic Time for Point 6

Table 4.7. PGA values for Landers Earthquake

Condition	Point 1	Point 2	Point 3	Point 4	Point 5	Point 6
Initial Condition	0.221	0.155	0.120	0.272	0.266	0.251
Raft Foundation	0.221	0.158	0.121	0.270	0.265	0.249
Deep Foundation	0.203	0.157	0.129	0.272	0.265	0.248

Table 4.8. Amplification Factors for Point 1,2 and 3

Condition	Amplification Factor (1/6)	Amplification Factor (2/6)	Amplification Factor (3/6)
Initial Condition	0.880	0.618	0.478
Raft Foundation	0.888	0.635	0.486
Deep Foundation	0.819	0.633	0.520

4.5.2. Kobe

According to results, there is a very slight change in response spectrum, however the peak points do not change. The shapes of curves at surface, at the end of piles and at just beneath the end of piles in sand layer, do not change for initial or deep foundation conditions based on Figure 4.43, Figure 4.44 and in Figure 4.45. Moreover, after a depth under the piles, there is a clear match among each curve as expected, except some differences between peak points, which means the pile construction does not affect the underlying layers of piles and it does not change soil class for the given conditions.

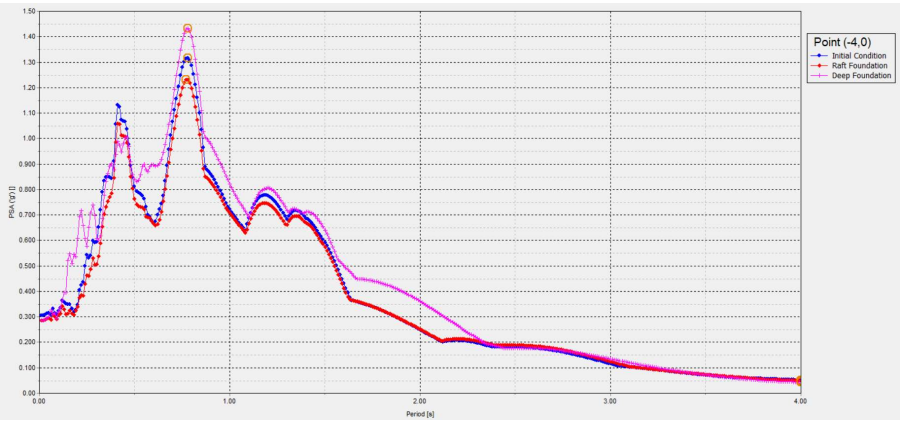

Figure 4.43. Acceleration response spectrum for point 1

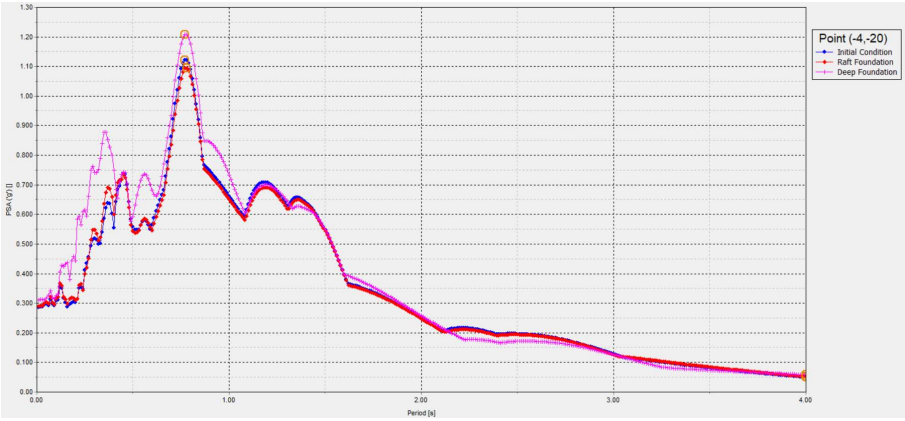

Figure 4.44. Acceleration response spectrum for point 2

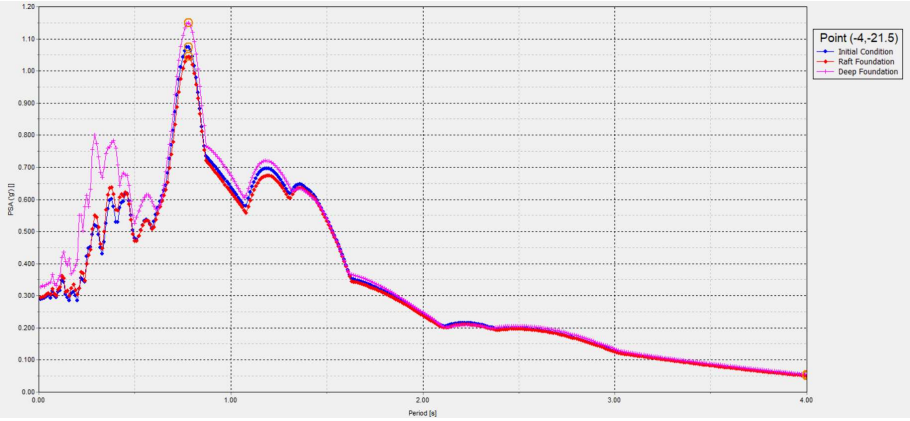

Figure 4.45. Acceleration response spectrum for point 3

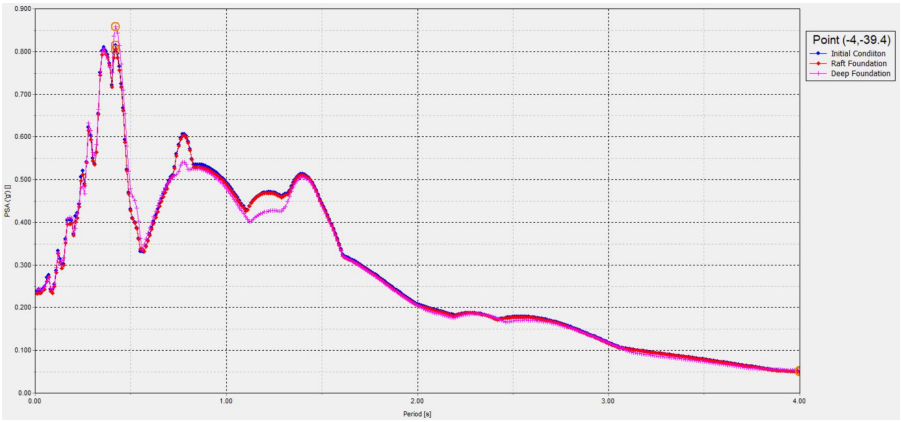

Figure 4.46. Acceleration response spectrum for point 4

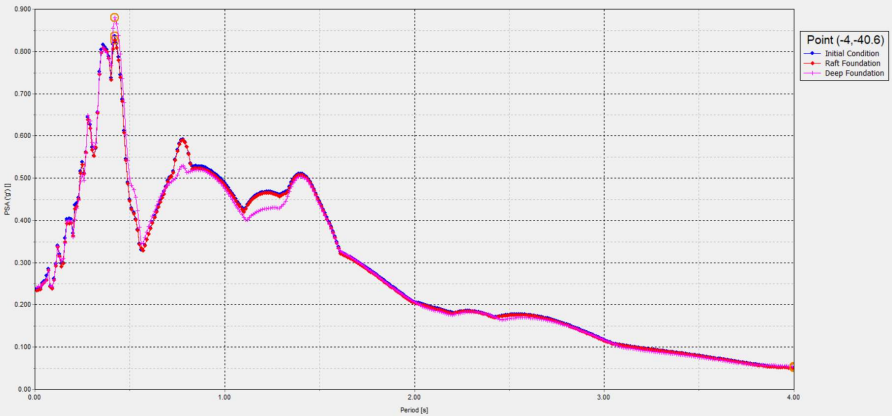

Figure 4.47. Acceleration response spectrum for point 5

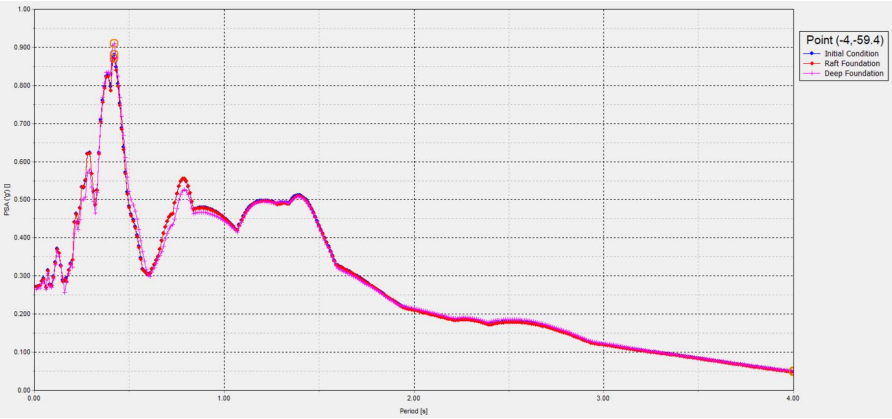

Figure 4.48. Acceleration response spectrum for point 6

Based on acceleration vs dynamic time graphs, like Landers earthquake, there is not a clear shift at a depth under the end of piles. There is not a significant shift at the end of piles too. In contrast there is a very clear change at base. At short periods and very long periods, acceleration of deep foundation increases when compared to other two cases. It may be due to increase in rigidity at free surface as stated previously.

According to amplification behavior given in Table 4.9 and Table 4.10, there is deamplification as the wave propagates through the sand layer. But as the waves reach the surface through clay layer the soil amplifies it for initial condition and deamplifies for other two conditions. Based on Table 4.10, it can be expressed that the deep foundations deamplify the soil better than initial condition. Therefore, construction of piles deamplifies dynamic

earthquake loading better when compared to natural conditions for the given soil parameters and the earthquake record.

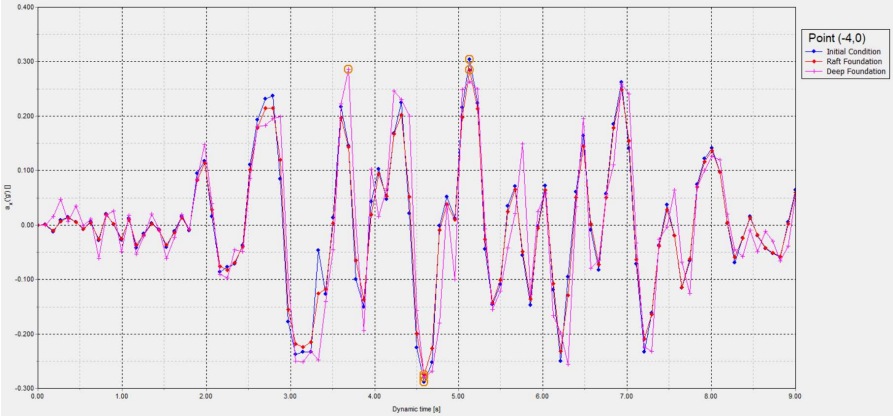

Figure 4.49. Acceleration vs Dynamic Time for Point 1

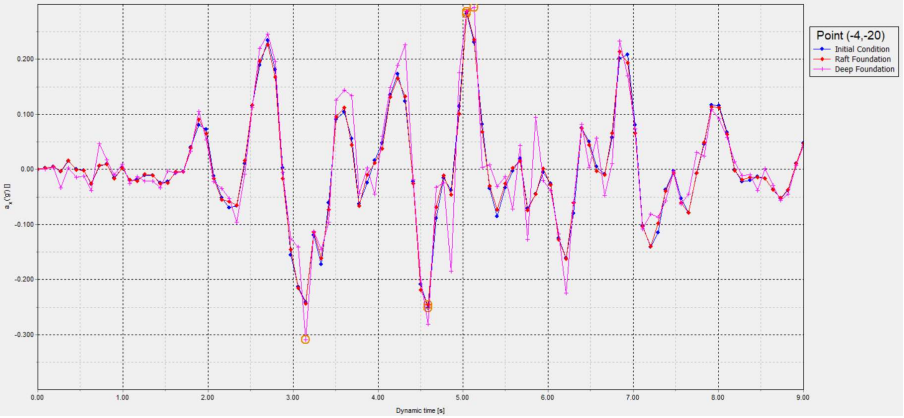

Figure 4.50. Acceleration vs Dynamic Time for Point 2

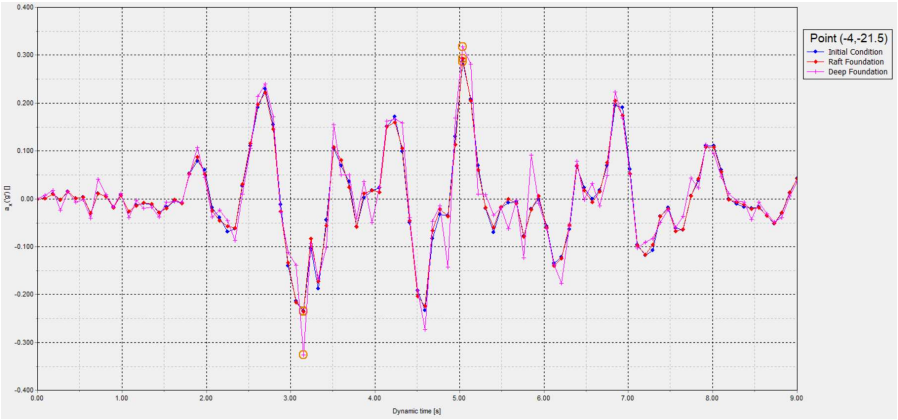

Figure 4.51. Acceleration vs Dynamic Time for Point 3

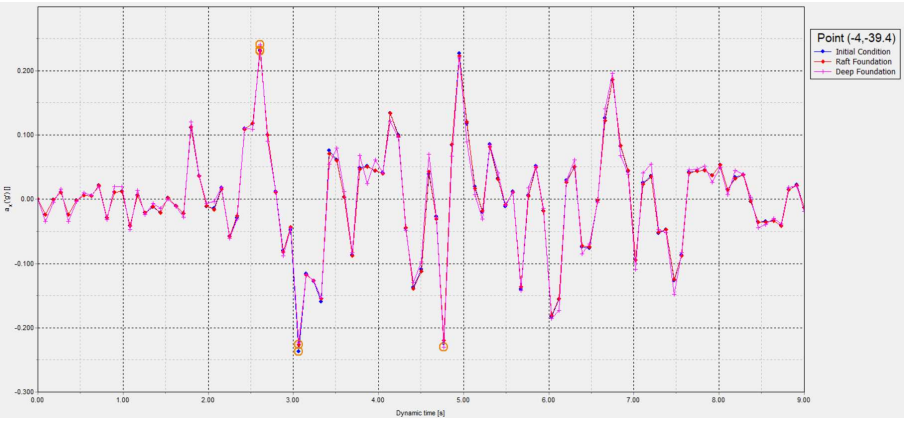

Figure 4.52. Acceleration vs Dynamic Time for Point 4

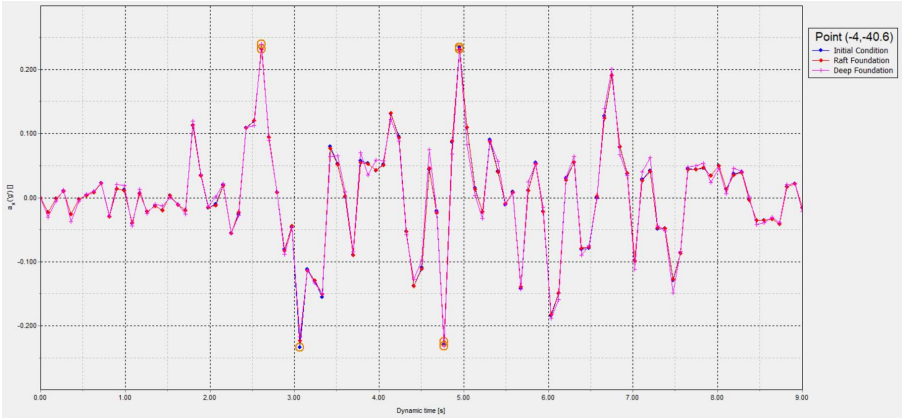

Figure 4.53. Acceleration vs Dynamic Time for Point 5

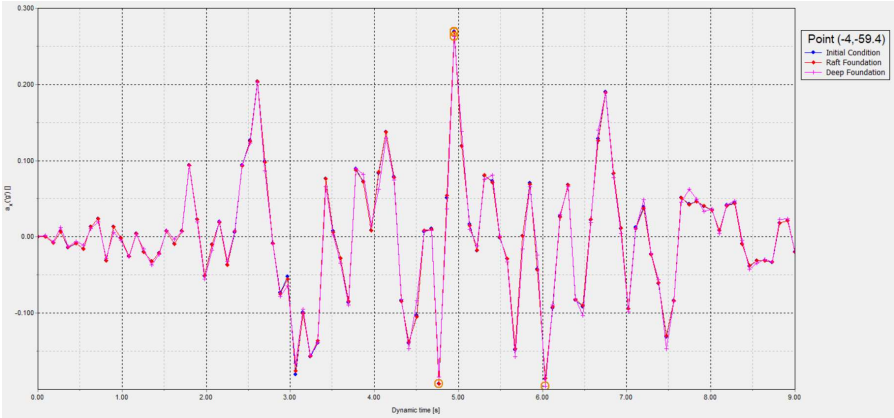

Figure 4.54. Acceleration vs Dynamic Time for Point 6

Table 4.9. PGA values for Kobe Earthquake

Condition	Point 1	Point 2	Point 3	Point 4	Point 5	Point 6
Initial Condition	0.304	0.282	0.287	0.237	0.235	0.269
Raft Foundation	0.205	0.287	0.293	0.231	0.232	0.269
Deep Foundation	0.213	0.309	0.318	0.24	0.24	0.263

Table 4.10. Amplification Factors for Point 1,2 and 3 of Kobe Earthquake

Condition	Amplification Factor (1/6)	Amplification Factor (2/6)	Amplification Factor (3/6)
"Initial Condition	1.130	1.048	1.067
Raft Foundation	0.762	1.067	1.089
Deep Foundation	0.810	1.175	1.209

4.5.3. Kocaeli-Gebze

According to results, there is not a clear change in response spectrums. The shapes of response spectrums at the end of pile or at the surface, given in Figure 4.55 and Figure 4.56, do not change. But there is just a little decrease just beneath the end of piles, which may be due to the improvement. At a depth under the pile, in sand layer or in rock layer, there is a nice match among curves. As result, it can be stated that the pile construction does not change the soil class and the improvement does not affect the underlying layers for that loading record and given soil conditions.

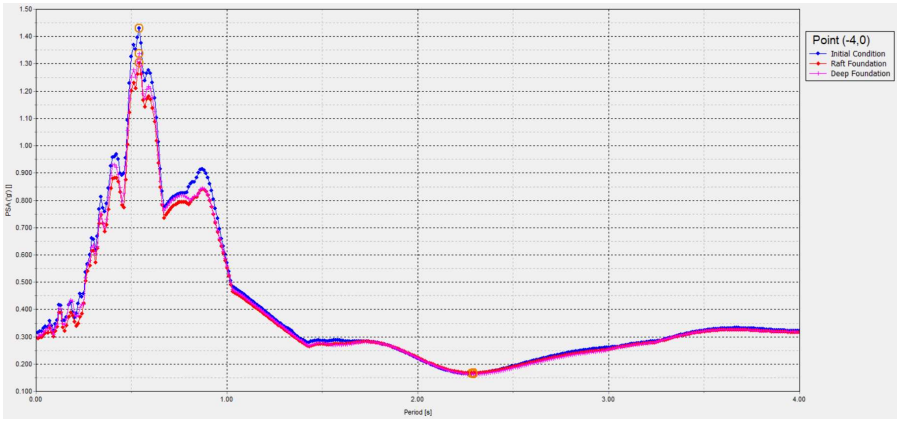

Figure 4.55. Acceleration response spectrum for point 1

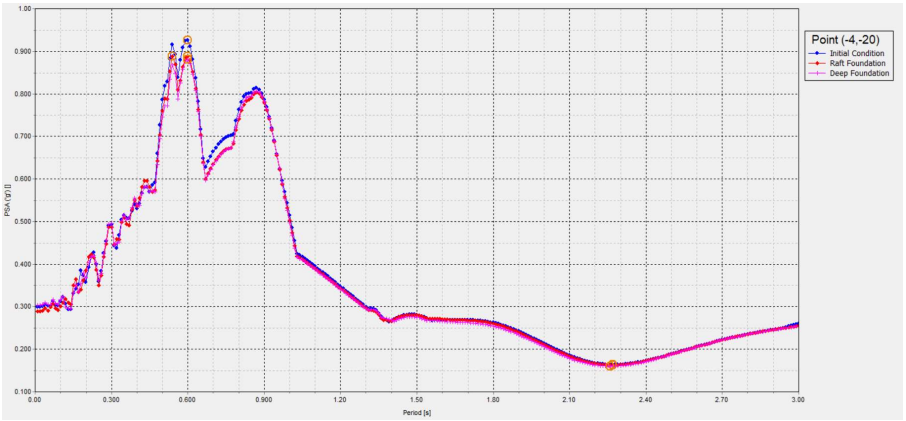

Figure 4.56. Acceleration response spectrum for point 2

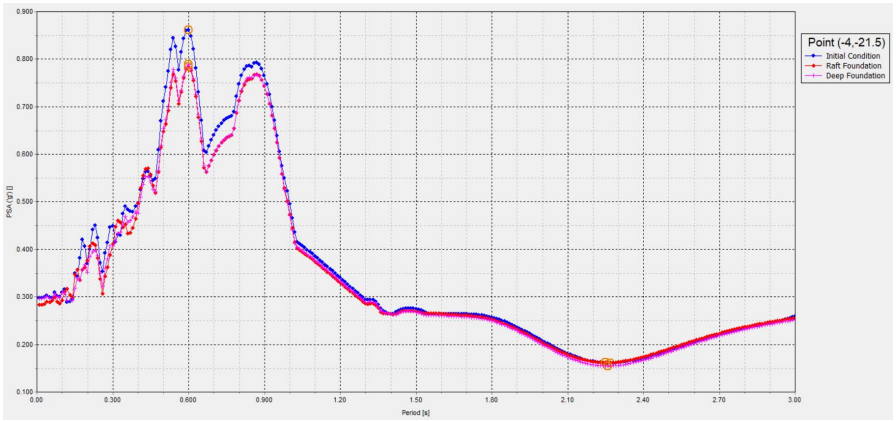

Figure 4.57. Acceleration response spectrum for point 3

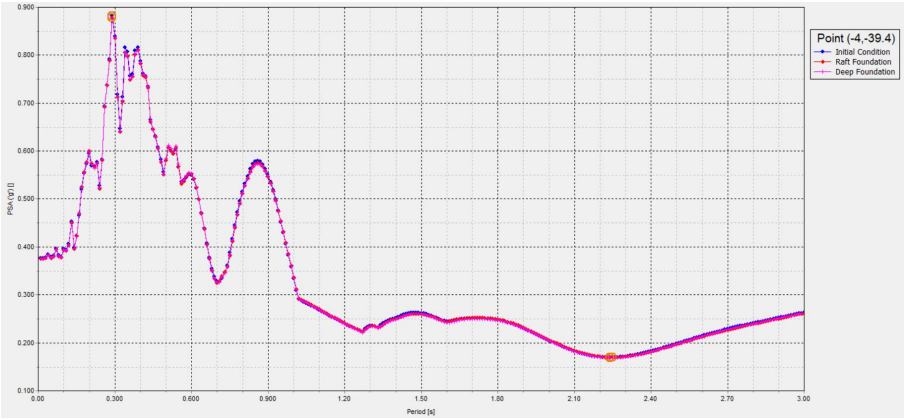

Figure 4.58. Acceleration response spectrum for point 4

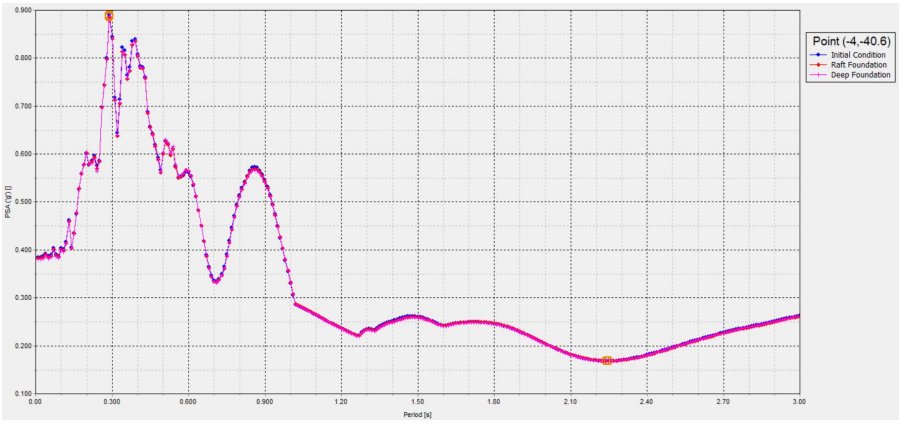

Figure 4.59. Acceleration response spectrum for point 5

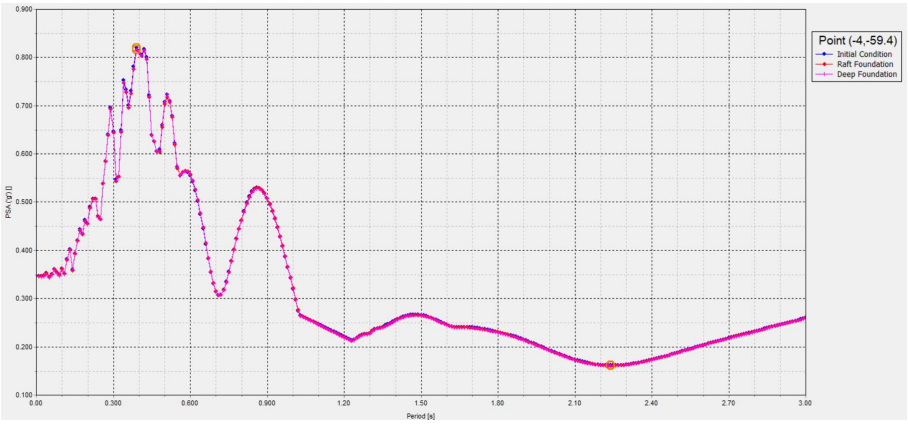

Figure 4.60. Acceleration response spectrum for point 6

Based on acceleration vs dynamic time graphs, like previous two cases, there is no shift at sand layer or rock layer at a depth under the piles. Indeed, there is not a very clear

shift in the improved part of sand and clay layer too. But there are decreases at most of peak values for that improved part. Contrary to other two cases, there is decrease at free surface at this case.

According to Table 4.11, there is a decrease in peak acceleration from the bottom to the upper layers, which means the wave is deamplified as it travels from rock to soil layers. Based on the amplification behavior given in Table 4.12, the soil deamplifies the dynamic loading as the waves propagate upward. Based on Table 4.12, it can be stated that the amplification factors decreased after improvement. Thus, it can be concluded as that the improvement has increased soil dynamic capacity against earthquake loading for the given conditions.

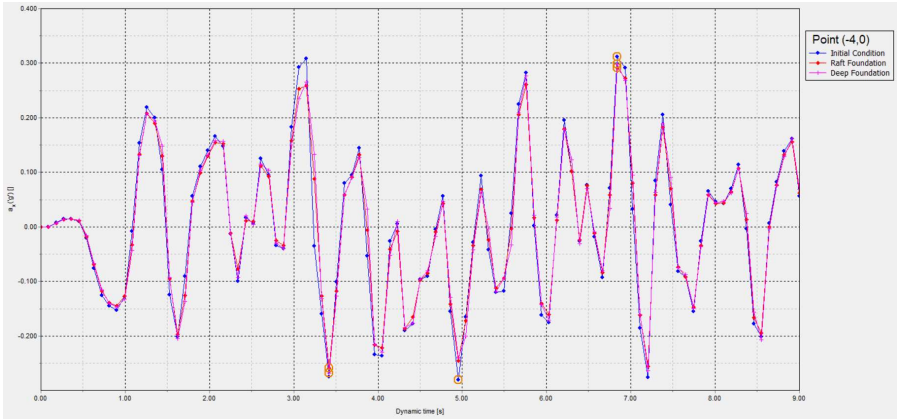

Figure 4.61. Acceleration vs Dynamic Time for Point 1

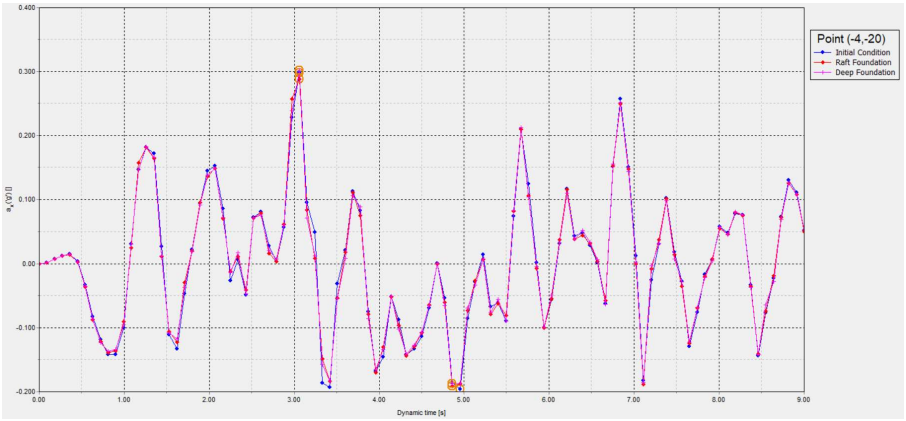

Figure 4.62. Acceleration vs Dynamic Time for Point 2

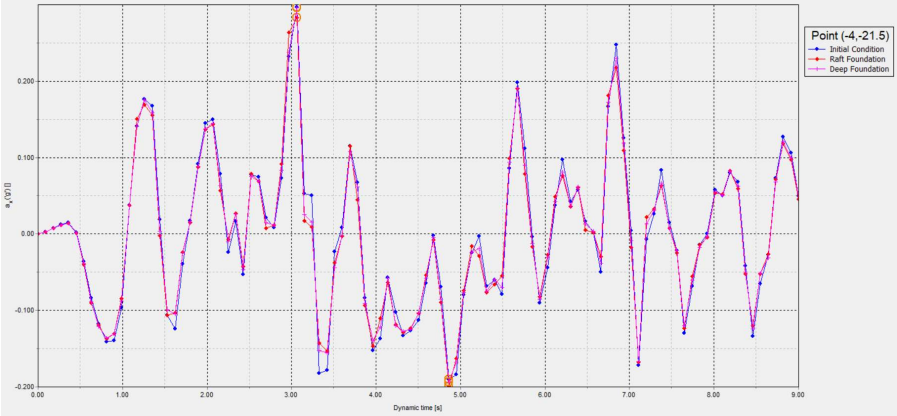

Figure 4.63. Acceleration vs Dynamic Time for Point 3

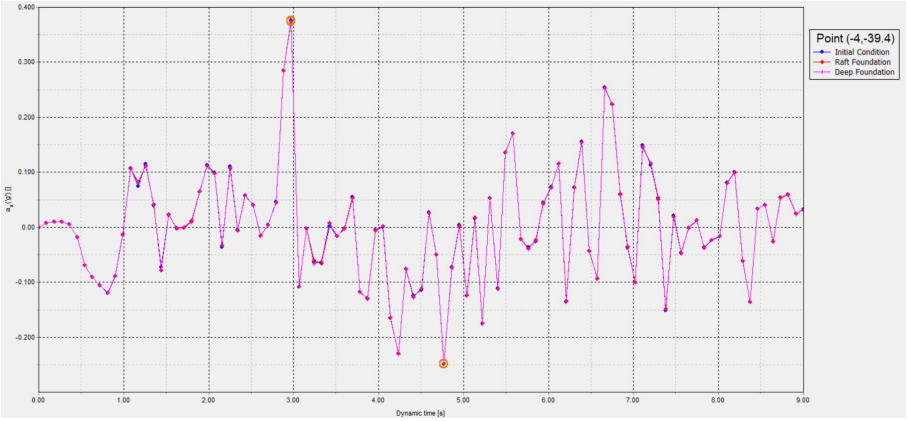

Figure 4.64. Acceleration vs Dynamic Time for Point 4

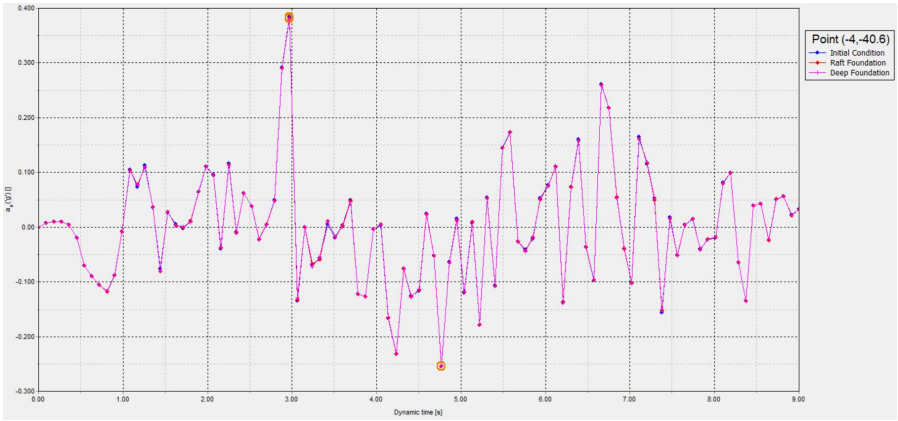

Figure 4.65. Acceleration vs Dynamic Time for Point 5

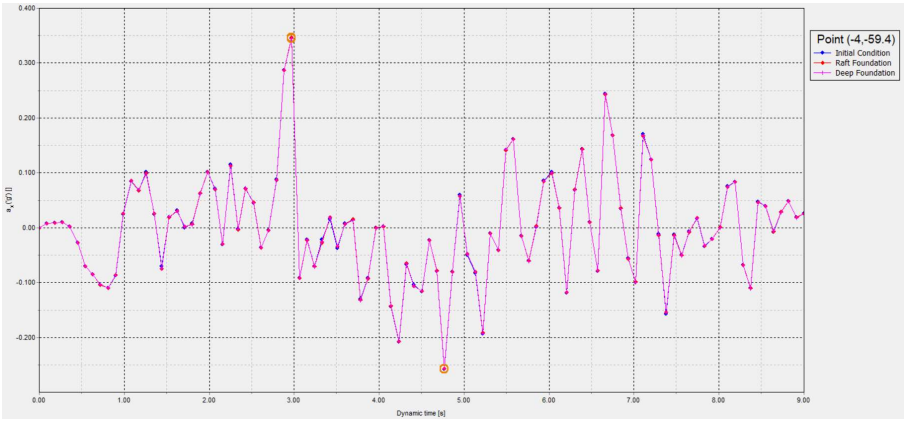

Figure 4.66. Acceleration vs Dynamic Time for Point 6

Table 4.11. PGA values for Kocaeli-Gebze Earthquake

Condition	Point 1	Point 2	Point 3	Point 4	Point 5	Point 6
Initial Condition	0.312	0.298	0.297	0.377	0.384	0.346
Raft Foundation	0.291	0.289	0.283	0.374	0.382	0.347
Deep Foundation	0.298	0.303	0.296	0.375	0.38	0.345

Table 4.12. Amplification Factors for Point 1,2 and 3 of Kocaeli-Gebze Earthquake

Condition	Amplification Factor (1/6)	Amplification Factor (2/6)	Amplification Factor (3/6)
Initial Condition	0.902	0.861	0.858
Raft Foundation	0.839	0.833	0.816
Deep Foundation	0.864	0.878	0.858

4.5.4. Kocaeli-Izmit

Results show that there is not a significant change in response spectrums based on the figures below. Moreover, there is a clear match among curves in the unimproved area as shown in Figure 4.70, Figure 4.71 and Figure 4.72. As result, it is clear that the improvement does not change soil class and it does not affect the underlying layers for the given loading and soil conditions.

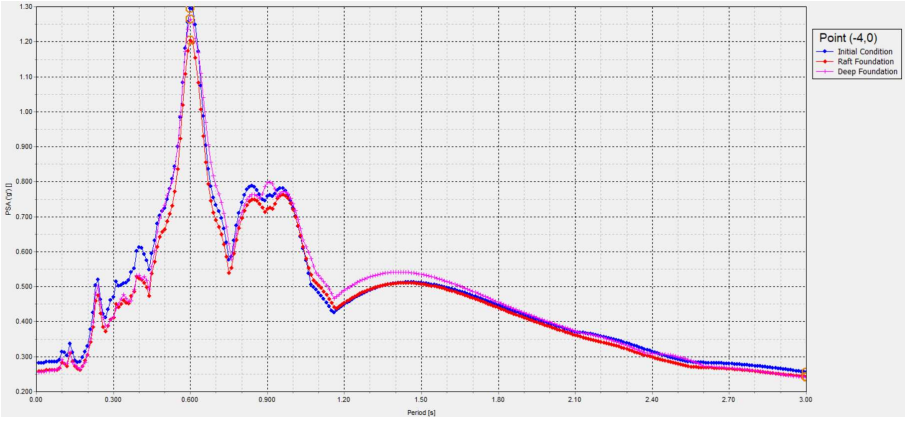

Figure 4.67. Acceleration response spectrum for point 1

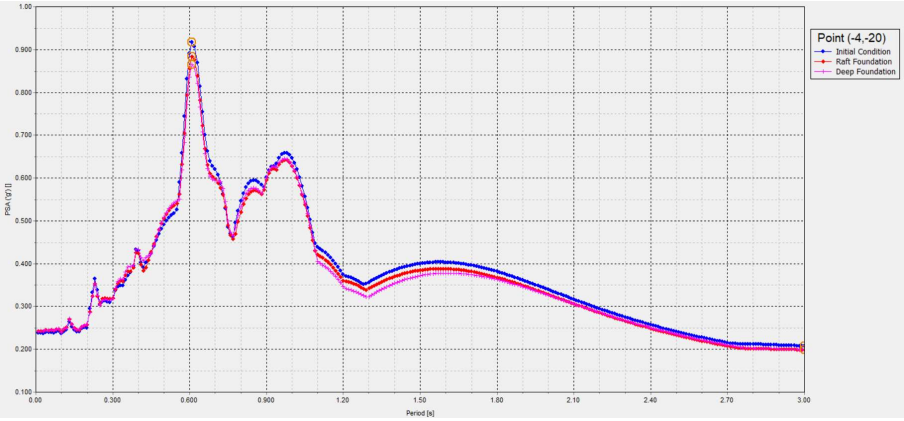

Figure 4.68. Acceleration response spectrum for point 2

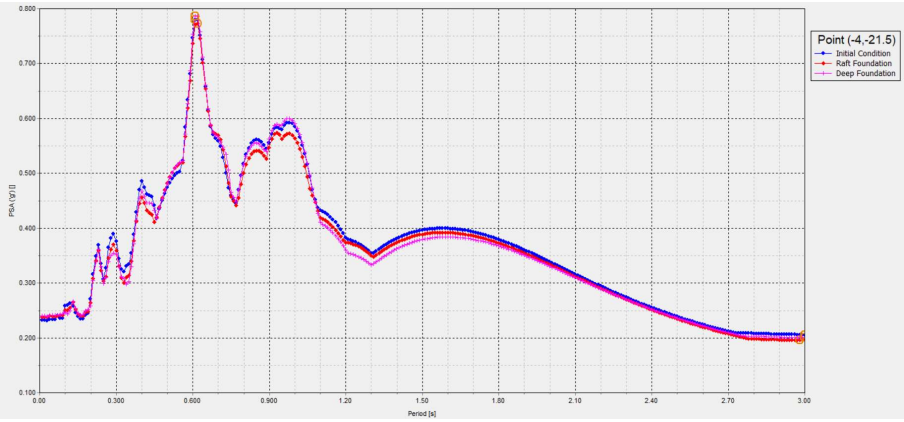

Figure 4.69. Acceleration response spectrum for point 3

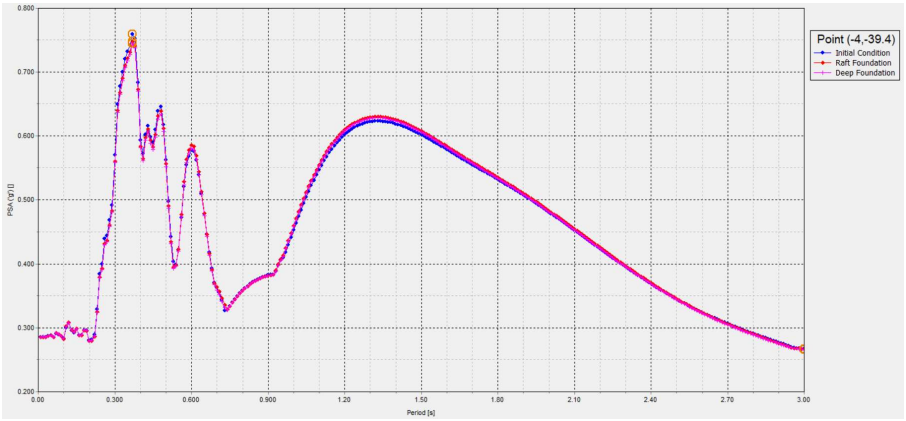

Figure 4.70. Acceleration response spectrum for point 4

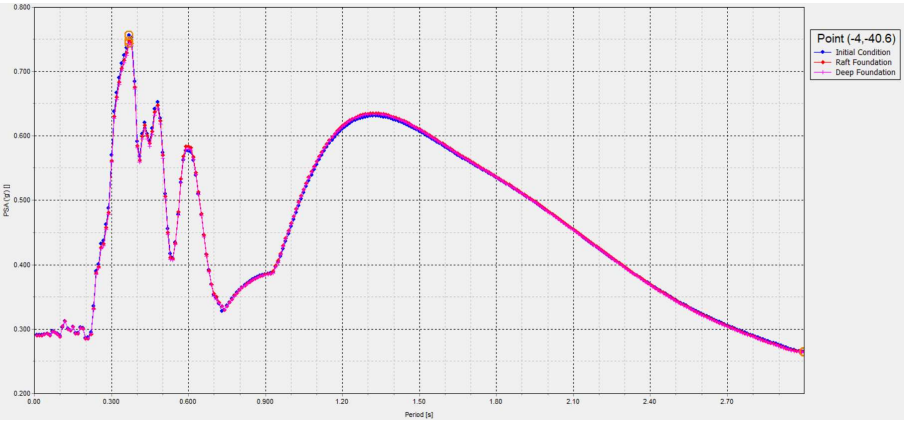

Figure 4.71. Acceleration response spectrum for point 5

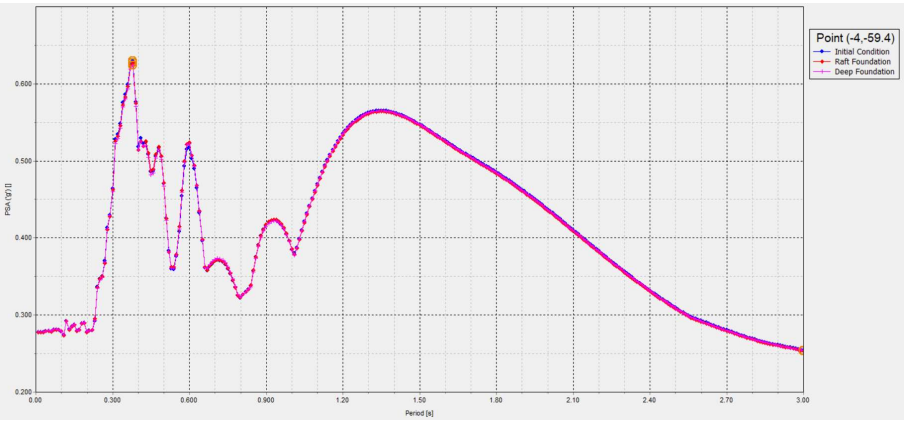

Figure 4.72. Acceleration response spectrum for point 6

According to the acceleration vs dynamic time graphs, like previous cases, there is no shift at unimproved locations. There is not a very clear shift at improved sand area too. There is a negligible shift at surface. At which, the peak values decreased after improvement.

When we look to the Table 4.13 and Table 4.14 , there is a decrease in peak acceleration from the bottom to the upper layers. Based on amplification factors given in Table 4.14, it can be expressed that the wave is not amplified while travelling through sand, however it is amplified in clay layer. And the amplification is lower in deep foundations while compared to initial condition. Therefore, it can be concluded that the construction of piles decreases the amplification of loading under the given conditions.

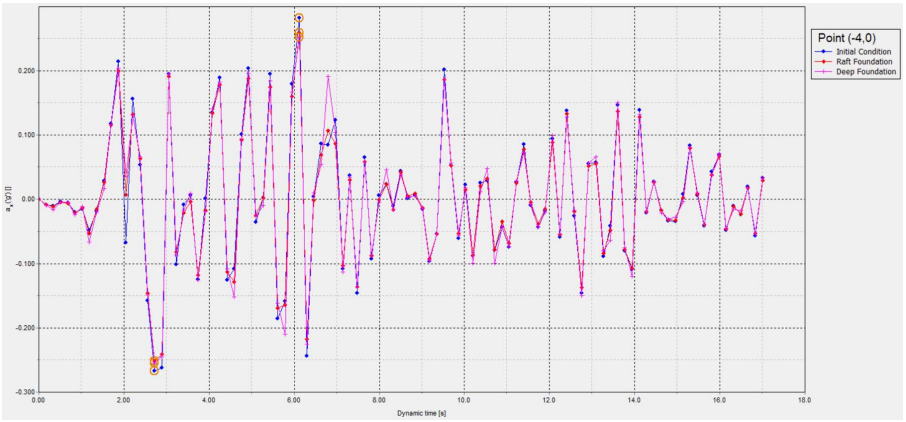

Figure 4.73. Acceleration vs Dynamic Time for Point 1

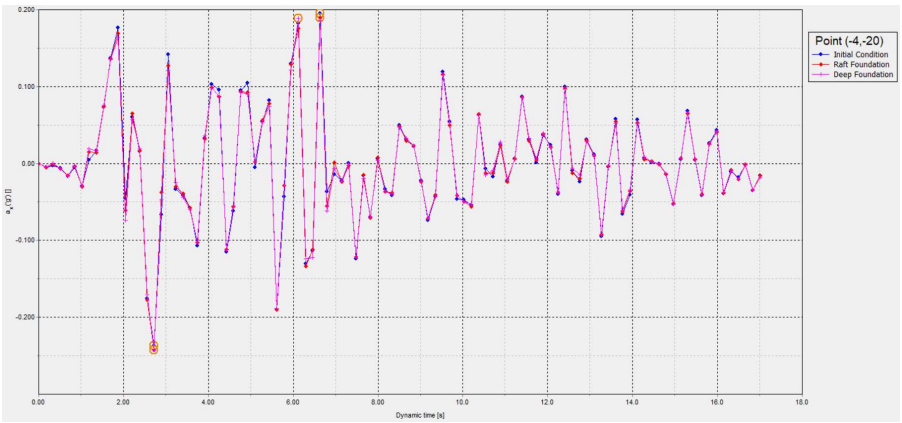

Figure 4.74. Acceleration vs Dynamic Time for Point 2

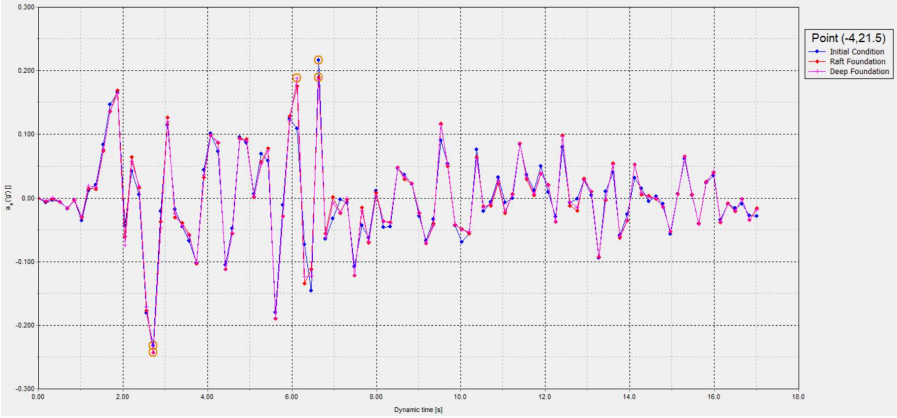

Figure 4.75. Acceleration vs Dynamic Time for Point 3

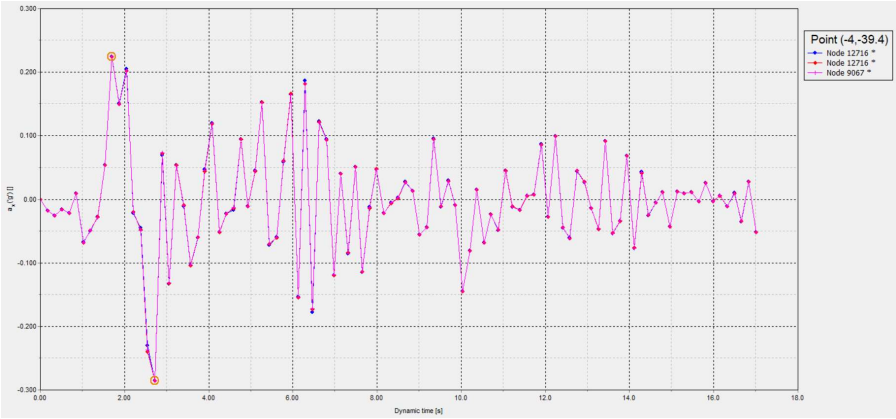

Figure 4.76. Acceleration vs Dynamic Time for Point 4

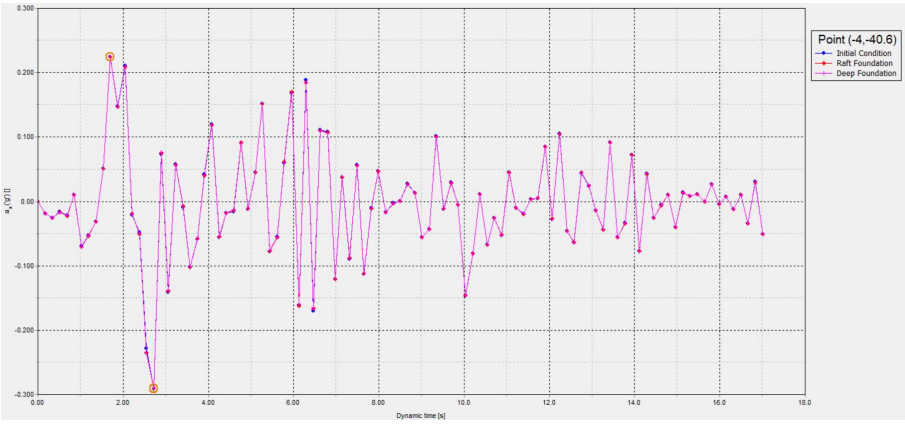

Figure 4.77. Acceleration vs Dynamic Time for Point 5

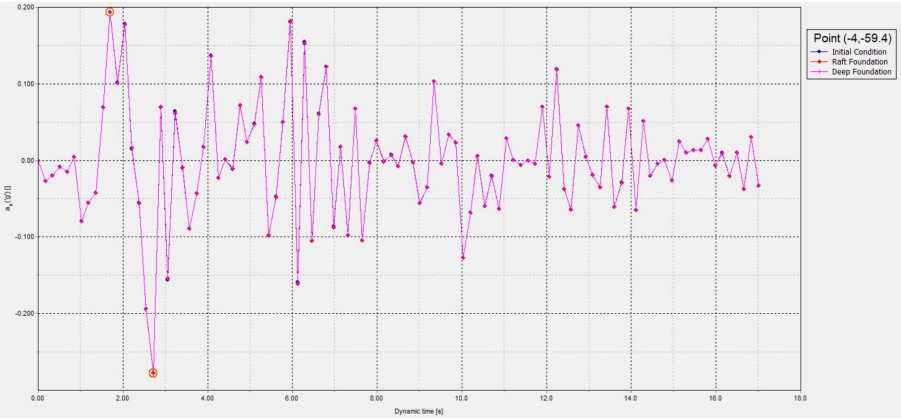

Figure 4.78. Acceleration vs Dynamic Time for Point 6

Table 4.13. PGA values for Kocaeli-Izmit Earthquake

Condition	Point 1	Point 2	Point 3	Point 4	Point 5	Point 6
Initial Condition	0.282	0.232	0.232	0.285	0.291	0.277
Raft Foundation	0.259	0.243	0.243	0.286	0.290	0.277
Deep Foundation	0.255	0.243	0.243	0.286	0.290	0.278

Table 4.14. Amplification Factors for Point 1,2 and 3 of Kocaeli-Izmit Earthquake

Condition	Amplification Factor (1/6)	Amplification Factor (1/6)	Amplification Factor (3/6)
Initial Condition	1.018	0.838	0.838
Raft Foundation	0.935	0.877	0.877
Deep Foundation	0.917	0.874	0.874

4.5.5. Hector Mine

According to the acceleration response spectrums, like the other cases, there is no change at unimproved locations based on Figure 4.82, Figure 4.83 and Figure 4.84. At other parts, given in Figure 4.79, Figure 4.80 and Figure 4.81, there is not a change or shift in curves too. Thus, it can be concluded that the improvement does not change soil class for that soil and loading conditions.

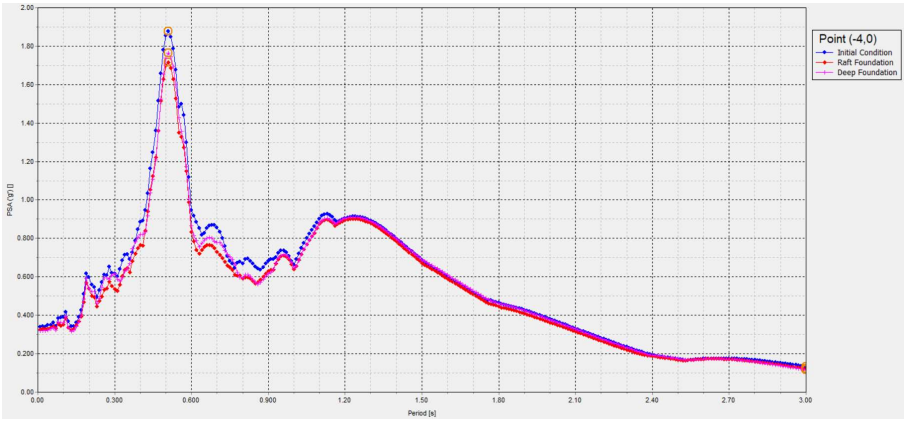

Figure 4.79. Acceleration response spectrum for point 1

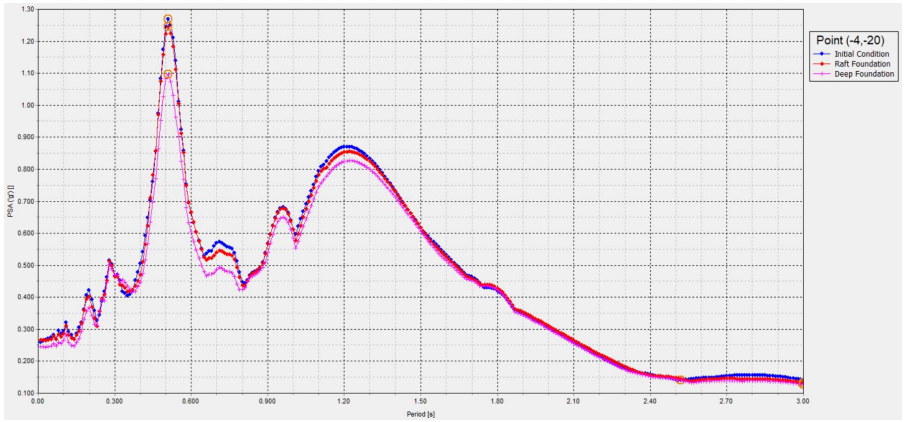

Figure 4.80. Acceleration response spectrum for point 2

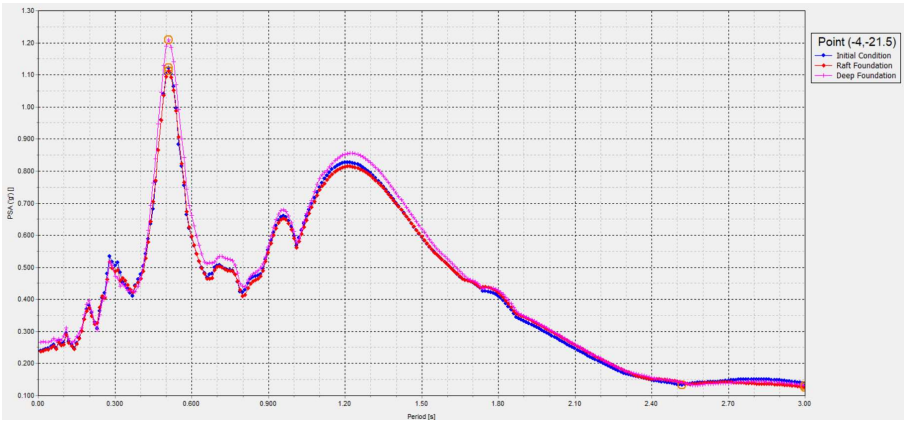

Figure 4.81. Acceleration response spectrum for point 3

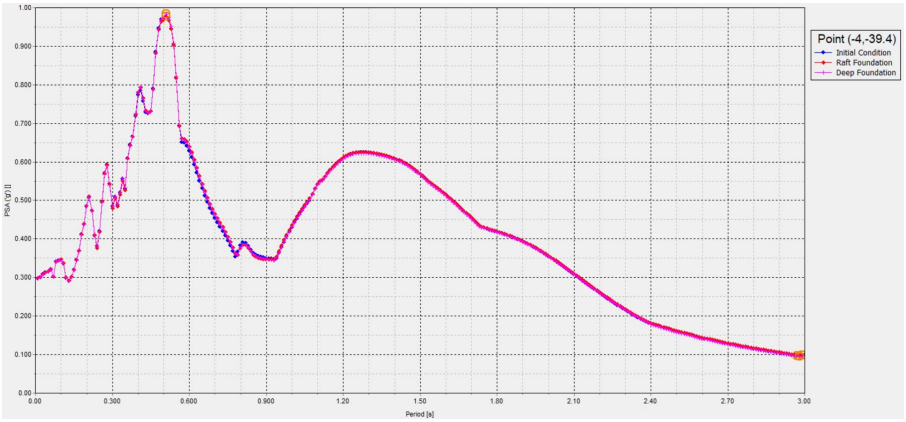

Figure 4.82. Acceleration response spectrum for point 4

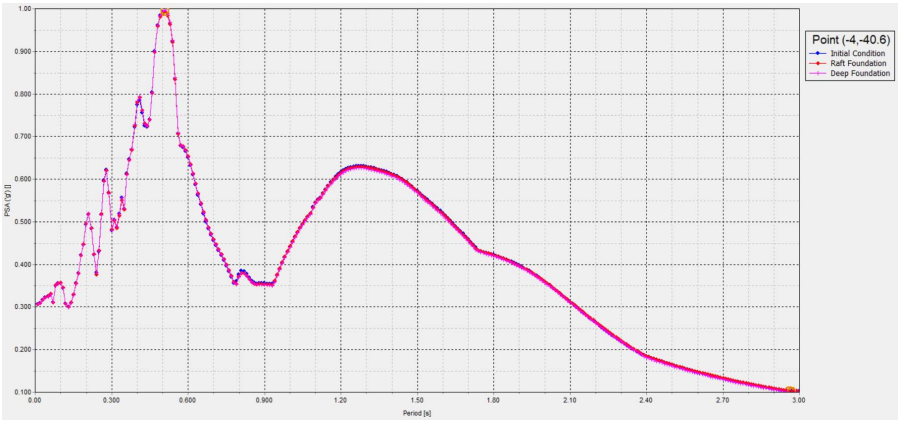

Figure 4.83. Acceleration response spectrum for point 5

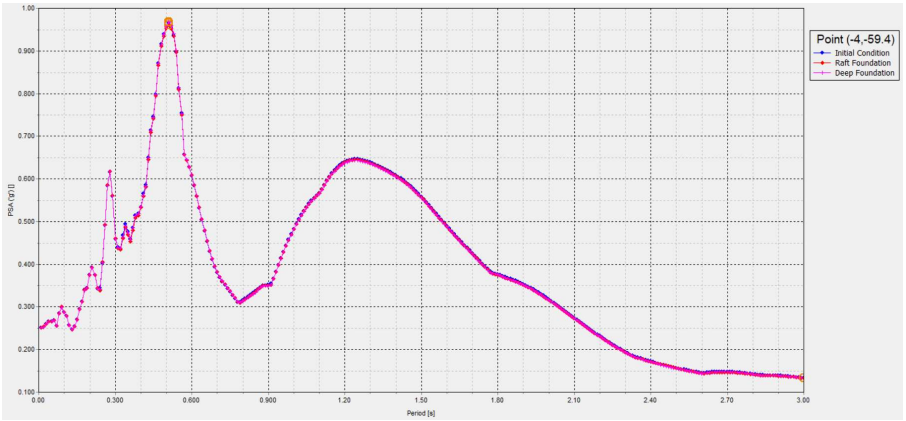

Figure 4.84. Acceleration response spectrum for point 6

Based on acceleration vs dynamic time graphs, like previous cases, there is no shift at base and unimproved part of sand layer. There is not a very clear shift at other locations too,

except some peak values. According to amplification behavior given in Table 4.15 and Table 4.16, there is an increase in peak acceleration as the wave propagates from rock layer to the sand and clay layers. Based on amplification behavior tabulated in Table 4.16, the soil amplifies the dynamic loading as the waves travels within soil layers. However, the loading is amplified less in deep foundations when compared to initial conditions. Thus, it can be stated that the construction of piles decreases the amplification for these loading and soil conditions.

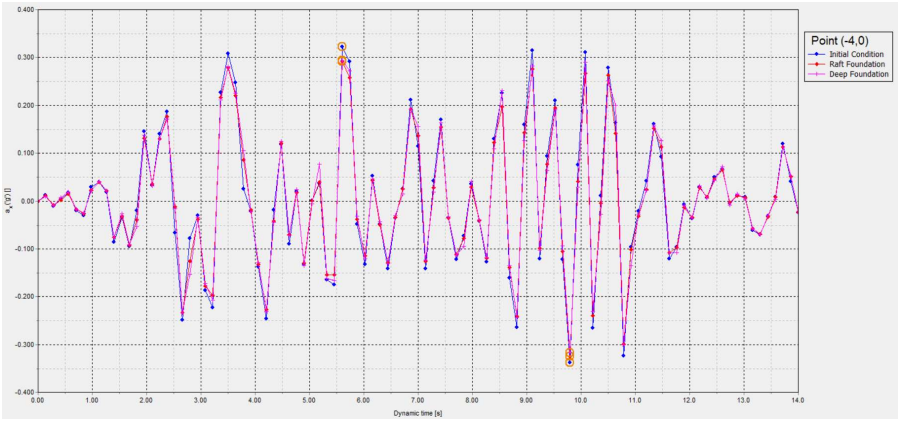

Figure 4.85. Acceleration vs Dynamic Time for Point 1

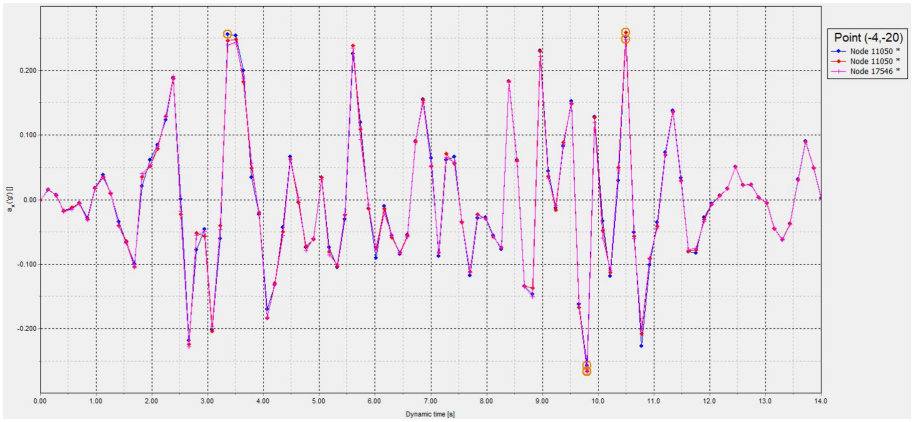

Figure 4.86. Acceleration vs Dynamic Time for Point 2

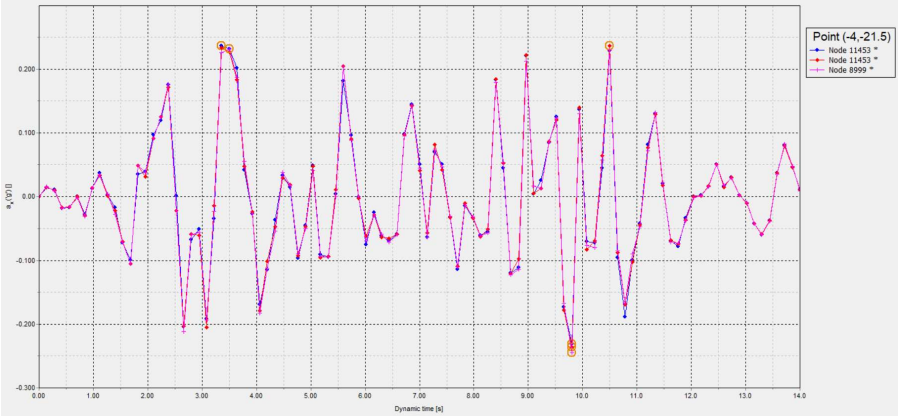

Figure 4.87. Acceleration vs Dynamic Time for Point 3

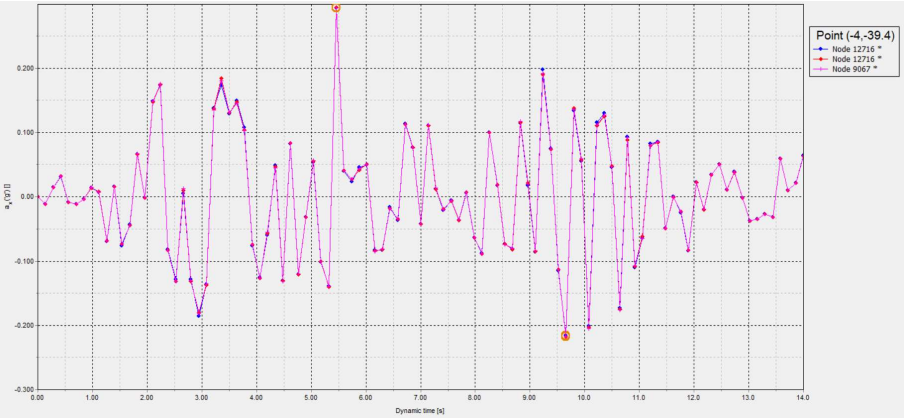

Figure 4.88. Acceleration vs Dynamic Time for Point 4

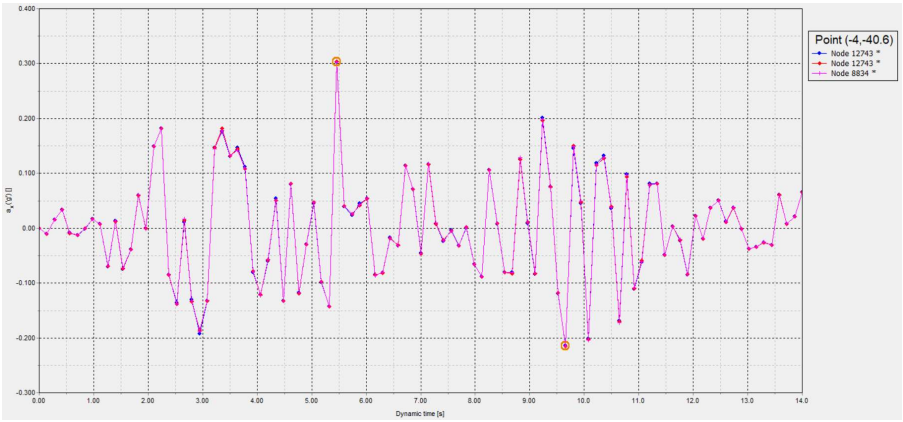

Figure 4.89. Acceleration vs Dynamic Time for Point 5

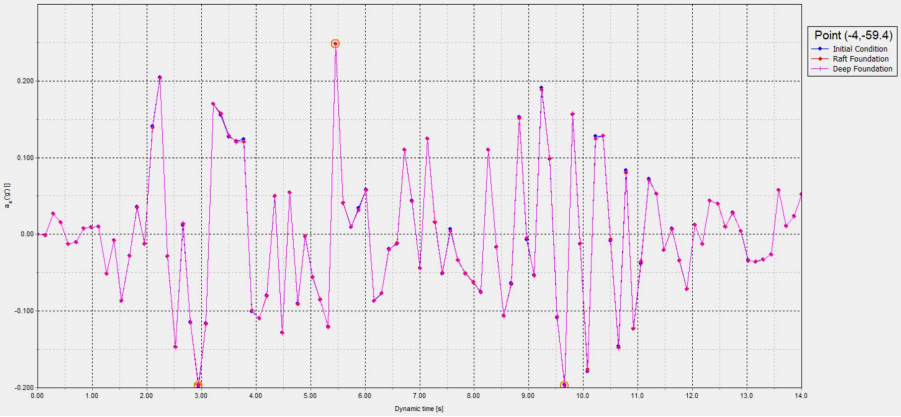

Figure 4.90. Acceleration vs Dynamic Time for Point 6

Table 4.15. PGA values for Hector Mine Earthquake

Condition	Point 1	Point 2	Point 3	Point 4	Point 5	Point 6
Initial Condition	0.339	0.257	0.237	0.294	0.303	0.248
Raft Foundation	0.326	0.266	0.237	0.295	0.303	0.248
Deep Foundation	0.318	0.267	0.245	0.295	0.303	0.248

Table 4.16. Amplification Factors for Point 1,2 and 3 of Hector Mine Earthquake

Condition	Amplification Factor (1/6)	Amplification Factor (2/6)	Amplification Factor (3/6)
Initial Condition	1.367	1.036	0.956
Raft Foundation	1.315	1.073	0.956
Deep Foundation	1.282	1.077	0.988

4.5.6. Tottori

According to acceleration response spectrums, in contrast to other cases, there are significant shifts at improved part. But at unimproved part, there is no change as usual. At improved part, given in Figure 4.91, Figure 4.92 and Figure 4.93, the shift is observed very clearly. That means the soil improvement has a significant effect on cyclic performance of soil in that case. Besides, for unimproved part it can be concluded that the improvement does not affect underlying layers.

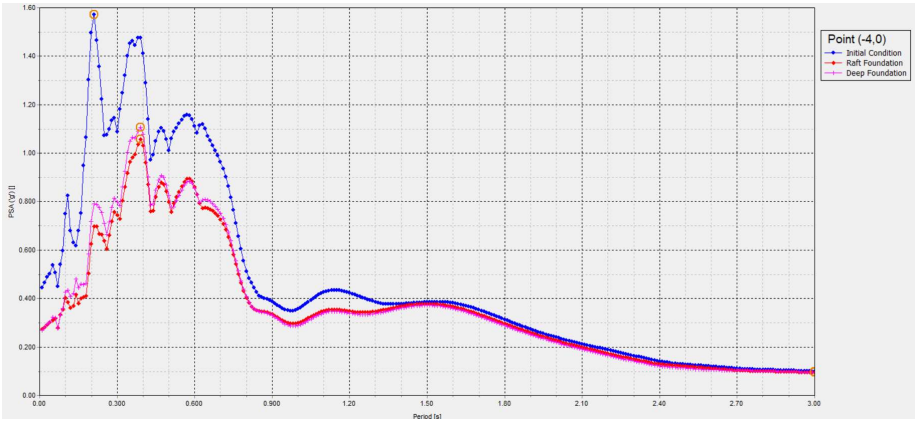

Figure 4.91. Acceleration response spectrum for point 1

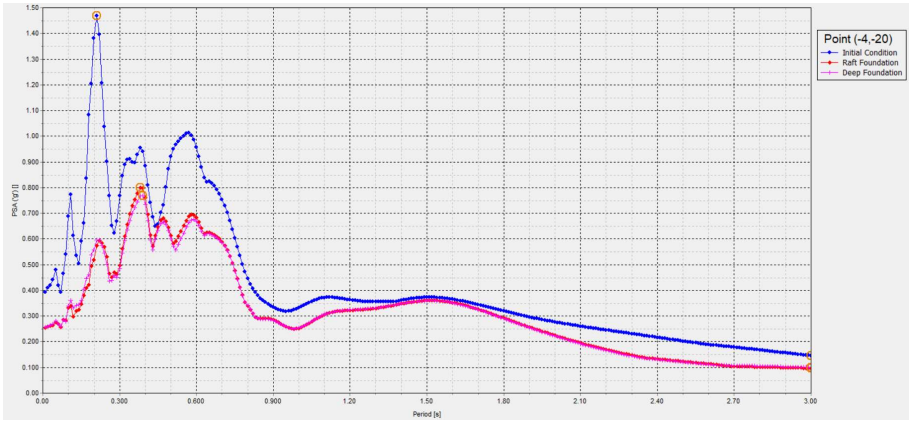

Figure 4.92. Acceleration response spectrum for point 2

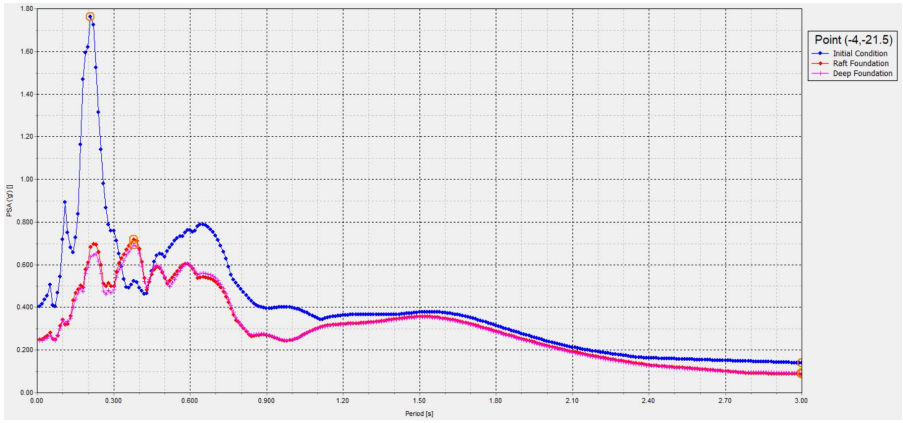

Figure 4.93. Acceleration response spectrum for point 3

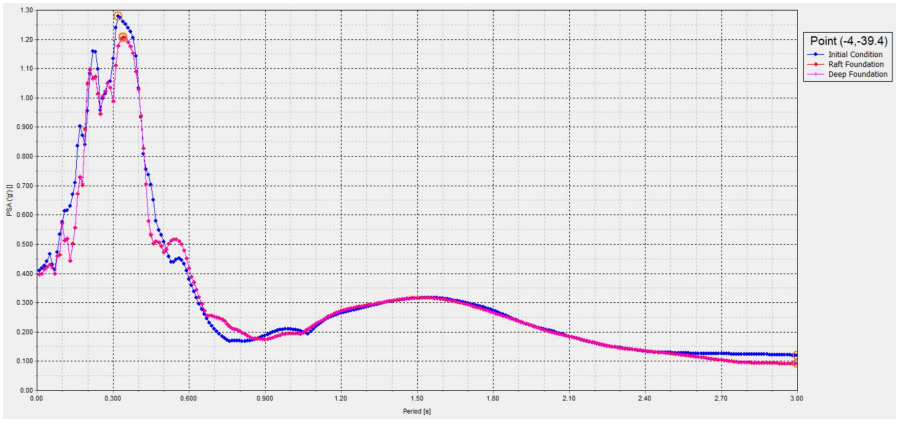

Figure 4.94. Acceleration response spectrum for point 4

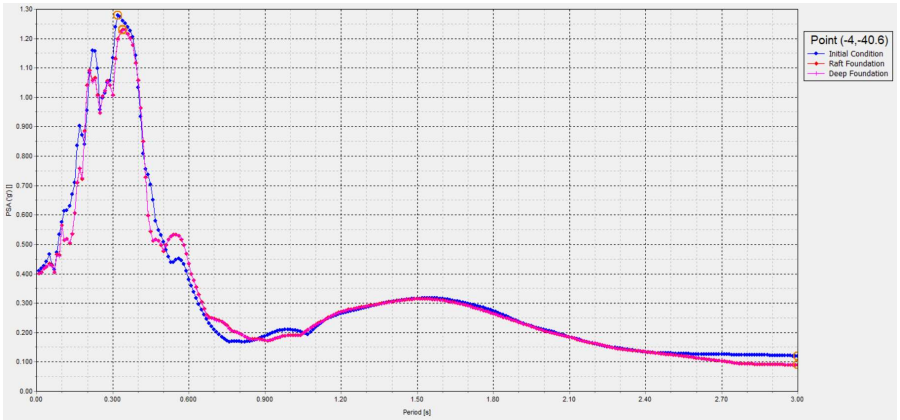

Figure 4.95. Acceleration response spectrum for point 5

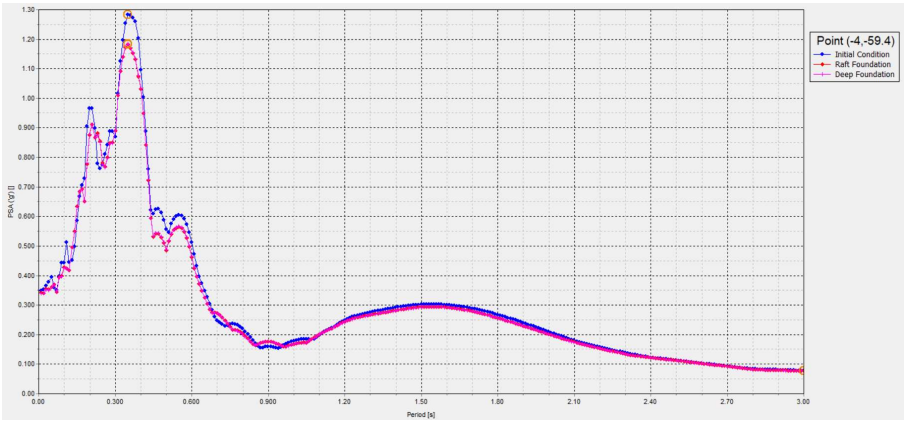

Figure 4.96. Acceleration response spectrum for point 6

Based on acceleration vs dynamic time graphs, there is a slight match between curves at locations under the piles. But the main concern is the improved part in that case. At surface

and improved sand layer, given in The Figure 4.97, Figure 4.98 and Figure 4.99, the peak acceleration values decreases after pile construction. Since the rigidity of soil increases at these locations, the capacity to response of earthquake loading advances too.

According to PGA values given in Table 4.17, the soil amplifies the earthquake loading as the wave travels from sand to clay. Moreover, according to the amplification factors given in Table 4.18, it can be stated that the amplification of soil is much less in deep foundations while comparing with initial conditions. Thus, the piled foundations deamplify the dynamic loading much better than natural conditions for that condition of soil and loading.

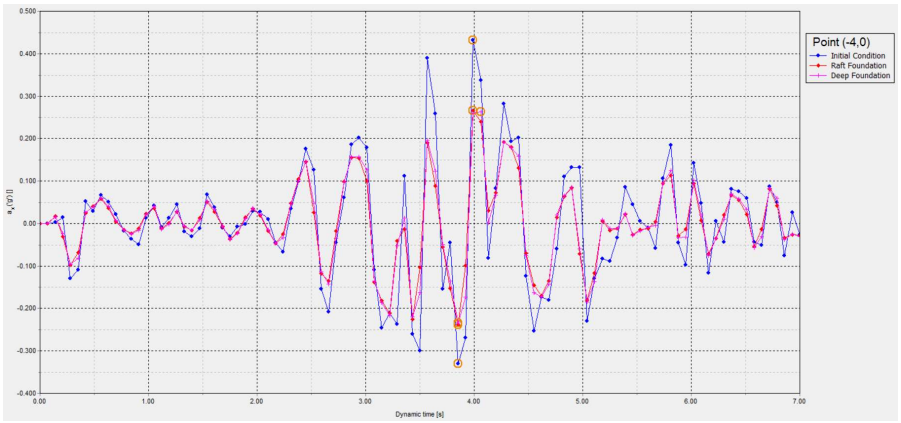

Figure 4.97. Acceleration vs Dynamic Time for Point 1

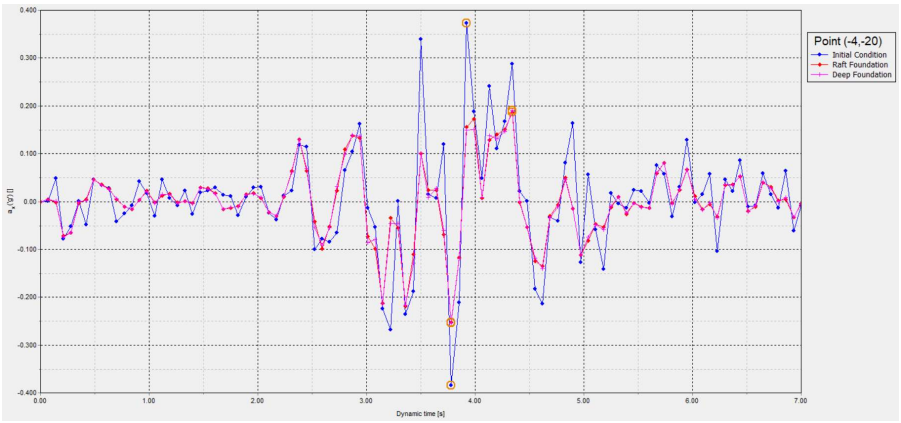

Figure 4.98. Acceleration vs Dynamic Time for Point 2

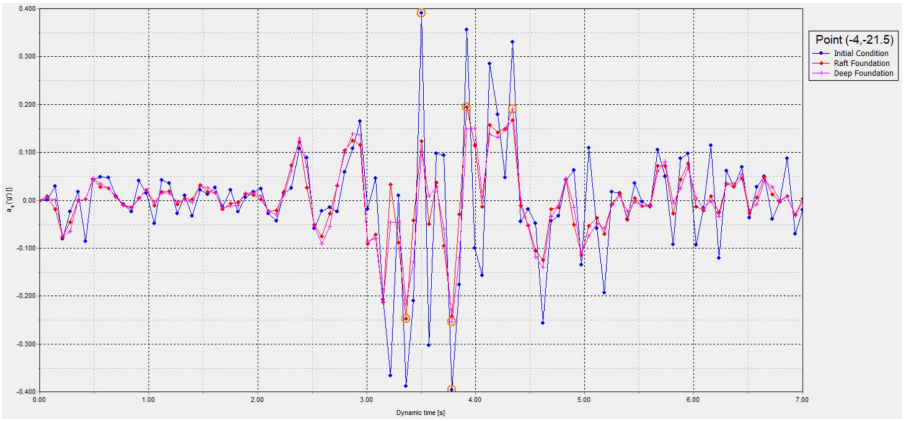

Figure 4.99. Acceleration vs Dynamic Time for Point 3

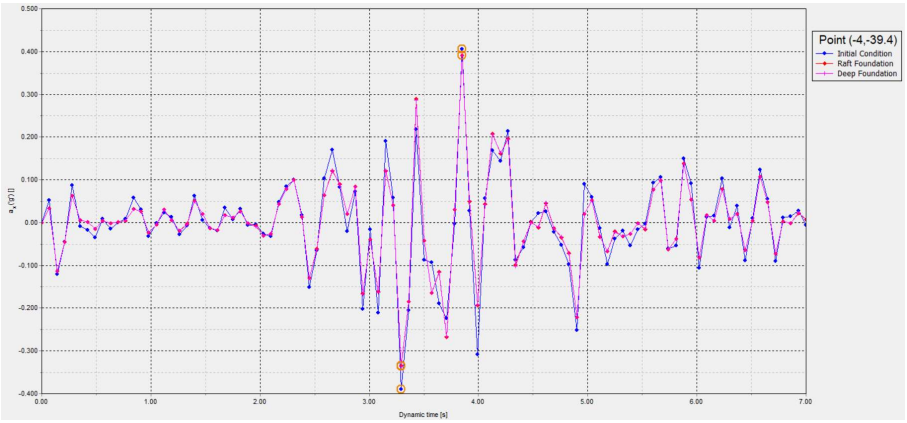

Figure 4.100. Acceleration vs Dynamic Time for Point 4

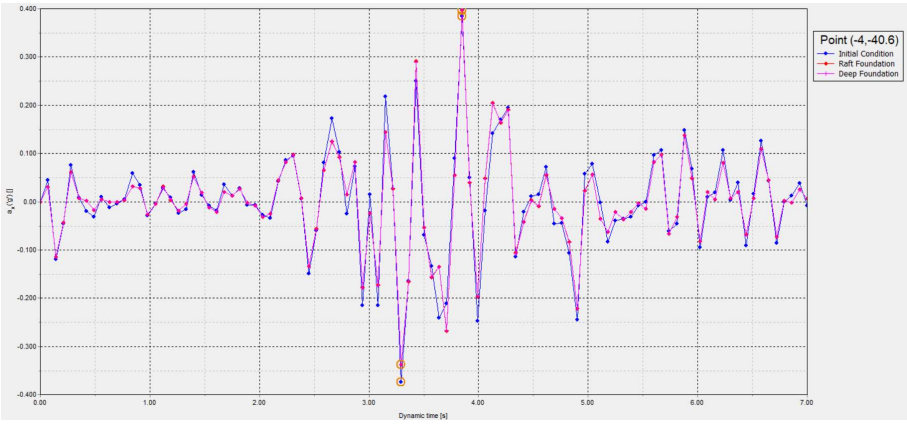

Figure 4.101. Acceleration vs Dynamic Time for Point 5

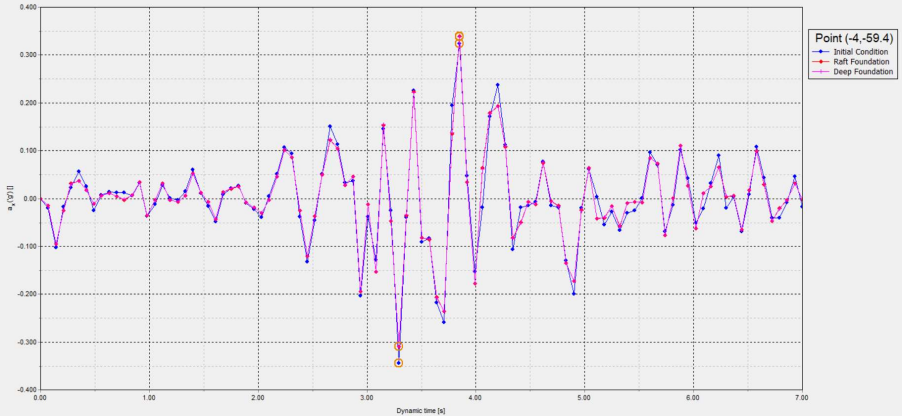

Figure 4.102. Acceleration vs Dynamic Time for Point 6

Table 4.17 PGA values for Tottori Earthquake

Condition	Point 1	Point 2	Point 3	Point 4	Point 5	Point 6
Initial Condition	0.432	0.384	0.391	0.405	0.384	0.344
Raft Foundation	0.266	0.252	0.247	0.391	0.397	0.339
Deep Foundation	0.263	0.254	0.254	0.390	0.397	0.338

Table 4.18 Amplification Factors for Point 1,2 and 3 of Tottori Earthquake

Condition	Amplification Factor (1/6)	Amplification Factor (2/6)	Amplification Factor (3/6)
Initial Condition	1.256	1.116	1.137
Raft Foundation	0.785	0.743	0.729
Deep Foundation	0.778	0.751	0.751

4.5.7. Duzce

Results show that there is a great match for unimproved part which means the improvement does not affect underlying layers. At improved part, given in Figure 4.103, Figure 4.104 and Figure 4.105, even there is small changes in curves of response spectrums, but there is not a significant shift among curves. Thus, the improvement does not affect the spectrum of site so much for the given soil and earthquake loading conditions.

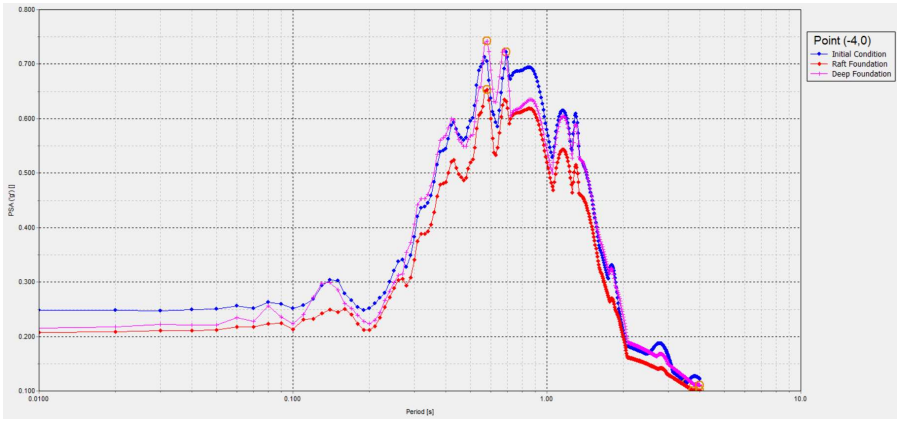

Figure 4.103. Acceleration response spectrum for point 1

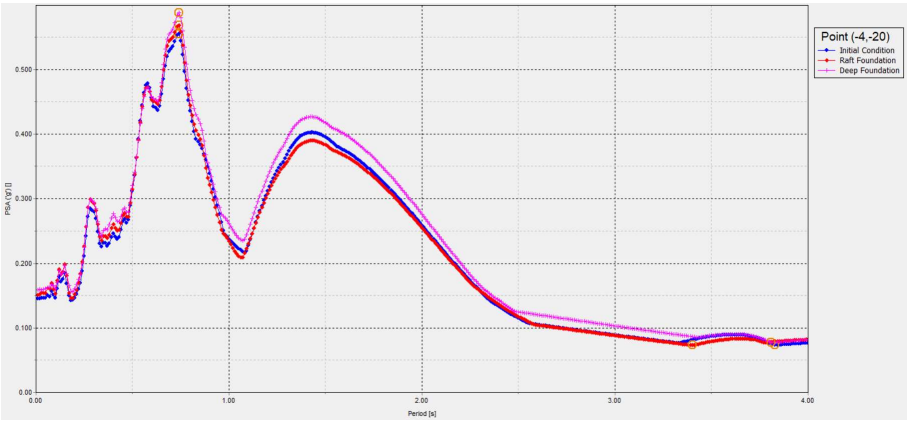

Figure 4.104. Acceleration response spectrum for point 2

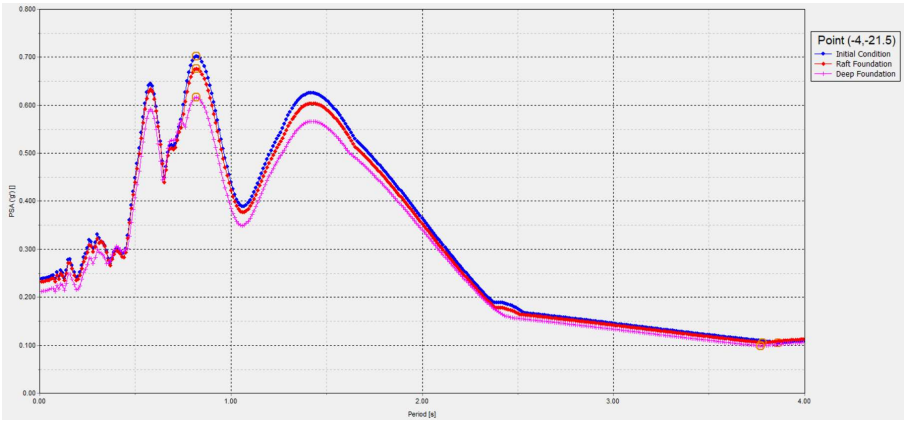

Figure 4.105. Acceleration response spectrum for point 3

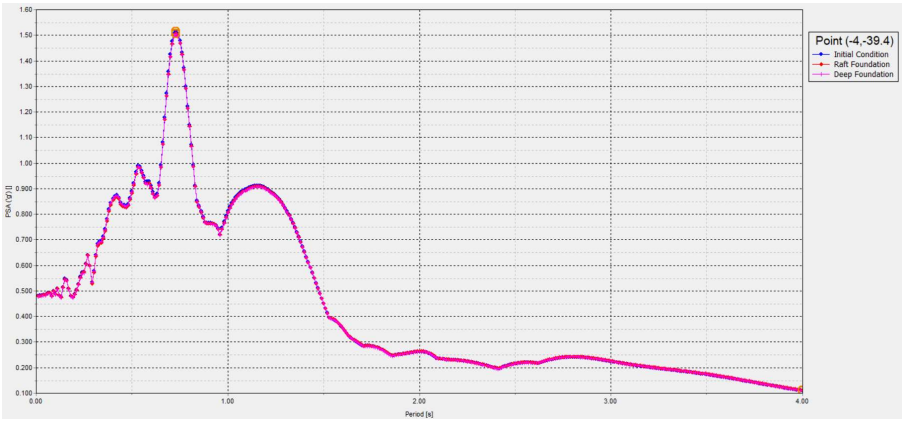

Figure 4.106. Acceleration response spectrum for point 4

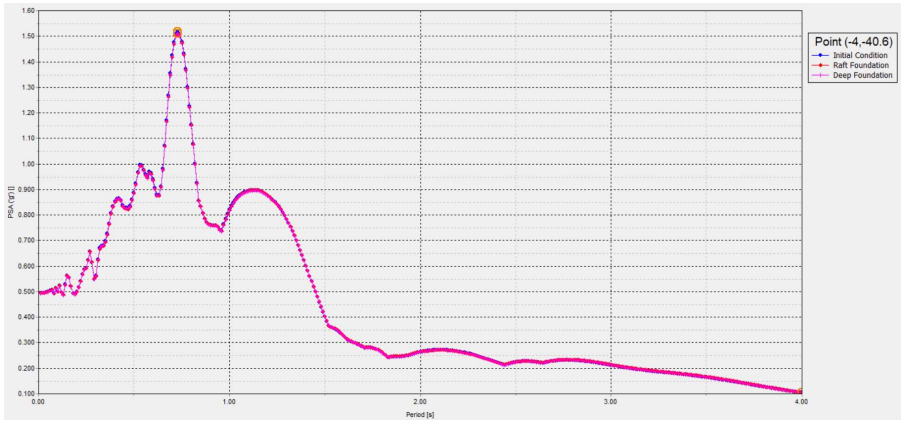

Figure 4.107. Acceleration response spectrum for point 5

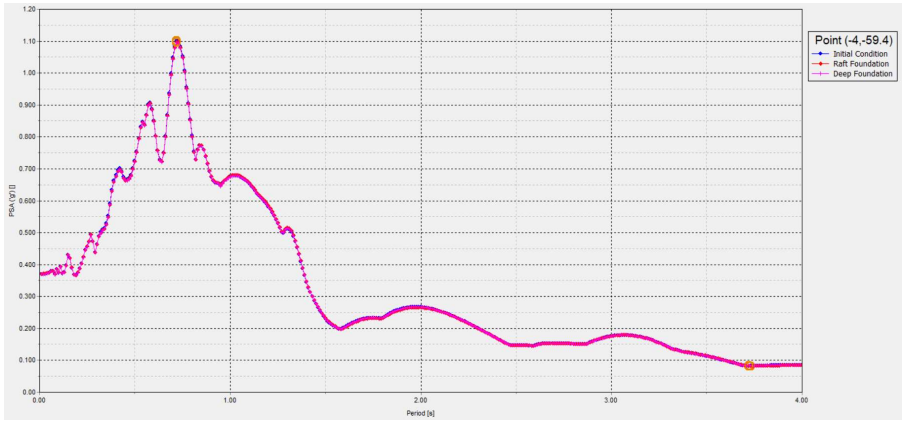

Figure 4.108. Acceleration response spectrum for point 6

According to the acceleration vs dynamic time graphs, there is a great match between curves for parts under piles. Indeed, there is not a clear difference for improved part too,

except some shifts in peak points. Moreover, according to the PGA values given in Table 4.19, the dynamic load is deamplified as waves travelling through sand layer, but it is amplified in clay layer. Besides, the amplification behavior given in Table 4.20 shows that the deep foundations allow the amplification much less than initial conditions. Therefore, the pile construction deamplify the dynamic loading much better than natural condition for the given loading and soil conditions.

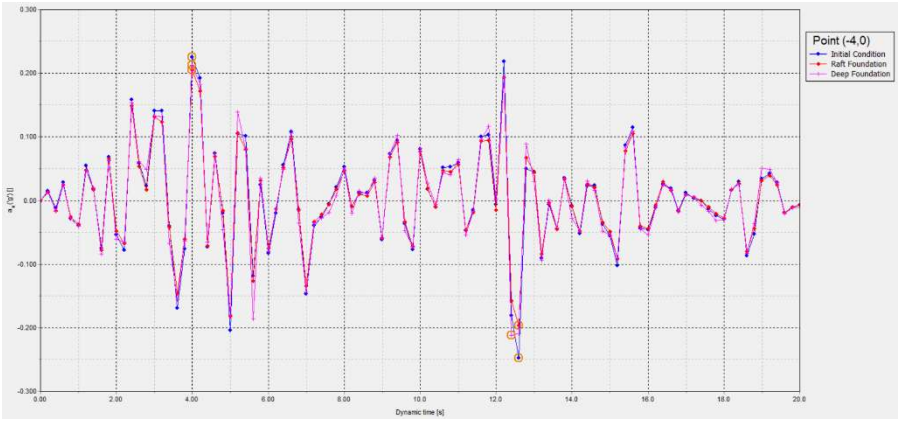

Figure 4.109. Acceleration vs Dynamic Time for Point 1

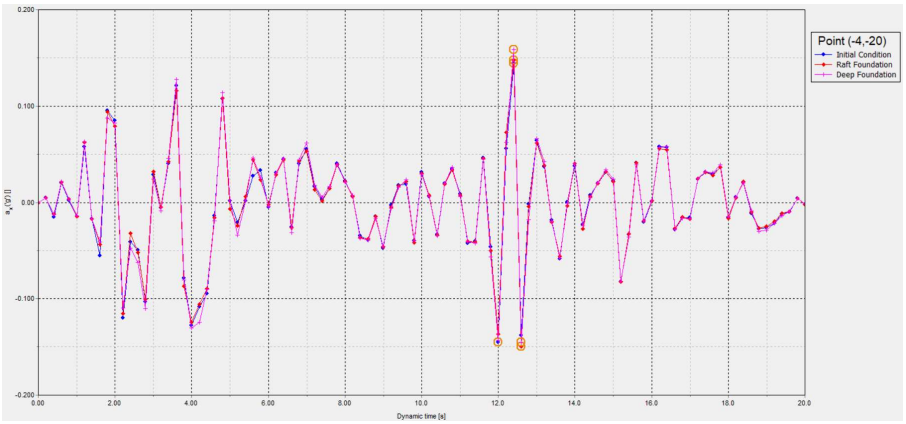

Figure 4.110. Acceleration vs Dynamic Time for Point 2

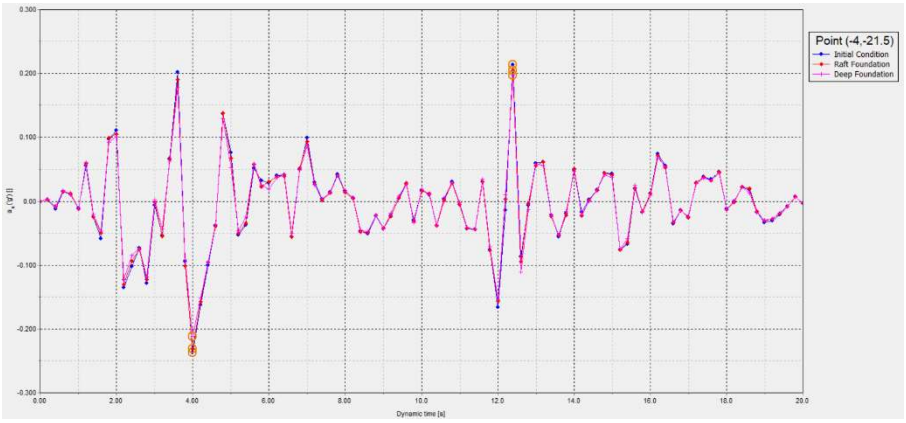

Figure 4.111. Acceleration vs Dynamic Time for Point 3

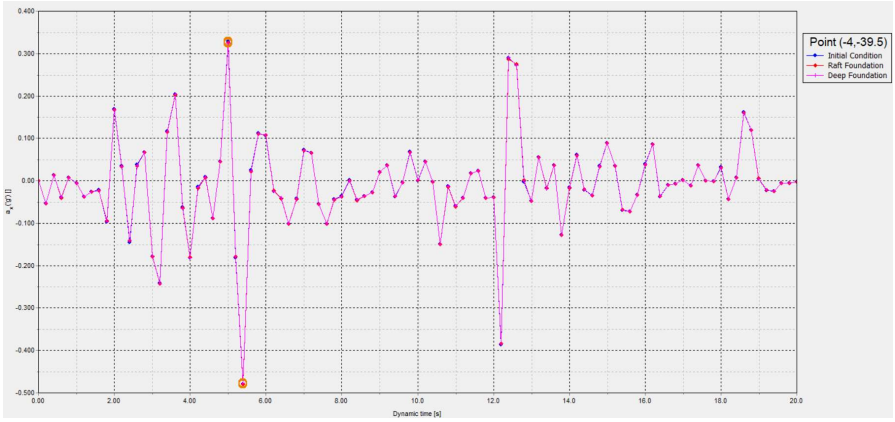

Figure 4.112. Acceleration vs Dynamic Time for Point 4

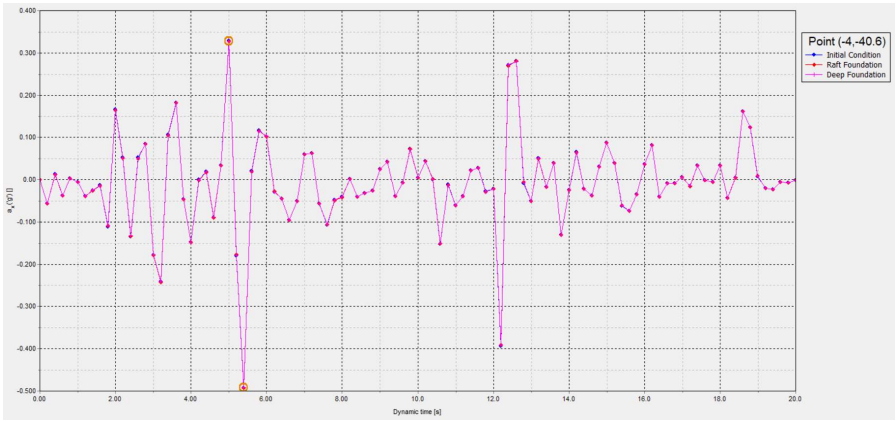

Figure 4.113. Acceleration vs Dynamic Time for Point 5

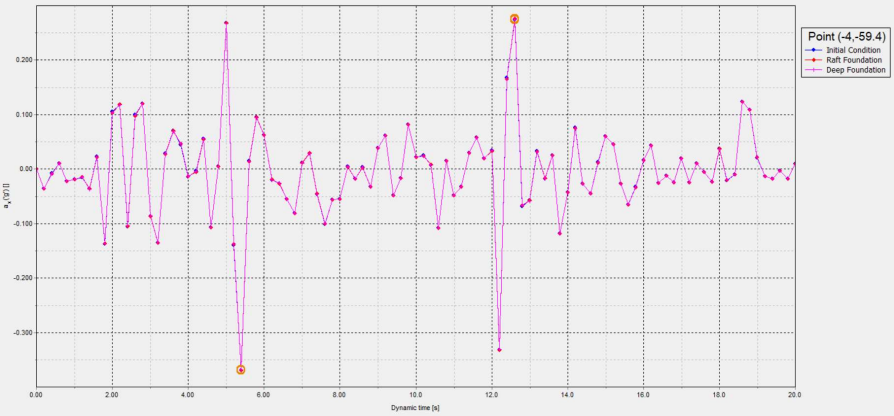

Figure 4.114. Acceleration vs Dynamic Time for Point 6

Table 4.19 PGA values for Duzce Earthquake

Condition	Point 1	Point 2	Point 3	Point 4	Point 5	Point 6
Initial Condition	0.248	0.145	0.237	0.48	0.493	0.369
Raft Foundation	0.205	0.149	0.232	0.479	0.493	0.369
Deep Foundation	0.213	0.159	0.211	0.477	0.491	0.369

Table 4.20 Amplification Factors for Point 1,2 and 3 of Duzce Earthquake

Condition	Amplification Factor (1/6)	Amplification Factor (2/6)	Amplification Factor (3/6)
Initial Condition	0.672	0.393	0.642
Raft Foundation	0.556	0.404	0.629
Deep Foundation	0.577	0.431	0.572

All in all, in this study, the effect of improvement is discussed through response spectrum, PGA value and amplification factors. The response spectrums show that the soil improvement or pile construction does not change the spectrum, does the soil class for the specified cyclic loading and soil conditions. And when we look to the PGA values from different levels of model, we see that the earthquake induced wave is amplified as it travels from rock to soil in most of the cases. But the amplification factors show that the construction of piles decreases the degree of amplification much better than the natural condition for the given conditions.

5. CONCLUSION

The aim of that study is to understand the effect of soil improvement (by pile construction) during dynamic loading (earthquake loading). It is expressed in terms of acceleration response spectrum, peak ground acceleration and amplification factor, which means the ratio of PGA at the specified point to the PGA at the outcrop bedrock.

The effect of soil improvement has been studying for long time. Many researchers studied different type of improvement such as rigid inclusions, jet grouting, foundation stabilization etc., on different soil types. In the past, the general acceptance was pseudo-static approach in dynamic analysis. However, todays by the development of software, it leads to enlargement in the field in terms of researches and studies on the analysis with real- or synthetic earthquake loading conditions.

In that study, seven-different acceleration-time records are selected from six different earthquakes, which are Landers, Kobe, Kocaeli (Gebze and Izmit stations), Hector Mine, Tottori and Duzce earthquakes. These data are scaled based on the scaling factor given by "https://ngawest2.berkeley.edu/" website. To get rid of unnecessary noise effects and to get healthy results the records are filtered by high pass and low pass filtering and corrected to throw off the linear errors of records. The scaling, filtering and correction processes are carried out by Seismosignal software. Then three models are created in Plaxis 2D finite element software, representing initial condition, raft foundation condition and deep foundation condition. At the result, response spectrum and acceleration-time graphs are drawn for six different locations, which are the surface, the end of pile, the point just beneath the pile, the locations at the top and bottom of change of soil layer and the base of rock layer.

Results show that, the soil improvement through pile construction does not create any shifts in the response spectrum, thus it does not change the soil class in most of the cases for the given loading and soil conditions, but for some records, the spectrum may change as seen in Tottori case. Beside we checked the PGA values at those six different points. It is seen that there is amplification as the wave travels within soil in most cases. And based on

amplification factors, it is stated that amplification factors of deep foundation are lower than initial condition. Thus, the soil improvement through the construction of piles deamplifies the earthquake loading much better than natural condition.

REFERENCES

1. FHWA, (August 2011), LRFD Seismic Analysis and Design of Transportation Geotechnical Features and Structural Foundations, NHI-11-032-Gec No:3.

2. Turkish Earthquake Code,2018 Disaster and Emergency Management Center, Ankara.

3. Kramer S,L.,(1996) Geotechnical Earthquake Engineering, Prentice-Hall USA.

4. Technical Report for the PEER Ground Motion Database Web Application, Beta Version, October 2001.

5. Naghizadehrokni M., A study of the effect of Soil Improvement Based on Numerical Site Response Analysis of Natural Ground in Babol City, Open Journal of Civil Engineering 2016,6,163-178, Babol, Iran.

6. Frankel, A. (1995), Mapping Seismic Hazard in the Central and Eastern United States, Seismological Research Letters, 66, (8-21).

7. Armstrong R.J, Boulanger R.W, Numerical Simulations of Liquefaction Effects on Piled Bridge Abutments, 6th International Conference on Earthquake Geotechnical.

8. Bouckovalas, G., Papadimitriou, A., Kondis, A. and Bakas, G. (2006) Equivalent-Uniform Soil Model for the Seismic Response Analysis of Sites Improved with Inclusions. Proceedings of 6th European Conference on Numerical Methods in Geotechnical Engineering, Graz, 6-8 September 2006, 801-807.

9. Vucetic, M. and Dobry, R. (1991) Effect of Soil Plasticity on Cyclic Response. Journal of Geotechnical Engineering, 117, 89-107.

10. Ge, G. and Liu, J.M. (2011) Effects of Ground Treatment on Site Seismic Response. 2011 International Conference on Consumer Electronics, Communications and Networks (CECNet), Xianning, 16-18 April 2011, 1198-1202.

11. Tamura S, Khorosvari M., Boulanger R.W., Wilson D.W., Olgun C.G, Rayamajhi D., Wang Y., Site Response of Soft Clay Reinforced by Soil-Cement Grid Based on Dynamic Centrifuge Tests, 6th International Conference on Earthquake Geotechnical Engineering, New Zealand.

12. Li Z., Li M., Feng Q., Dynamic Response of Mud in the Field Soil Improvement with Dynamic Drainage Consolidation, 4th International Conference on Recent Advances in Geotechnical Engineering and Soil Dynamics, Missouri University of Science and Technology, 2001.

13. Klimis N., Anastasiadis A., Gazetas G., Apostolu M., Liquefaction Risk Assessment and Design of Pile Foundations for Highway Bridges, 13th World Conference on Earthquake Engineering, Vancouver, B.C. Canada, 2004.

14. Mavituna O., Teymur B., Effect of Improving Soil as a Countermeasure for liquefaction, 14th World Conference on Earthquake Engineering, October 2008, Beijing, China.

15. Hashad Dr. A., El-Hakem Dr. Y., El-Ashaal Dr. A., Improving seismic resistance of Hydraulic Structures using soil improvement techniques, 16th International Water Technlogy Conferencec, IWTC 16 2012, Istanbul, Turkey.

16. Remediation of Liquefaction effects for a dam using soil-cement grids: Centrifuge and numerical modelling, Proceedings of the 19th International Conference on Soil Mechanics and Geotechnical Engineering, Seoul 2017.

17. Haselton C.B., Whittaker A.S., Hortacsu A., Baker J.W., Bray J., Grant D.N., Selecting and Scaling Earthquake Ground Motions for Performing Response-History

Analyses, 15th World Conference on Earthquake Engineering, Lisbon, Portugal 2012.

18. Armstrong R.J, Boulanger R.W, Beaty M.H., Liquefaction Effects on piled Bridge abutments: Centrifuge Tests and Numerical Analyses, Journal of Geotechnical and Geoenvironmental Engineering, ASCE, March 2013.

19. Armstrong R.J, Boulanger R.W, Beaty M.H., Equivalent Static Analysis of Bridge Abutments Affected by Earthquake-Induced Liquefaction, Journal of Geotechnical and Geoenvironmental Engineering, ASCE, March 2014.

20. Alkaya D., Çobanoğlu I., Yeşil B., Yıldız Ş., The evaluation of stone column and jet grouting soil improvement with seismic refraction method: Example of Poti (Georgia) Railway, International Journal of the Physical Sciences vol. 6(28) pp6565-6571, November 2011.

21. Franke Dr. K., Geotechnical Analysis of Earthquake, Lecture Notes, https://www.youtube.com, accessed in May 2019.

22. Üstünay E., (2018), Designing a Quay Structure with Steel Sheet pile and Investigating it under Earthquake effect (Master Thesis), ITU, Geotechnical Engineering Master Program, Istanbul.

23. Tönük G., Factors Affecting Site Response Analysis, Ph.D Thesis, Graduate program in Earthquake engineering , Boğaziçi University, Istanbul.

24. Yılmaz D., Site Response and Settlement of Buildings, In Adapazarı Basin, Ph.D Thesis, Graduate program in civil engineering, Bogazici University, Istanbul.

25. Çetiner B., Evaluating Site Effeccts for Estimation of Seismic Ground Response: A practical Approach, Master Thesis, Graduate program in Earthquake engineering, Boğaziçi University, Istanbul.

26. Bozkurt B.H., A Geotechnical Earthquake Engineering Investigation for Soils of Southern Coast of Izmir Bay, (Master Thesis), Dokuz Eylul University, Geotechnical Engineering Master Program, Istanbul.

27. Kirkit M., Investigation of Dynamic Soil-Pile-Structure Interaction in Clayey Soils by Numerical Analyses, Ph. D. Thesis, Yıldız Technical University, Geotechnical Engineering Program, Istanbul.

28. Pacific Earthquake Engineering Research Center, https://ngawest2.berkeley.edu, accessed in April 2019.

29. Disaster and Emergency Management Presidency, Turkish Hazard Map, https://tdth.afad.gov.tr, accessed in September 2018.

30. Seismosoft Software User Manual, http://www.seismosoft.com/seismosingal-documentation/, accessed in April 2019.

31. Plaxis 2D, Plaxis Manuals, http://www.plaxis.nl, accessed in September 2018.